FACULTY OF SCIENCE AND TECHNOLOGY

MASTER THESIS

Study programme / specialisation:

Marine and Offshore Technology

The spring semester, 2022

Open / ~~Confidential~~

Author: **Anuraj Karuvathil**

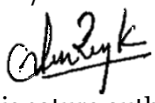

(signature author)

Course coordinator: **Yihan Xing**

Supervisor(s): **Yihan Xing**

Thesis title: **Estimation of Extreme Load Responses in a Gearbox of 10-MW Floating Offshore Wind Turbine**

Credits (ECTS):30

Keywords:

Offshore Wind Turbine
Acer method
Extreme load estimation
Gumbel Distribution

Pages: .....36.....

+ appendix: ...52.....

Stavanger, ...14/06/2022...

Abstract

This thesis studies the extreme load responses experienced by a 10-MW floating wind turbine situated in the North sea. With a plan to minimise fossil fuels and redefine the energy sector by adopting more safe, efficient, and cleaner solutions, countries have started investing in wind energy to harness the enormous untapped potential contained in the wind. Developing countries have begun building wind turbines to meet their energy needs. Countries started moving away from hydrocarbon and investing more in offshore wind turbines and solar energy parks to meet the expanding population needs and economy and reach net zero emission by 2050. The global average wind turbine size increased from 1.5-MW to 7.58-MW from 2000 to 2020. The future of wind turbines will be in 10-MW to 15-MW class wind turbines as the scientific research community has started to analyse more about the large offshore wind turbine(OWT). The gearbox is considered one of the most critical components in a wind turbine that drives a significant part of operating expenses. Reliability of the gearbox is often crucial for wind turbines which comes as a package with an efficient design and proper load estimation matching the ULS (Ultimate Limit State) condition. The costs of gearbox repair and upkeep and the costs of output losses associated with faulty gearboxes account for a significant portion of the operating costs of the offshore wind turbine. In this thesis, the accuracy and robustness of ACER (Average Conditional Exceedance Rate) as a tool are analysed to estimate extreme loads on the wind turbine gearbox and structure. This is done by analysing varying quantities of accessible data from the North Sea, where most large floating wind turbines are installed. The extreme loads estimated are compared with the Gumbel method under operating conditions of 8m/s, 12 m/s and 16m/s wind speed representing below, rated and above rated wind speed. It is vital to analyse the extreme loads under the dynamics operating condition and analyse the response in a fully coupled state. The aim is to show the accuracy and reliability of ACER in estimating the extreme load's responses and 1,2 & 5 year return period of large OWT. The results show that the extreme loads' responses on the 10-MW wind turbine gearbox and structure estimated by ACER gave more accurate and reliable values independent of other extreme value prediction methods like the Gumbel method. This study develops and estimates load responses in large OWT and guides the ultimate limit state load (ULS) calculation for 10-MW wind turbines.

Table of Contents

List of figures and tables

Abbreviations

GW	–	Giga Watt
kW	–	Kilo Watt
MW	–	Mega Watt
OWT	–	Offshore Wind Turbine
FOWT	–	Floating Offshore Wind Turbine
ULS	–	Ultimate Limit State
HAWT	–	Horizontal Axis Wind Turbine
VAWT	–	Vertical Axis Wind Turbine
DTU	–	Danmarks Tekniske Universitet
RWT	–	Reference Wind Turbine
NREL	–	National Renewable Energy Laboratory
DNV	–	Det Norske Veritas
N	–	Newton
kN	–	Kilo Newton
ACER	–	Average Conditional Exceedance Rate
EVD	–	Extreme Value Distribution
MBS	–	Multi-Body System
LC	–	Load Case
NREL	–	National Renewable Energy Laboratory

Acknowledgement

This thesis is a part of my master's programme, Marine and Offshore Technology, at the University of Stavanger under the Department of Mechanical and Structural Engineering and Material Science, Faculty of Science and Technology

First and foremost, I would like to thank my supervisor Professor. Yihan Xing for his immense support, constant guidance, and encouragement. I couldn't have made it this far without the help of him, who kindly shared his knowledge and skills. I would also like to express my gratitude to Professor Shuaishuai Wang at NTNU for the invaluable assistance, guidance, and information that helped me complete my thesis.

I am very thankful to my friend Mr. Rajiv Balakrishna for sharing his knowledge and guiding me in writing papers. A special thank goes to my classmates, especially Mr. Laksri Jayathilake and Mr.Andre Eltervaag, for providing me with moral support during the last two years

Lastly, I owe my deepest gratitude to my parents for giving me the best education and constant support throughout my studies and life. I would also like to thank my wife Ms Preetha Antony for her belief in me, which has kept my spirit and motivation high.

Chapter 1 - Introduction

The world countries are making an international effort to tackle climate change, a major concern for the rise in global temperature and melting of glaciers. This is a significant challenge both developed and developing countries are facing. Most of them have pledged to reduce their dependency on fossil fuels and move toward clean energy to limit the rise in global temperature to 1.5 degrees Celsius. Wind and solar power have been at the forefront of the energy transition, enabling countries and industries to adopt clean and efficient utilisation of renewable energy sources to meet energy demands. Global Wind Energy Council (GWEC) is leading the way by supporting the development of wind energy technology to achieve or meet the target of reaching a carbon-neutral economy by 2050.

Wind energy is a clean and readily available renewable energy source with vast energy potential. Due to the higher wind potential and continuous unobstructed availability of offshore, there has been a considerable shift in the trends towards wind turbine installation in the offshore sector. Wind turbine technology was developed and advanced to a stage where wind turbines started getting bigger to meet the increasing energy demand and needs of the growing economy. The two main reasons for wind turbine development moving offshore where the availability of undisturbed wind due to the lower surface roughness offshore and higher power output by increasing the rotor diameter. The maximum power output available in the wind given by Eq. (13) is influenced by wind speed, i.e. doubling the wind speed will lead to an eight-fold increase in power, and doubling the rotor diameter will lead to a four times increase. This, together with the improvement in wind turbine technology, has led to wind turbines moving further offshore.

There has been a tremendous increase in the wind industry in the past decade. Figure 1 shows the worldwide wind turbine installation offshore and onshore. The report published by Global Wind Energy Council (GWEC) [1] in 2022 showed that 837 GW of wind capacity was installed to date worldwide. A total of 93.6-GW wind capacity was installed in 2021, which was only 1.8% less than the previous year, even though the world went through a pandemic. Most of the development came from the Asia Pacific, especially the People's Republic of China, leading the race in wind power installation. The offshore industry saw a tremendous growth of 21-GW wind power installed, which as per the GWEC, is the second highest till now. Even though the growth of wind energy was high, it was not enough. The GWEC forecast would require an increase of wind energy installation four times from 93.6-GW in 2021 to contain the temperature rise by 1.5 degrees Celsius and reach the net-zero target by 2050.

Figure 1: New Wind turbine installation worldwide 2017-2021

As more and more wind turbines got installed and the size of the wind turbine increased to capture more power from the wind, it became necessary to design wind turbines economically while maintaining the safety margin within the operational limits. Robust design is required to avoid downtime to keep the wind turbines' operational readiness and condition. For achieving reliability, an accurate load prediction was crucial to understanding the dynamic loads that wind turbines had to undergo during their lifespan. As the industry evolved, wind turbines moved offshore for various reasons apart from the aforementioned technical reasons. As we go more away from the shore, the resistance to airflow gets reduced considerably, and we get a consistent and uninterrupted airflow. The Floating Offshore Wind Turbine(FOWT) can be installed and pre-commissioned on the shore and towed to the installation site. Floating wind turbines have the advantage of towing them back to shore when more significant repair workers are required to be carried out, thus enabling easy operation and maintenance. All these reasons led to 80% of OWT to be Floating Offshore Wind Turbine(FOWT) located away from the shore where bottom fixed wind turbines were not economical.

Studies were conducted to make OWT economical and reduce the installation cost, which led to an increase in the size and capacity rating of the FOWT. This also helped reduce the number of offshore structures, cables, and mooring systems, which thereby helped bring down

the cost of maintenance. The balance of system cost is reduced by installing a large wind turbine and plant, as shown by Shield et al. [2]. His research shows that increasing the wind turbine capacity will reduce the energy cost. Also, as the size of the wind turbine grew, it was difficult to transport the new wind turbines on land and faced many hurdles in the transportation. As the size of the wind turbine increased, OWT enjoyed the benefit of easiness of transport compared to the constraints in onshore wind turbines, which was reached study conducted by Bilgili et al.[3]. Major wind turbine manufacturers like Vestas, General Electric (GE) and Siemens Gamesa are upsizing the next-generation wind turbine and reducing the cost as per the Offshore Wind Market Report,2021 [4]. Figure 2 shows the global increasing wind turbine size trend from 2001 to 2026.

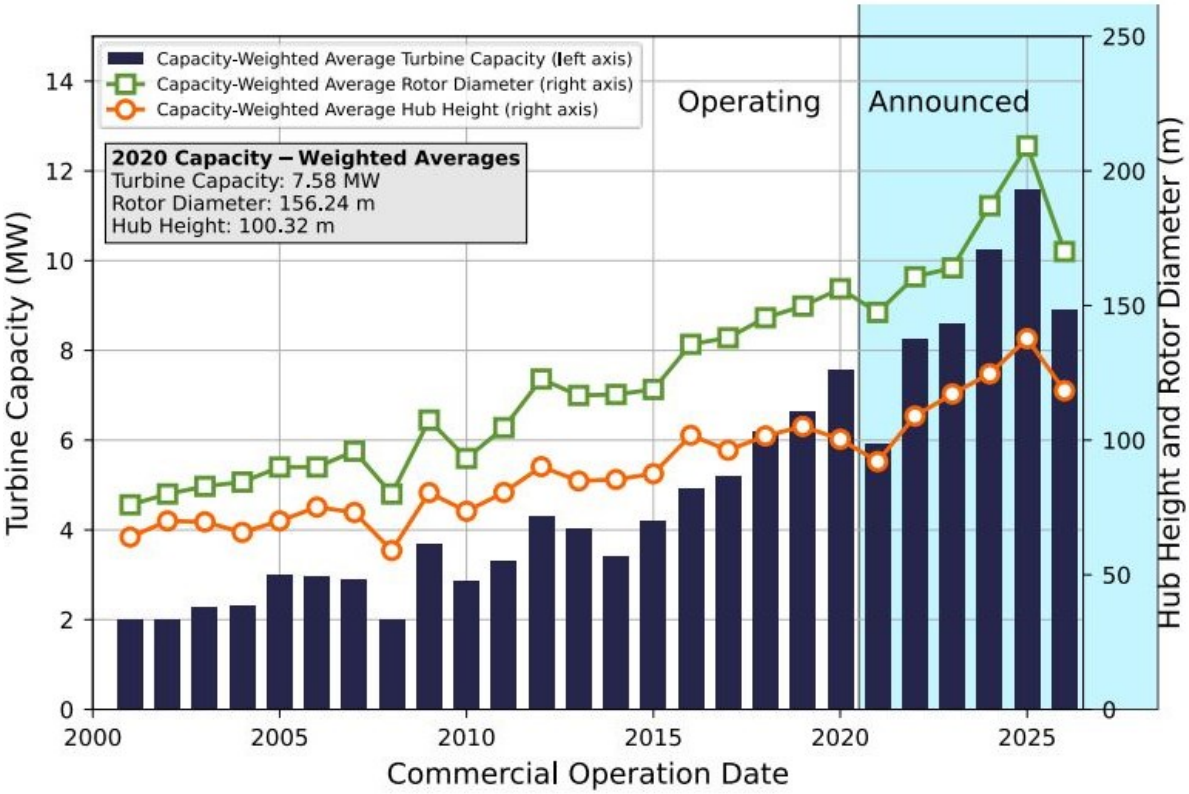

Figure 2: OWT capacity and size[4]

As wind turbine technology developed, the wind turbine size increased gradually, capturing more and more energy and making wind turbines economically viable. As the size increased, the wind turbine technology met with a new hurdle of not achieving the design life span as intended, which had a cost implication. A study on the wind turbine condition monitoring by

Keller J et al.[5] showed that the gearbox in the drivetrain system caused the highest downtime per failure. The gearbox is one of the expensive components, and if faulty will affect the operation and increase production losses due to downtime. Figure 3 shows the failure of two large wind turbines in 13 years in Europe.

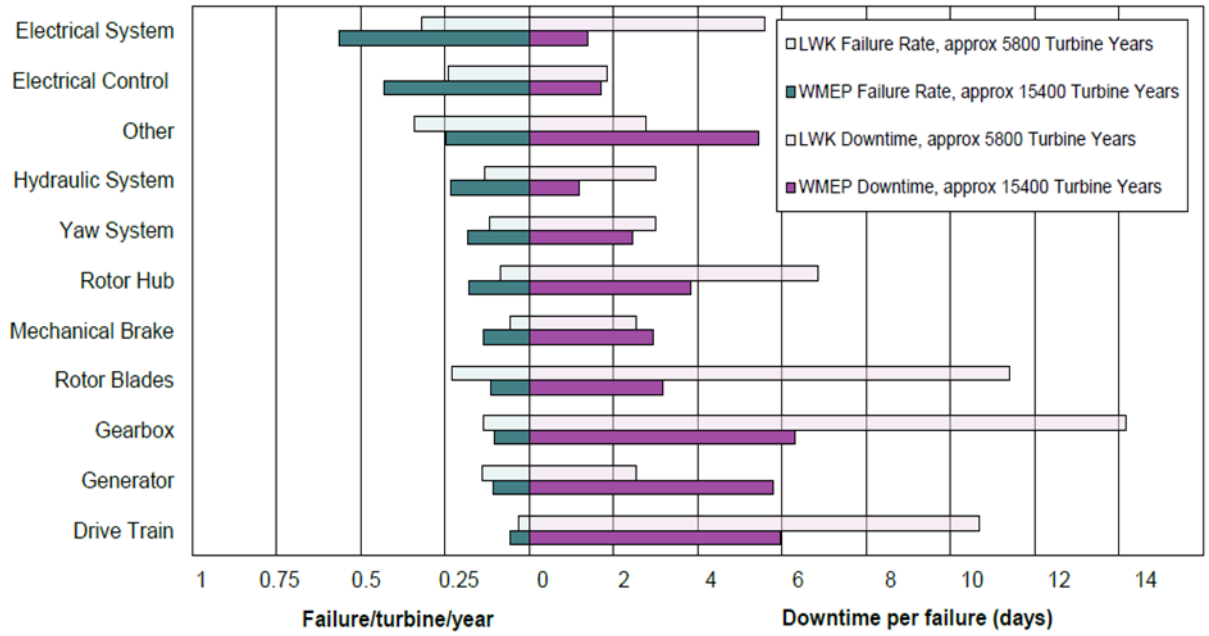

Figure 3: Reliability and downtime in wind turbine subassemblies [6]

As most of the wind turbines were designed and planned to be installed in the offshore environment, there was a need to understand the dynamic behaviour of the wind turbine under different environmental conditions. FOWT are generally exposed to various environmental loads like waves, currents, wave slamming, wave breaking loads on the structural, turbulent wind loads, wake turbulence, ship and ice impact loads etc. Since the wind turbine is prone to all these extreme environmental conditions and the coupled behaviour between the FOWT and the environmental condition, it is necessary to estimate the extreme loads acting on the wind turbine. Also, since the responses are highly random, irregular, and dynamic, it became important to develop a numerical tool that can accurately estimate the effects of wind and waves on the wind turbine. In the ULS design, it is very important to estimate the extreme dynamic load responses and identify accurate safety factors so the design is efficient. Many kinds of research were done to determine the extreme loads, but most required numerous dynamic simulations, which were time-consuming and had high computational costs. Scientific studies were done in estimating and developing a numerical tool estimating the extreme responses

offshore. Xu K et al. [7] 2019 studied the extreme responses of a semi-submersible FOWT and showed how the fatigue damages could be nonlinear. Extensive studies were done to understand the responses in the drive train gearbox. In his paper, Y. Xing et al. [8] studied the multi-body body modelling and the responses from the planetary gear. Later in 2014, Y. Xing et al.[9] showed the coupled environmental responses on spar-type platforms and their effects on the gearbox. Offshore wind turbines had to face more uncertainty in load estimation due to the challenging environmental condition than onshore wind turbines. As a result of development in wind turbine technology and engineering and with an eye on the future wind turbines, S. Wang, A. R Najed and T. Moan 2020 [10]came up with a design for a compact 10-MW OWT with a compact drive train arrangement and studied the dynamic response analysis. This paper used an innovative power split and compound epicyclic transition method in the new compact wind turbine design. S. Wang et al. [10], [11] made a significant contribution to the design modelling and analysis of 10-MWT FOWT.

A compressive knowledge of the dynamic behaviour of the wind turbine drive train and structures is required to minimise the downtime and improve the life span and service life of the wind turbine. IEC 61400-3 [12] has put forward a statistical extrapolation method that has helped identify the ultimate strength while estimating the extreme loads' responses. Most of the research was then conducted to analyse the effectiveness of the extrapolation method. A. Naess et al.[13] proposed a statistical technique called Average Conditional Exceedance Rate (ACER) for extracting the extreme values of sampled data. This method is considered more accurate when comparing the peak-over-threshold and Gumbel methods. Xu et al.[14] used ACER to predict the extreme loads to reduce downtime due to the environment loading on the semi-submersible wind turbine that was used in the design phase of a 5-MW wind turbine. Cheng et al. [15] studied the dynamic structural and fatigue response of HAWT and VAWT on a 5-MW semi-submersible wind turbine

Most of the research was done on the 5-MW FOWT, and the contribution to very large FOWT has been less since the future wind turbines are large FOWT from 10-15 MW. Based on the ACER method, only very few studies have been conducted on extreme load responses on the gearbox of 10-MW semi-submersible FOWT. This thesis will characterise the importance of ACER as a statistical tool in estimating extreme gear pair meshing load responses and load responses from the structure of a 10-MW semi-submersible wind turbine during the operating conditions

Chapter 2 – Theoretical Background

2.1 Overview

FOWT is a complex structure consisting of parts like the tower, support structure, rotor and drivetrain. It is necessary to assess the loads from the waves excitation (hydrodynamic), the load from the wind (aerodynamic), the loads on the structure (elastic) and the control system (servo) in the time domain to analyse the dynamic response in the wind turbine. Since all the components are coupled together, assessing the dynamic behaviour of the global structure is a complex process. It is therefore subjected to a two-step decoupled analytical technique. In the first step to analyse the loads and moments, we use global hydro-servo-aero-elastic studies. This is done in FAST (Fatigue Aerodynamics Structure Turbulence). The loads obtained from FAST results are then used in Multi-Body Simulation (MBS) to forecast the dynamic behaviour of the moving parts. Upon getting the time domain data from the MBS, we analyse the extreme load responses using ACER and compare it with Gumbel to estimate the accuracy of the robustness.

2.2 Hydro-Servo-Aero-Elastic Analysis

To study the effect of fully coupled hydro-servo-aero elastic analysis, we have three-time domain tools SIMPACK, FAST and SIMA. FAST is an open-source code software by National Renewable Energy Laboratory (NREL). FAST or Open FAST [16] is a physics-based tool for simulating the coupled nonlinear simulation of a wind turbine. It includes coding to analyse the aero-hydro-servo-elastic loads. The wind flow data is used in the aerodynamic model to estimate the aerodynamic loads, and this is very useful for analysing the loads on the rotor blades. For analysing the irregular wave loads, the hydrodynamic model in the FAST solves the hydrostatic, diffraction, radiation loads, etc. This helps solve the hydrodynamic stresses on the wind turbine structure and mooring system. The control system solves the electrical, sensor, and pitch control analysis. Global analysis of 10-MW on a semi-submersible floating concept wind turbine in Paper 1 is done in FAST

SIMA[17] is software used to analyse marine operations and floating systems. This software has significant capability in dynamic analysis of FOWT from wind turbine modelling, 3D simulation, lifting operation, towing operation, and documentation analysis report. Global

analysis of 10-MW OWT on bottom-fixed monopile concept, spar-type concept and semi-submersible floating concept in Paper 2 is done SIMA as estimates the hydrodynamic loads, complex dynamic motion of floating structures, structural responses and has the option to add control system externally

2.3 Multi-Body Simulation using Simpack

Simpack [18] is multi-body simulation software that helps engineers simulate and solve the dynamics of motion of a moving mechanical system and visualise the coupled forces, bending moment etc., acting on the body. The Simpack is engineered to solve the dynamic behaviour of interconnected bodies. It is fully aligned to determine the dynamic responses of FOWT, containing moving components like the hub, main shaft, bearing, and gearbox. The bodies are made up of stiff and flexible parts linked together by various joints and other restricting factors. This software is mostly used in the wind turbine industry and automobiles to solve complex and irregular models with flexible and interconnected bodies. Joints like force or stiffness elements are used to connect different bodies, and these joints restrict the relative motion between the bodies. Simpack is a multi-body simulation software that analyses the dynamics of body behaviour by solving the equation of motion. Forces elements model gear tooth contact, and bearing and gear meshing stiffness are modelled by a spring element in Simpack. Also, Simpack analyses the model and can be used to generate the natural frequencies inside a drivetrain. The natural frequencies obtained from Simpack can be used along with excitation frequencies in a Campbell diagram to check for the likelihood of resonance in the drivetrain model.

2.4 Extreme Value Distribution (EVD)

Extreme value distributions are limiting distributions for extreme values, i.e. smallest extreme or the largest extreme of a stochastic variable. The extreme values obtained from the EVD are mostly used as design parameters. EVD is defined as the largest of the maximum value from the individual maximum value from a series of discrete maxima, and more detail is given by Leira et [19].

$$Y_{ext} = \max (Y_{max1} , Y_{max2} , Y_{max3} \ldots\ldots\ldots Y_{max\,n}) \quad (1)$$

Where Y_{ext} is the largest maximum value, and Y_{max} is the individual maximum value. It is assumed that the individual maxima are independent and also distributed identically with the distribution function $F_{Ymax}(y)$ where

$$F_{Yext} = P(Y_{ext} \leq y) = [F_{Ymax} (y)]^n \quad (2)\ (1)$$

There are three types of extreme value distribution (EVD) that can show the extreme from any data set. It should satisfy the following conditions: a continuous probability distribution, the data set must be identical and independently distributed random sample and should have an inverse. The three types of EVD differentiated based on the tail behaviour of the initial distribution are:

i. EVD Type I (Gumbel Distribution)
ii. EVD Type II (Fréchet Distribution)
iii. EVD Type III (Weibull Distribution)

The most common type of EVD is the Type I distribution or the Gumbel distribution, which is mostly used to estimate natural disaster occurrence. Frechet distribution or Type II EVD are used to model the largest values, and the Type III or the Weibull Distribution are often used in product reliability. In this thesis, we will be comparing two techniques: the Gumbel technique (Section 2.4.1 Gumbel Distribution) and the ACER technique (Section 2.5 Average Conditional Exceedance Rate (ACER))

2.4.1 Gumbel Distribution

Gumbel Distribution is the most common type of extreme value distribution, also referred to as Type I EVD. The generalised extreme value distribution (GEV) combines or the Gumbel, Fréchet and Weibull distribution. The parameters of a distribution function are the shape parameter γ, location parameter μ and scale parameter σ. The CDF of general extreme value distribution is given by:

$$\mathrm{Fx(x)} = exp\left\{-[1 + \gamma\left(\frac{x - \mu}{\sigma}\right)]\right\}^{-\frac{1}{\gamma}} \quad (3)$$

The gear meshing forces or the circumferential forces in the wind turbine gear are fitted to the Gumbel distribution to estimate the maximum gear contact forces and assess the return period. When the shape parameter γ= 0, the GEV is equal to the Gumbel or Type I EVD. This is mostly used in estimating extreme values in marine structures and is given by:

$$Fx(x) = \exp\left\{\exp\left(\frac{x-\mu}{\sigma}\right)\right\} \tag{4}$$

When the shape parameter γ is greater than 0 and less than 0, the GEV will be equivalent to Fréchet Distribution (EVD Type II) and Weibull Distribution (EVD Type III), respectively.

Above Eq (*4*)when written in Logarithmic form:

$$-\ln\left(\ln\left(F_X(x)\right)\right) = \frac{x}{\sigma} - \frac{\mu}{\sigma} \tag{5}$$

The scale σ and location parameters μ is be found by the least-square fitting method. We get a straight line when plotted, as shown in Figure 4.

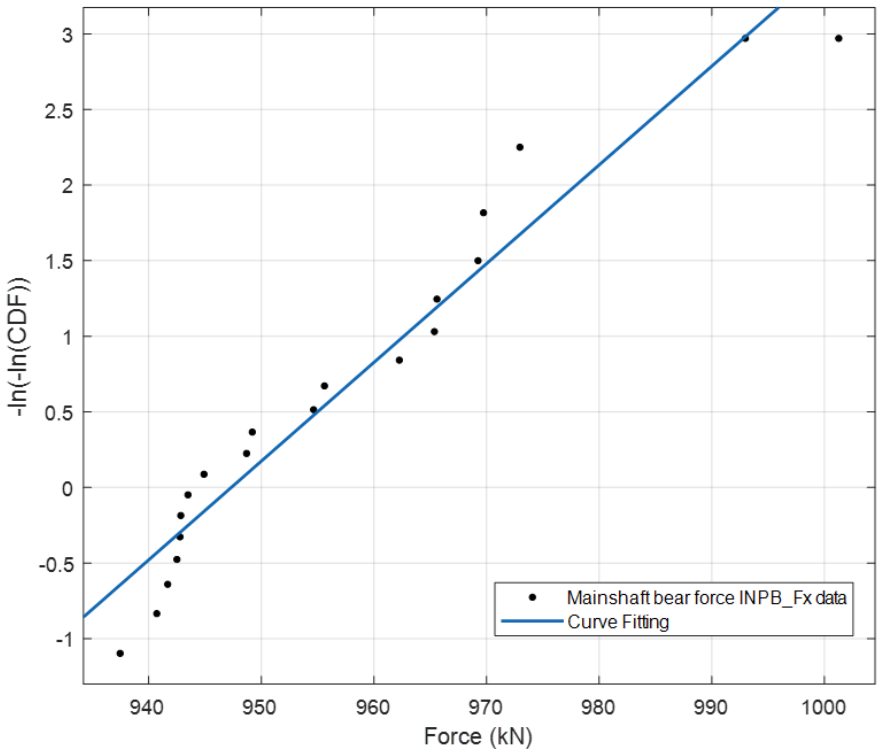

Figure 4: Gumbel probability

2.5 Average Conditional Exceedance Rate (ACER)

Naess et al. [13] established the Average Conditional Exceedance Rate (ACER), which predicts the extreme value distribution by building a series of non-parametric functions. It is helpful for both stationary and non-stationary processes because it incorporates all maximum global peaks and the correlation between subsequent peaks in a sampled time series. All the peaks from the 20 observations are used, and the number of exceeding peaks is analysed by multiplying the total number of peaks by the number of seeds. The ACER function k (x) is presented in Figure 5 with an order k scale from 1 to 6.

For example, consider a drivetrain load as a random stochastic process Y(t) observed over a time period [0, T]. The extreme value of the process is defined as the largest maximum from a sequence of individual maxima. Let us assume that the drive train loads or the gear contact forces peak values are Y1, Y2, …, Y_N allocated over a discrete-time t_1, t_2, ….t_N in the interval [0, T]. N is the number of peak loads that have been observed. The distribution function for the extreme values of the process Y(t) can be written as:

$$M_N = \max(Y_1, Y_2, Y_3 \dots \dots . Y_N) \tag{6}$$

The probability of occurrence or the extreme value distribution function (Cumulative Density Function CDF) can be expressed as:

$$P(\eta) = \text{Prob}(Y_1 \leq \eta, Y_2 \leq \eta \dots . Y_N \leq \eta) \tag{7}$$

The time series of drive train loads like main shaft loads, bearing loads etc., are not stationary. This non-stationary set of data from the short-term condition is used to assess the extreme values using the ACER method.

The method's primary premise is that a series of non-parametric functions based on ACER functions of various orders are developed to approximate the extreme value distribution shown in Eq(1). With the time series of the peak gear contact forces analysed, the extreme value distribution can be written as:

$$P(M_N \leq \eta) = P_k(\eta) = \exp(-(N - k + 1)\varepsilon_k(\varepsilon)) \tag{8}$$

Where ε_k is known as the empirical ACER function with the order of k

An extrapolation strategy is used to anticipate the extreme value distribution when the η is considerably big. The tail of the ACER function is assumed in the same manner as exp{-a(η-b)c}

$$\varepsilon \approx q \times \exp(-a(\eta - b)^c) \quad (9)$$

Where a, b, c and q are constants which are dependent on the order k and q varies as per the Eq(8). The constants a,b,c and q can be determined by the Levenberg Marquardt Least square method. Naess et al.[20] and Chai et al. [21] have shown that the extrapolation method by this method provides extreme value accurately, and the time taken for this method was significantly less.

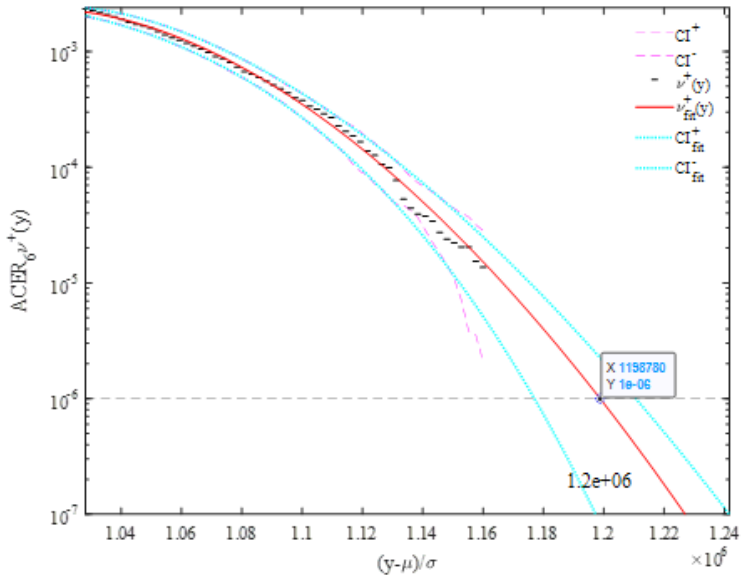

Figure 5: ACER function

2.6 Environment Condition & Load Cases

This thesis's wind and wave data is taken from the MARINA Platform project. The environmental data is obtained from Site 14, in the North Sea, located 30km from the shore, having a water depth from 100 to 202m which is suitable for floating wind turbines. The wind and wave data were developed from the hindcast model from 2001 to 2010 studied by Li et al. [22]. This location is selected due to the water depth and the high wind and wave power density

available at site 14. The environment conditions are determined based on wind and wave from the above site, and joint wind and wave distribution was established considering 1-hr mean wind speed at 10m above sea water level (U_{10}), significant wave height (H_S) and peak period (T_p)

$$f_{U10,Hs,Tp}(u, h, t) = f_{U10}(u) \cdot f_{Hs|U10}(h|u) \cdot f_{Tp|U10,Hs}(t|u, h) \quad (10)$$

Where $f_{U10,Hs,Tp}(u, h, t)$ is the marginal distribution of wind speed U_{10} above sea water level.

$f_{Hs|U10}(h|u)$: conditional distribution of peak period for the given wind speed U_{10}

$f_{Tp|U10,Hs}(t|u, h)$: conditional distribution of T_p for U_{10} and H_s.

This thesis selects the environmental conditions based on the significant wave height, peak period, and mean wind speed at 10m hub height. The most common wind speed profiles are logarithmic wind speed profile and power-law shown in Eq (11) and Eq (12), respectively, where wind speed profile is the variation of mean wind speed taken from a height H above the sea water level. More details of the wind speed profile can be obtained from the DNV guideline for environmental conditions and loads [23]

$$U(z) = \frac{u^*}{k_a} \ln \frac{z}{z_0} \quad (11)$$

Where $u^*$is the friction velocity, k_a is the von Karman's constant = 0.4, z is the height and z_0 is the terrain roughness factor. The terrain roughness factor can be obtained from table 2-1 from the DNV-RP-C205 recommendation practice. The roughness factor lies between 0.0001 and 0.01m for offshore areas. We can use power-law Eq (12) instead of logarithmic profile where α is the power-law coefficient which depends on the terrain roughness, and this is taken as 0.14 as per International Standard IEC 61400-3.

$$U(z) = U_H(\frac{z}{H})^{\alpha} \quad (12)$$

The load cases are selected to show the most common operating condition that an offshore wind turbine operates listed in Table 1. Wind speed speeds 8m/s is the cut-in, rated speed is 12m/s, and 16m/s is the above rated. Speeds below 8m/s are not considered as the wind turbine generally will not generate much power. Above 16m/s, the wind turbine blades pitch to maintain

the optimum power. The average wind speed analysed in this thesis is based on the operational conditions of the turbines. The average wind speed is different during rated speed and cut-out, and this increases by 4m/s.

Load cases	U_{Hub} (m/s)	T_I	H_s (m)	T_p (s)	Samples	Simulation length (s)
LC1	8	0.1740	1.9	9.7	20	4000
LC2	12	0.1460	2.5	10.1	20	4000
LC3	16	0.1320	3.2	10.7	20	4000

Table 1: Load cases for simulation

All the analyses run for a total of 4000 seconds. To account for the initial starting error impact commonly present during a turbine's start-up, the first 400 seconds of these simulations are ignored, which produces the correct estimate of extreme conditions. As a result, the extreme value is analysed using just 3600 seconds of data. Also, 20 seeds of wind data are used for each load case for the numerical analyses.

2.7 Available wind power

The power available in the wind through a wind turbine is the mass of airflow through the rotor disc area, and this is explained by J F Manwell et al. [24]

Kinetic energy per unit time or power in the wind is given by:

$$P = \frac{1}{2}\,\rho\, A\, U^3 \tag{13}$$

where A is the area of the rotor disc of diameter D, U is the airflow velocity

Also, wind power per unit is given by:

$$\frac{P}{A} = \frac{1}{2}\,\rho\, U^3 \tag{14}$$

The above Eq (13) and Eq (14) clearly show the reason for wind turbines moving offshore and becoming more significant in size. Constant unobstructed higher mean wind speed will increase the power captured threefold times, and an increase in rotor diameter will increase the power generated twice. Moving offshore helps engineers achieve both conditions, i.e. getting higher unobstructed wind speed and getting rid of space constraints to upscale the wind turbine rotor diameter.

Chapter 3 – System Description

3.1 Overview

We use a semi-submersible FOWT in this thesis and Paper 1 for global analysis based on Denmarks Tekniske Universitet (DTU) 10-MW RWT. The 10-MW bottom fixed monopile, 10-MW floating spar type and 10-MW semi-submersible wind turbine are used in Paper 2. Section 3.2 DTU 10-MW RWT describes the RWT and properties of the DTU 10-MW RWT. An overall description and properties of the floater and mooring lines are described in section 3.3 O-O Star Semi-Submersible. In section 3.4 10-MW Drive Train , we will look at the arrangement and configuration of the drivetrain model used in MBS for the response analysis of the gear meshing forces.

Figure 6: OO Star Floater [25]

3.2 DTU 10-MW RWT

The 10-MW RWT was developed as part of the Light Rotor project by DTU Wind Energy and Vestas Wind System. DTU developed the Light Rotor project to set a design platform for future wind turbine developments above 10-MW. Scaling the NREL 5-MW RWT[26], characterised by an efficient, lightweight rotor and a medium-speed drivetrain, yielded the DTU

10-MW RWT that serves as the drivetrain design in this work. The DTU 10-MW RWT [27] provided extensive details comparing aero-elastic aerodynamic tools. There was a need to compare the design results with a baseline, and a robust design DTU RWT was established.

Description	**Value**
Rating	10 MW
Rotor orientation, configuration	Upwind, 3 blades
Control	Variable speed, collective pitch
Drivetrain	Medium speed, Multiple stage gearbox
Rotor, Hub diameter	178.3m, 5.6m
Hub height	119m
Cut-in, Rated, Cut-out wind speed	4m/s, 11.4m/s, 25m/s
Cut-in, Rated rotor speed	6RPM, 9.6RPM
Rated tip speed	90m/s
Overhang, Shaft tilt, Pre-cone	7.07m, 5°, 2.5°
Pre-bend	3m
Rotor mass	229tons (each blade ~41tons)
Nacelle mass	446tons
Tower mass	605tons

Table 2: Design properties of DTU 10-MW RWT [27]

3.3 O-O Star Semi-Submersible

The DTU 10-MW RWT model is installed on the semi-submersible floater platform. The semi-submersible platform used is OO Star Wind Floater , designed and developed through the LIFES50+ project, which aimed to create the latest generation floaters for the FOWT. The floater was designed by Dr.techn. Olav Olsen AS [28] is a simple and robust design concept adaptable and scalable in all environments. The floater is made of hybrid concrete consisting of a central column supporting the wind turbine and tri-star-shaped pontoons that caters the stability and buoyancy. Suspended weights are added to the catenary mooring line to increase the tension in the station-keeping lines. These catenary mooring lines connected to the outer columns keep the floater in position during a rough sea state. Central and outer heave plates are installed below the pontoon to improve the heave response of the floater.

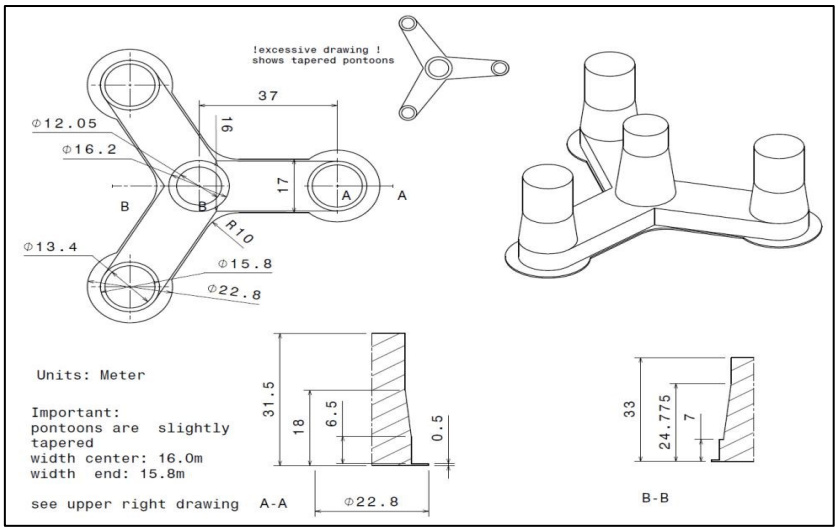

Figure 7: Dimension of OO Star Floater [29]

3.4 10-MW Drive Train

3.4.1 Overview

The drivetrain used in this thesis for studying the extreme loads on the gear contact forces is based on the DTU 10-MW RWT. Many studies on the dynamics of the wind turbine structure were done, but very few studies have been done on the future 10-MW wind turbine drive train. National Renewable Energy Laboratory (NREL) made a drive train model of 750-kW [30]. Xing et al.[9] studied the dynamic drivetrain analysis on a 750-kW spar-type floating wind turbine. Guo et al.[31] established the drivetrain model and studied the effects of moment and torque on the planetary gear inside the gearbox. Since 10-MW is the future wind turbine and medium-speed wind turbine has the advantage of low failure than high speed and less weight from the direct-drive Wang et al.[32] established10-MW drivetrain model multi-body simulation method and compared it with DTU for accuracy and fidelity.

3.4.2 Medium Speed 10-MW Drive train

The drive train is built to the international standard IEC 61400-4 [33]. The gearbox model used in this thesis is a four-point support configuration model with two supports on the main shaft bearing and two torque arms. The gearbox consisted of three stages, two planetary stage helical gears and one parallel stage helical gears. The 10-MW drivetrain gearbox is modelled

in a multi-body system (MBS) and is shown in Figure 8. The configuration of the main bearing is based on the research done by Torsvik et al.[34] who studied the design and operations of the main bearing on FOWT larger than 10-MW. The first stage planetary gear has five planet gears meshing, and the second stage planetary gear consists of three planet gears meshing. The third parallel stage gear is the high-speed gear connected to the generator shaft. Figure 9 shows the general arrangement of medium-speed gear with the main shaft bearing INP A and INP B

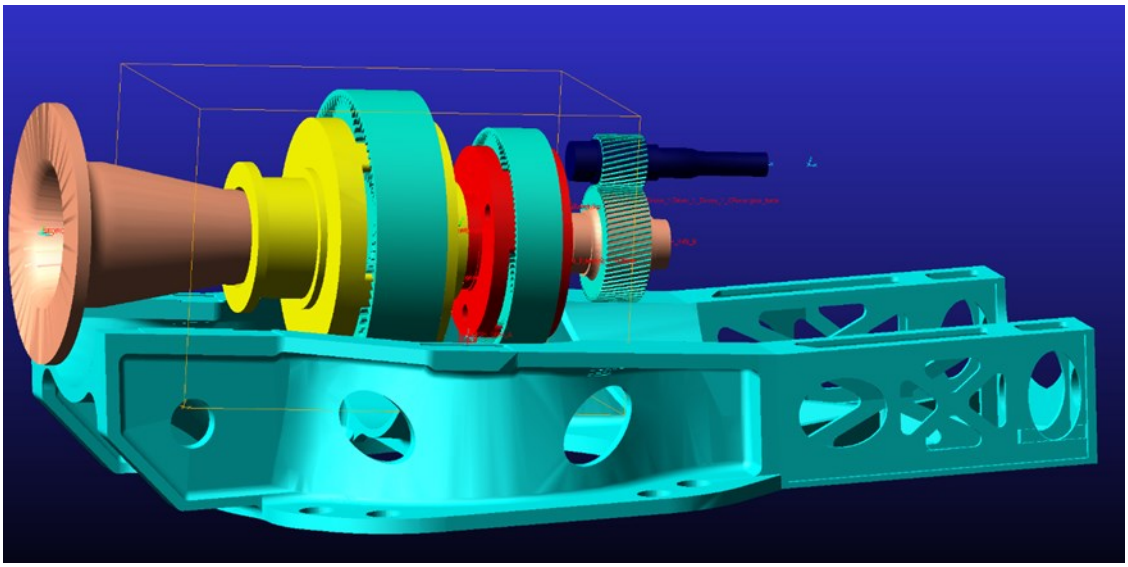

Figure 8: Multi-body system (MBS) model of 10-MW drive train

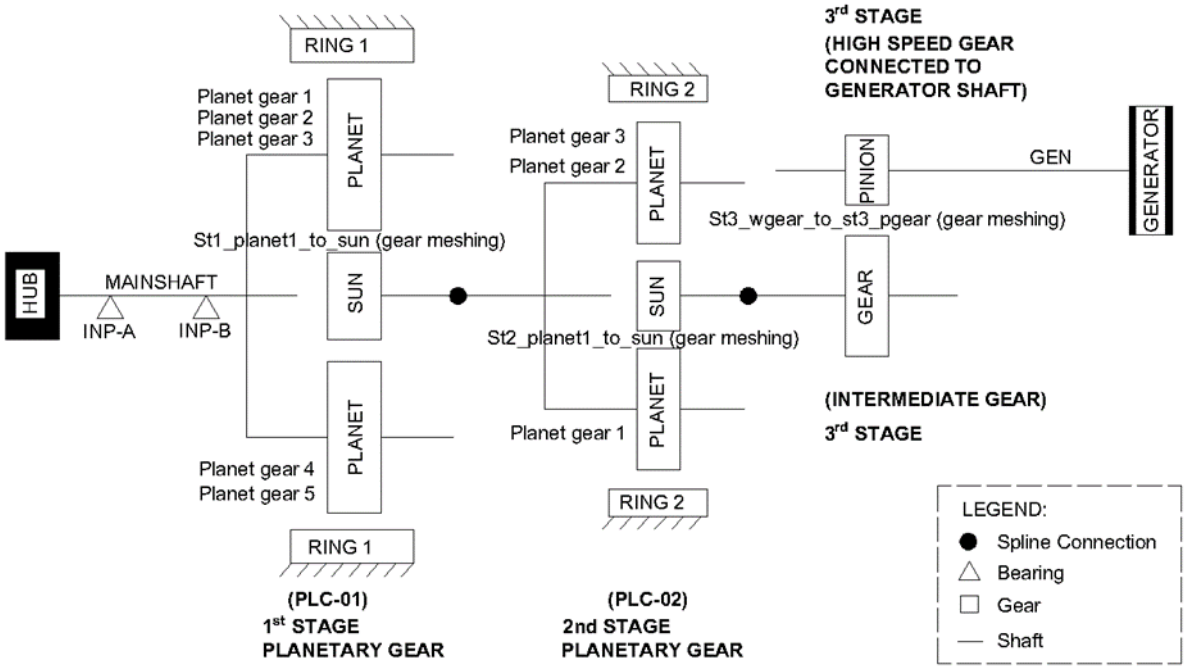

Figure 9: Schematic diagram of 10-MW turbine drivetrain

The quality and consistency of the numerical model established in MBS and the natural frequency compared with the DTU 10-MW RWT. Since the responses generated from the 10-MW model and natural frequencies match with the DTU model, this high-fidelity numerical model suit well in this thesis.

3.4 Response Variables

In this thesis, for estimating the extreme load responses in the drivetrain using ACER and comparing the results with the Gumbel method, the following measurement points are considered: Forces on the main shaft bearing A in the x-direction (INP A Fx), force on the main shaft bearing A in the y-direction (INP A Fy), force on the main shaft bearing A in the z-direction (INP A Fz), Forces on the main shaft bearing B in the x-direction (INP B Fx), force on the main shaft bearing B in the y-direction (INP B Fy), force on the main shaft bearing B in the z-direction (INPB Fz), the gear pair meshing force between stage 1 planet gear one and sun gear (st1_planet_to_st1 _sun), the gear pair meshing force between stage2 planet gear one and stage 2 sun gear(st2_planet1_to_sun) and gear pair meshing force between stage 3 intermediate gear and stage 3 high-speed pinion gear (st3_wgear_to_st3_pgear). We consider these variables because of the following reason:

- Sun gear has the highest tooth pitting fatigue damage caused by high tooth contact stresses.
- Pinion gear undergoes high tooth bending and pitting fatigue damage.
- Bearing INP-A observe the most serious bearing fatigue damage

These are reasons are based on the study conducted by S.Wang et al. [32] and Niemann G et al. [35]

Chapter 4 – Results & Response Analysis

We use the ACER and Gumbel methods to estimate the extreme value responses and compare the results. We neglect the first 400 seconds of observation during the analysis to cater to the turbine's sudden changes in magnitude or torque during the start-up process.

4.1 Acer Vs Gumbel Drive train

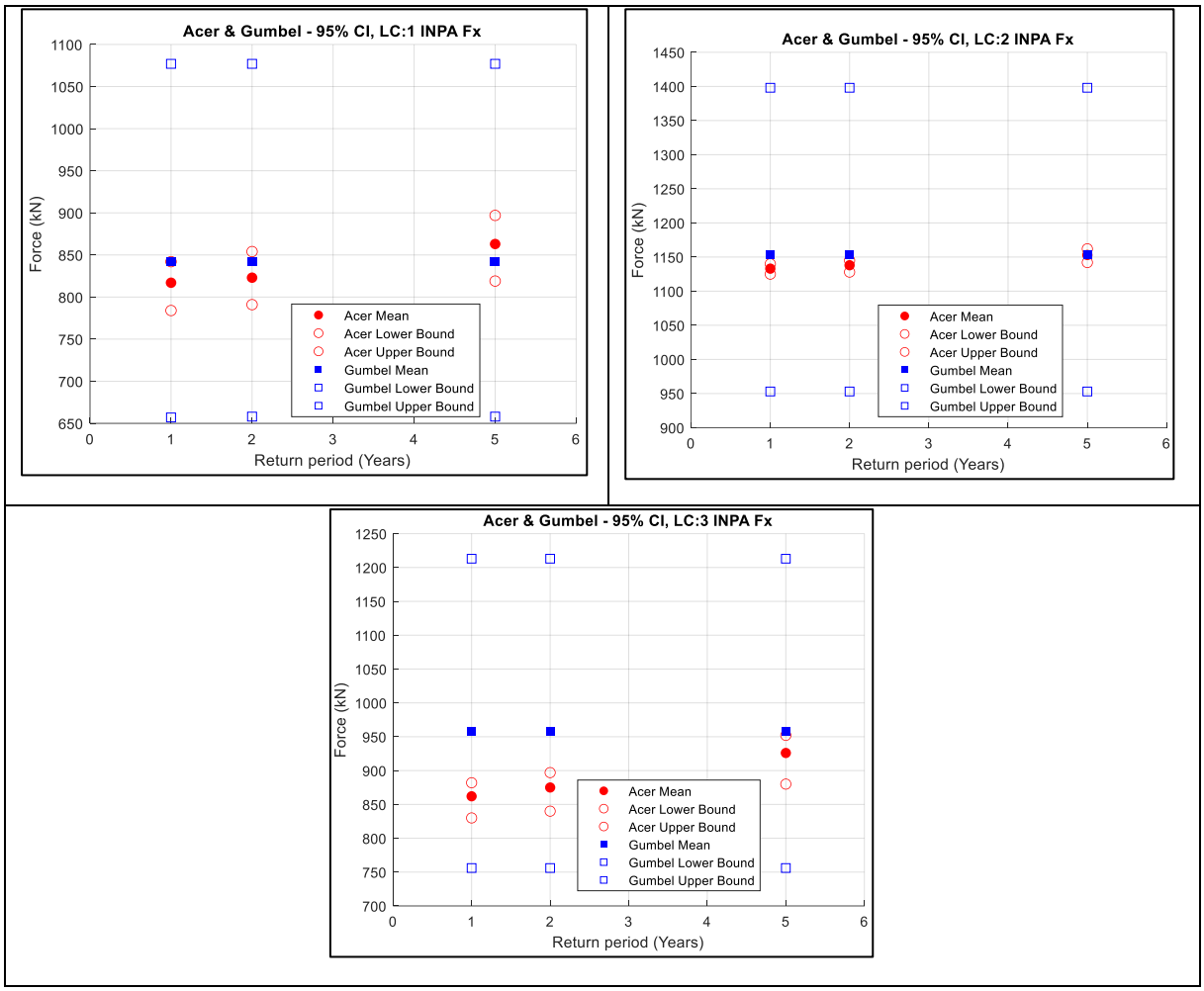

Figure 10: INPA_Fx Force. ACER and Gumbel with 95 % CI; Top-left: LC1 Vhub = 8 m/s; Top-right: LC2 Vhub = 12 m/s; Bottom: LC3 Vhub = 16 m/s

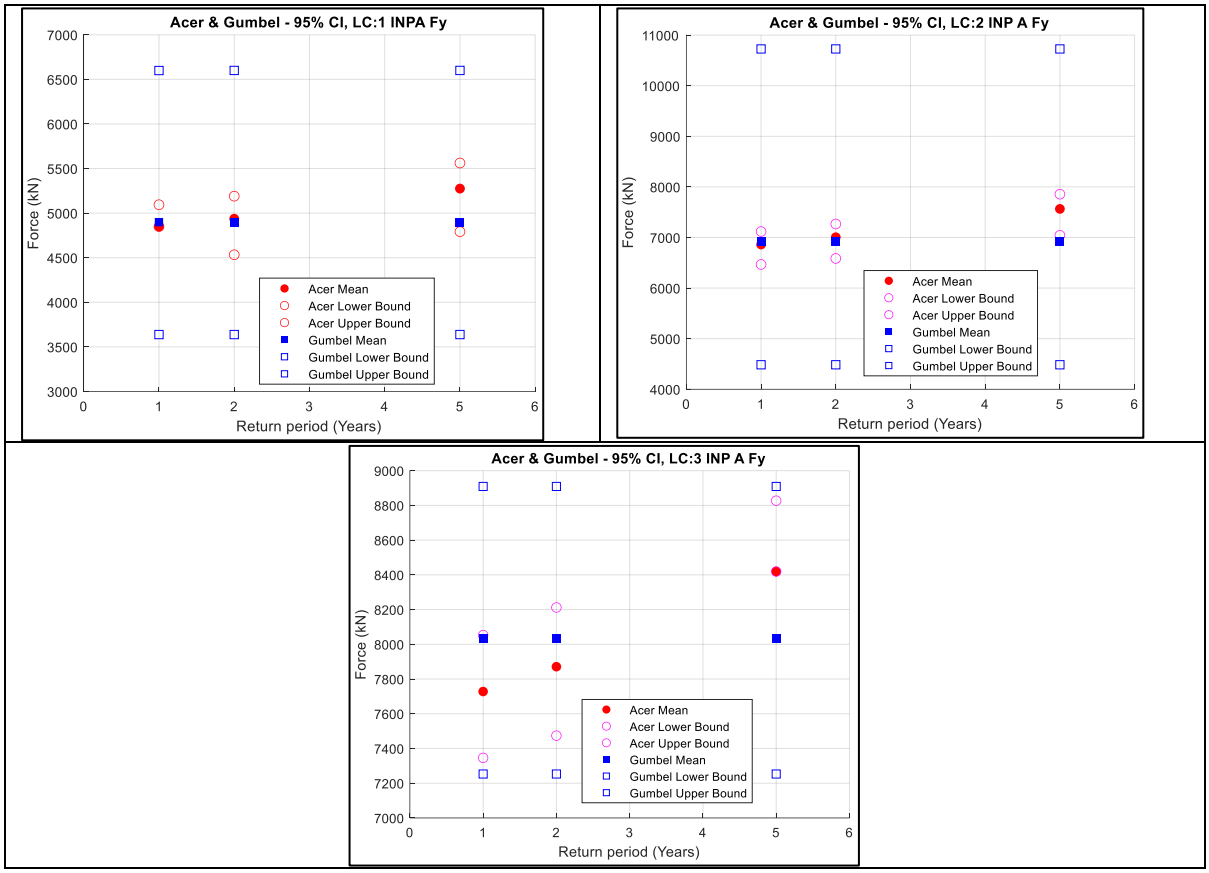

Figure 11 INPA_Fy Force. ACER and Gumbel with 95 % CI; Top-left:LC1 Vhub = 8 m/s; Top-right: LC2, Vhub = 12 m/s; Bottom: LC3, Vhub = 16 m/s

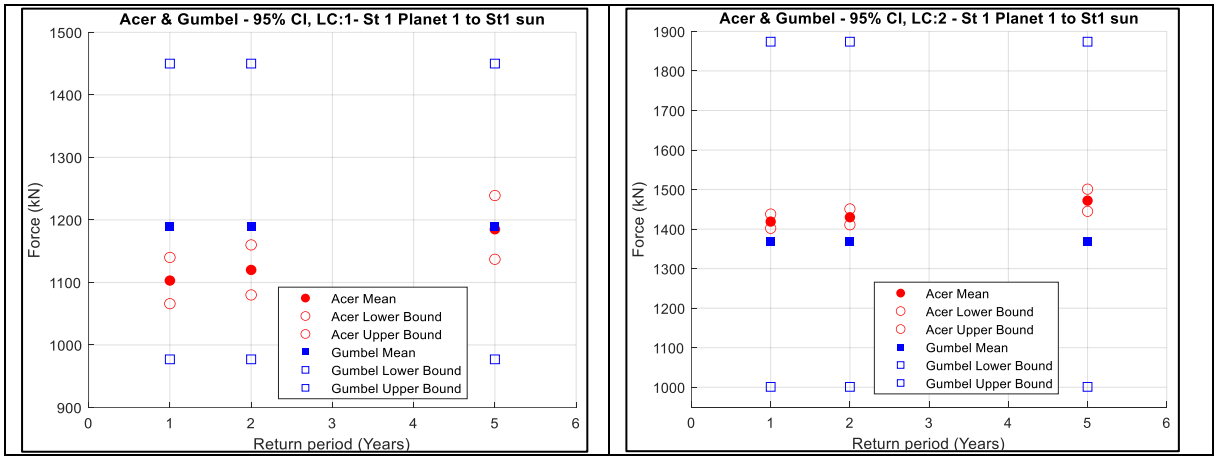

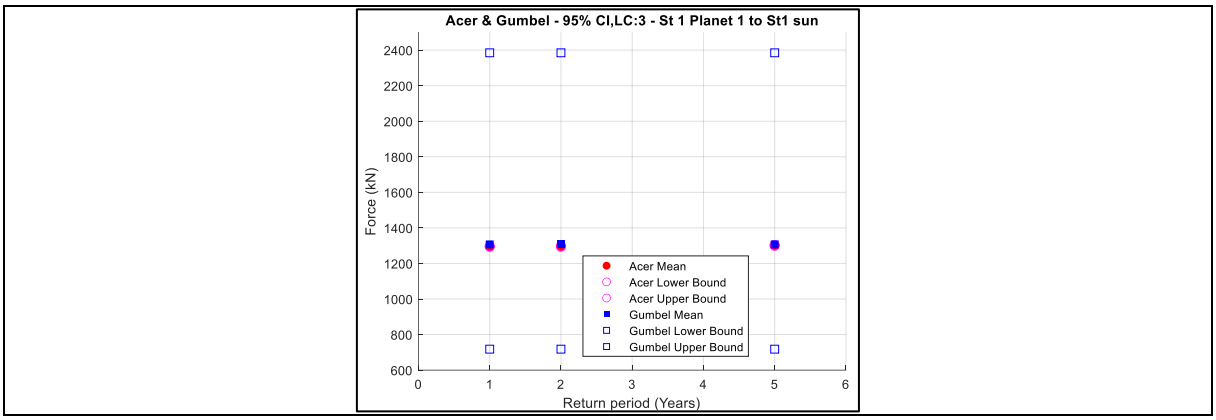

Figure 12 Stage 1 planet 1 to stage 1 sun gear meshing force. ACER and Gumbel with 95 % CI; Top-left:LC1 Vhub = 8 m/s; Top-right: LC2, Vhub = 12 m/s; Bottom: LC3, Vhub = 16 m/s

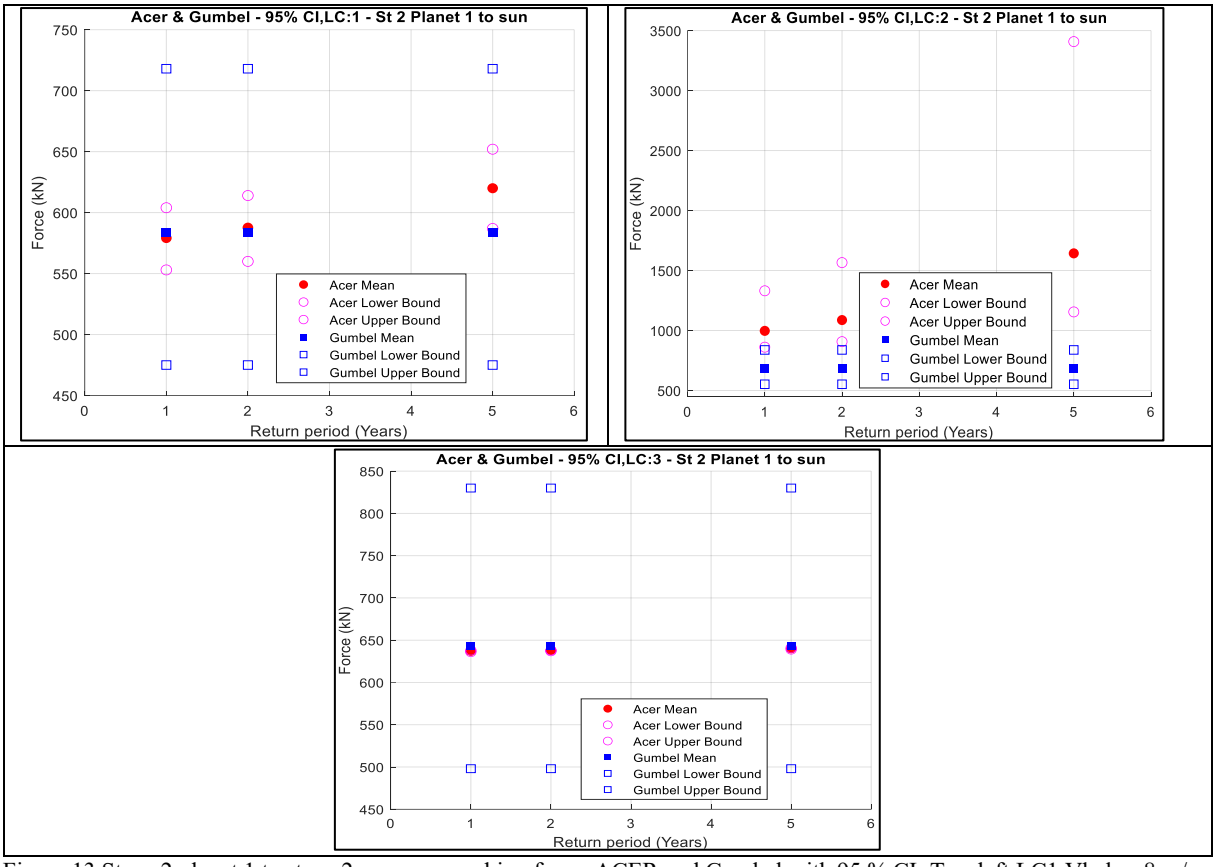

Figure 13 Stage 2 planet 1 to stage 2 sun gear meshing force. ACER and Gumbel with 95 % CI; Top-left:LC1 Vhub = 8 m/s; Top-right: LC2, Vhub = 12 m/s; Bottom: LC3, Vhub = 16 m/s

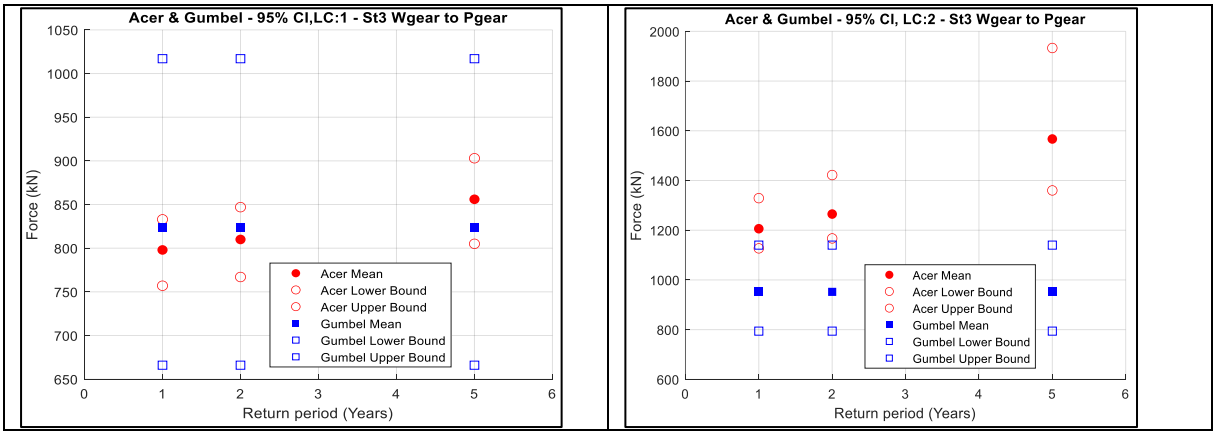

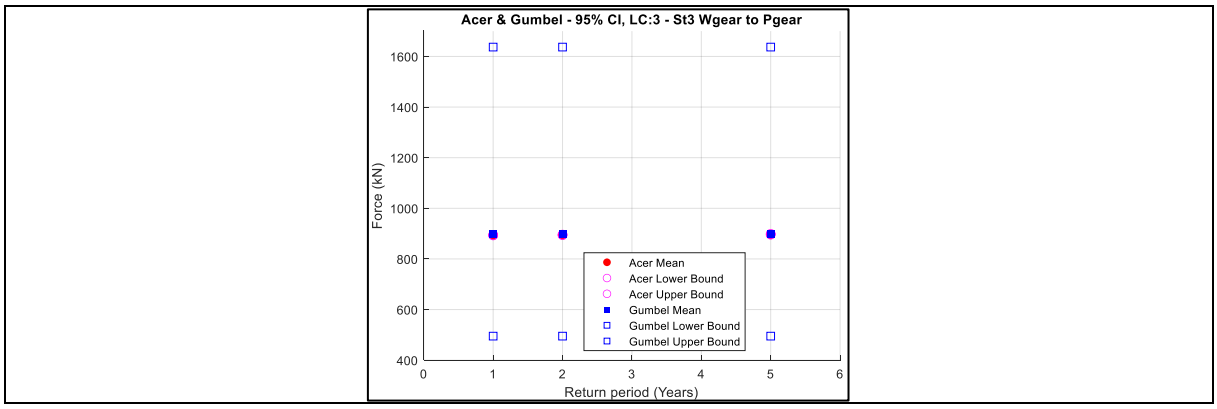

Figure 14 Stage 3 Wgear to high speed pinion gear meshing force. ACER and Gumbel with 95 % CI; Top-left:LC1 Vhub = 8 m/s; Top-right: LC2, Vhub = 12 m/s; Bottom: LC3, Vhub = 16 m/s

In comparing ACER and the widely approved Gumbel method in Figure 10 to Figure 14, the ACER method gives a smaller 95 % confidence interval. The confidence interval range of ACER is narrower than the values estimated by the Gumbel method, which tells that ACER is more accurate. The ACER mean value representing the extreme value response gradually increases as the return period increases. The extreme values obtained through the Gumbel method for the 10-MW wind turbine drive train are almost similar, which means the Gumbel distribution will not suit the extreme responses adequately.

4.2 Power Spectral Density

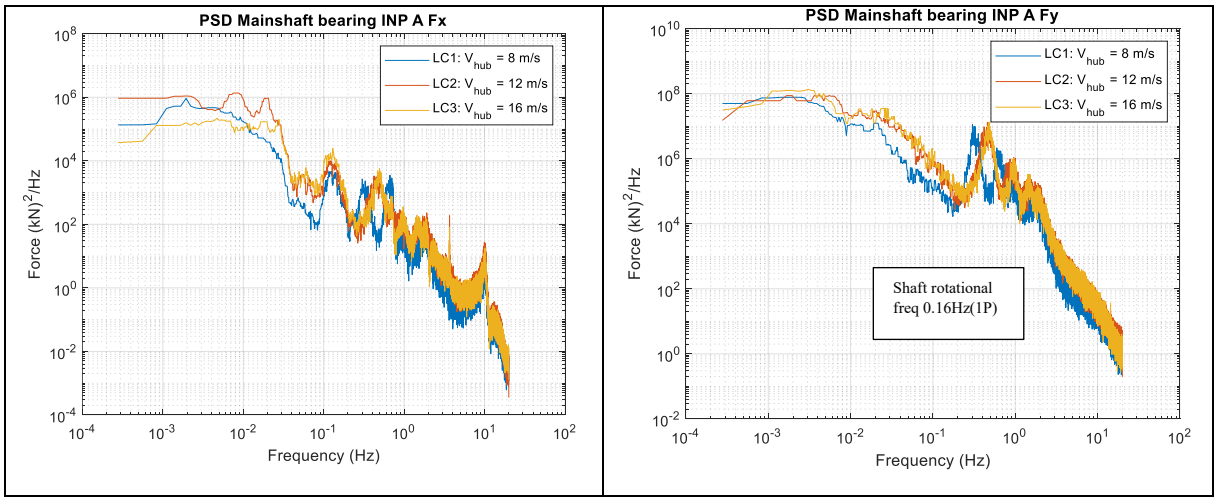

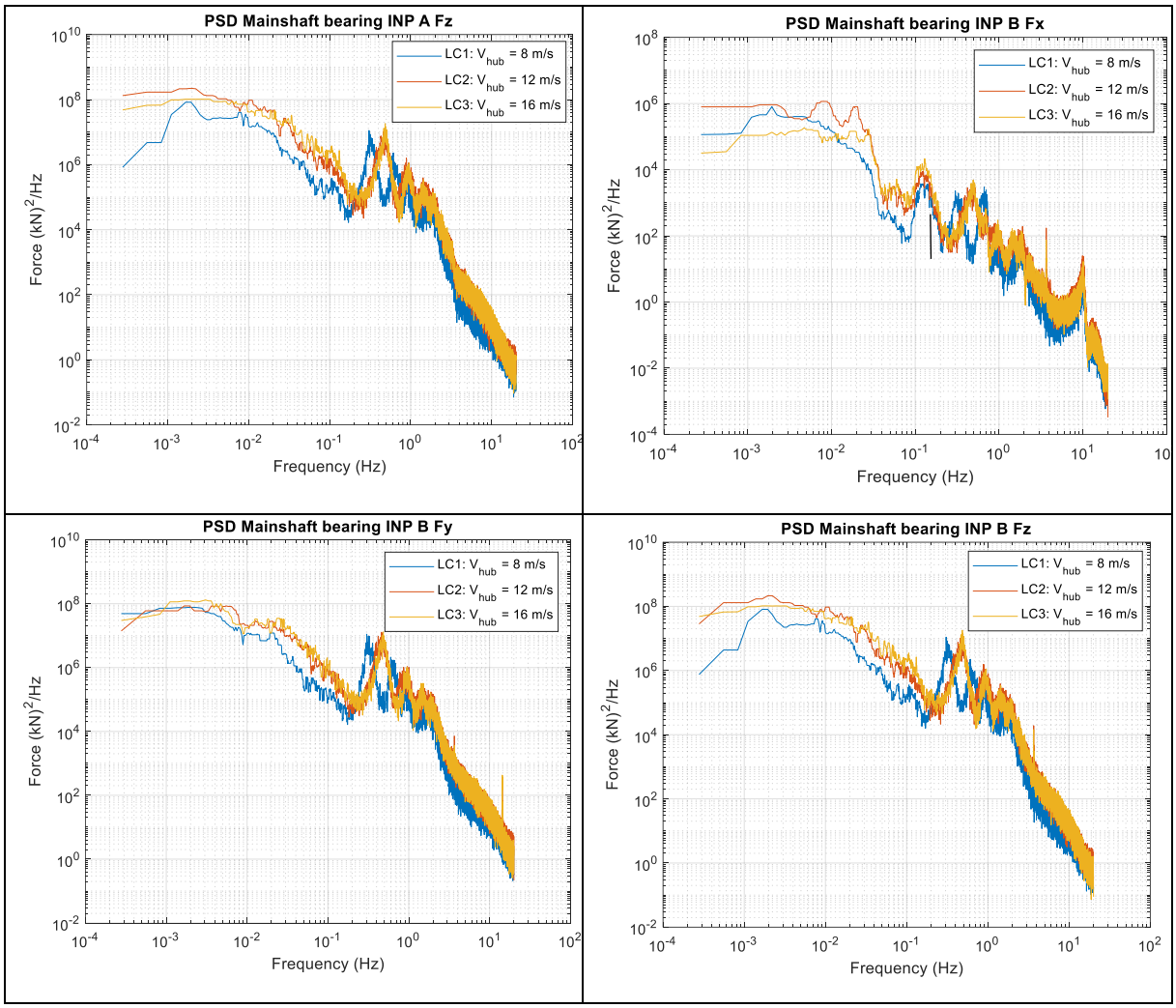

Figure 15: Power spectral density (PSD) of main shaft bearing

The main bearing INP A and INP B components in different directions (Fx, Fy, Fz) are outside the gearbox and near the rotor. The rotor is connected to the main shaft and supported on the two main bearings. The response on the main bearing excitation is from the wind loads because the aerodynamic loads produced by the rotor will be applied to the shaft. The load will be transferred to the main bearing as the shaft is supported on the main bearing. So it is highly possible that the response of the main bearing (INP A and INP B) shown in Figure 15 is caused by the aerodynamic loads. It is likely that the peak values are caused corresponding to aerodynamic loads because aerodynamic loads are not constant loads with different frequencies affected by turbulences, thereby making them dynamic. Figure 15 shows the drive train response caused by the load excitation. From Figure 15 and Figure 16, it is evident that most of the peaks are located at different frequencies. This means that the peaks are caused by external

excitation because the drive train model is the same for the three load cases, and the only difference is the wind speed.

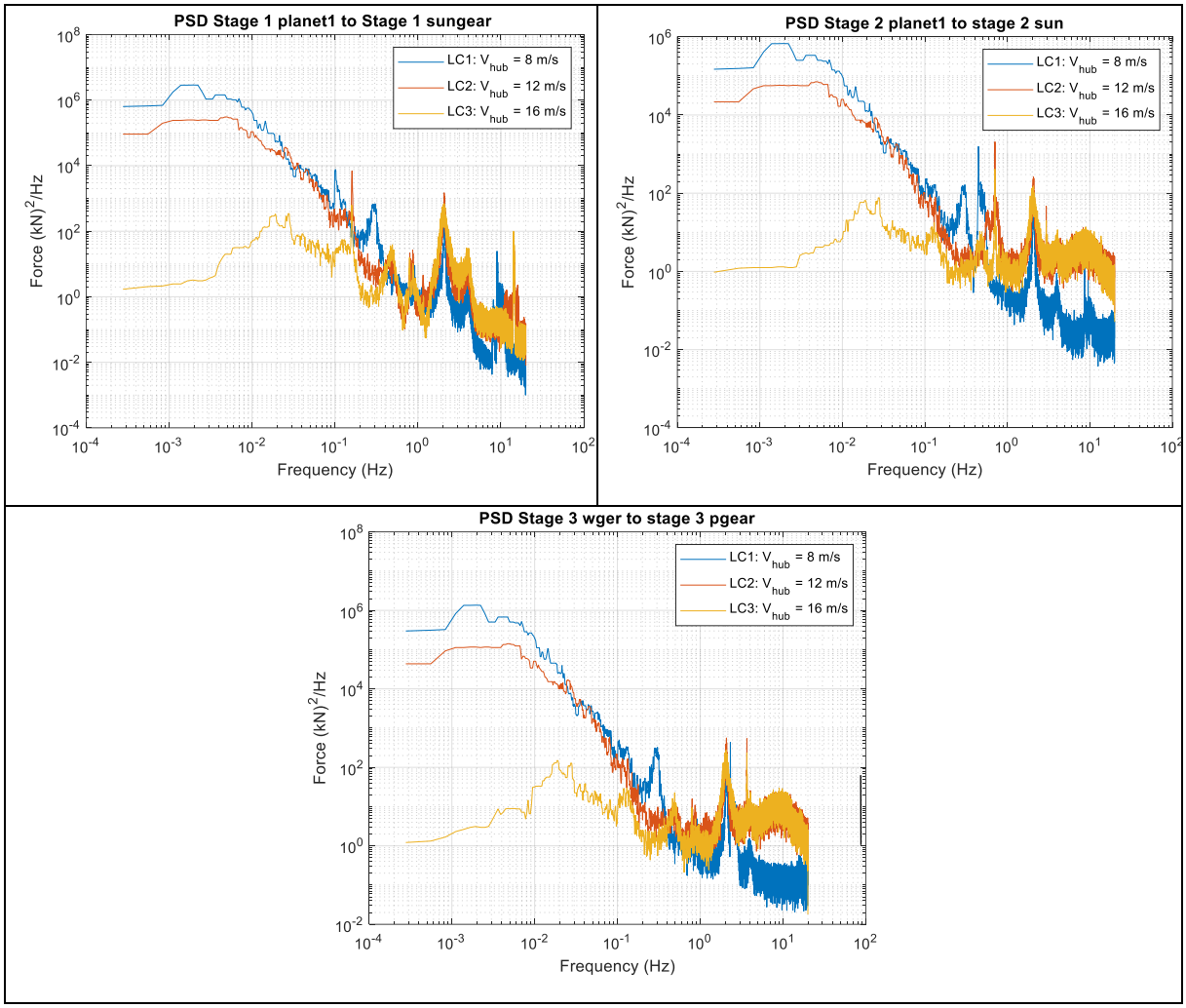

Figure 16: Power spectral density (PSD) of the response of gears in different load cases

The shaft-rotational frequency will also have some effect on the bearing response. But the difference in peak value is observed, which can also be due to aerodynamic load. Also, for the wind speed of 8m/s (LC1), our turbine is not rated wind speed. The shaft frequency will lie below 0.16Hz. But for the environmental condition of 12m/s(LC2) and 16m/s (LC3) corresponding to rated and above-rated conditions because of the wind turbine controller, we will see the same shaft rotating speed. That means the frequency for the case LC2 and LC3 will be more consistent than the LC1 because LC1 is not rated, and there will be a small difference in frequencies. The aerodynamic loads also affect the gearbox, shown by low-frequency peak values in Figure 16. This is because the torque values from the rotating shaft will get transferred inside the gearbox. So the gearbox is also affected by the aerodynamic loads

4.3 Solution of k-value

Load Case	q value :	1E-6		
	k value :	2.00	4.00	6.00
LC 1, V_{hub} = 8 m/s	INPA_Fx (kN)	992	977	977
	INPA_Fy (kN)	6,167	6,292	6,335
	INP A _Fz (kN)	3,451	3,454	3,422
	INP B_Fx (kN)	813	806	809
	INP B_Fy (kN)	6,866	7,022	6,890
	INP B_Fz (kN)	7,959	8,063	7,907
	st1_planet_to_st1 _sun (kN)	1,404	1,420	1,371
	st2_planet1_to_sun (kN)	739	712	716
	st3_wgear_to_st3_pgear (kN)	1,142	1,045	988
LC 2, V_{hub} = 12 m/s	INPA_Fx (kN)	1,204	1,196	1,199
	INPA_Fy (kN)	9,092	9,119	9,384
	INP A _Fz (kN)	7,962	7,758	8,009
	INP B_Fx (kN)	1,010	1,007	1,004
	INP B_Fy (kN)	10,135	9,912	9,895
	INP B_Fz (kN)	11,466	11,515	11,979
	st1_planet_to_st1 _sun (kN)	1,236	1,246	1,249
	st2_planet1_to_sun (kN)	9,144	8,334	9,228
	st3_wgear_to_st3_pgear (kN)	865	847	841
LC 3 , V_{hub} = 16 m/s	INPA_Fx (kN)	1,111	1,099	1,095
	INPA_Fy (kN)	9,981	9,971	10,128
	INP A _Fz (kN)	9,062	9,052	8,740
	INP B_Fx (kN)	922	913	906
	INP B_Fy (kN)	10,237	10,386	10,587
	INP B_Fz (kN)	10,237	10,386	10,600
	st1_planet_to_st1 _sun (kN)	1,313	1,317	1,316
	st2_planet1_to_sun (kN)	646	647	648
	st3_wgear_to_st3_pgear (kN)	905	906	906

Table 3: Extreme values using ACER with different degrees of conditioning

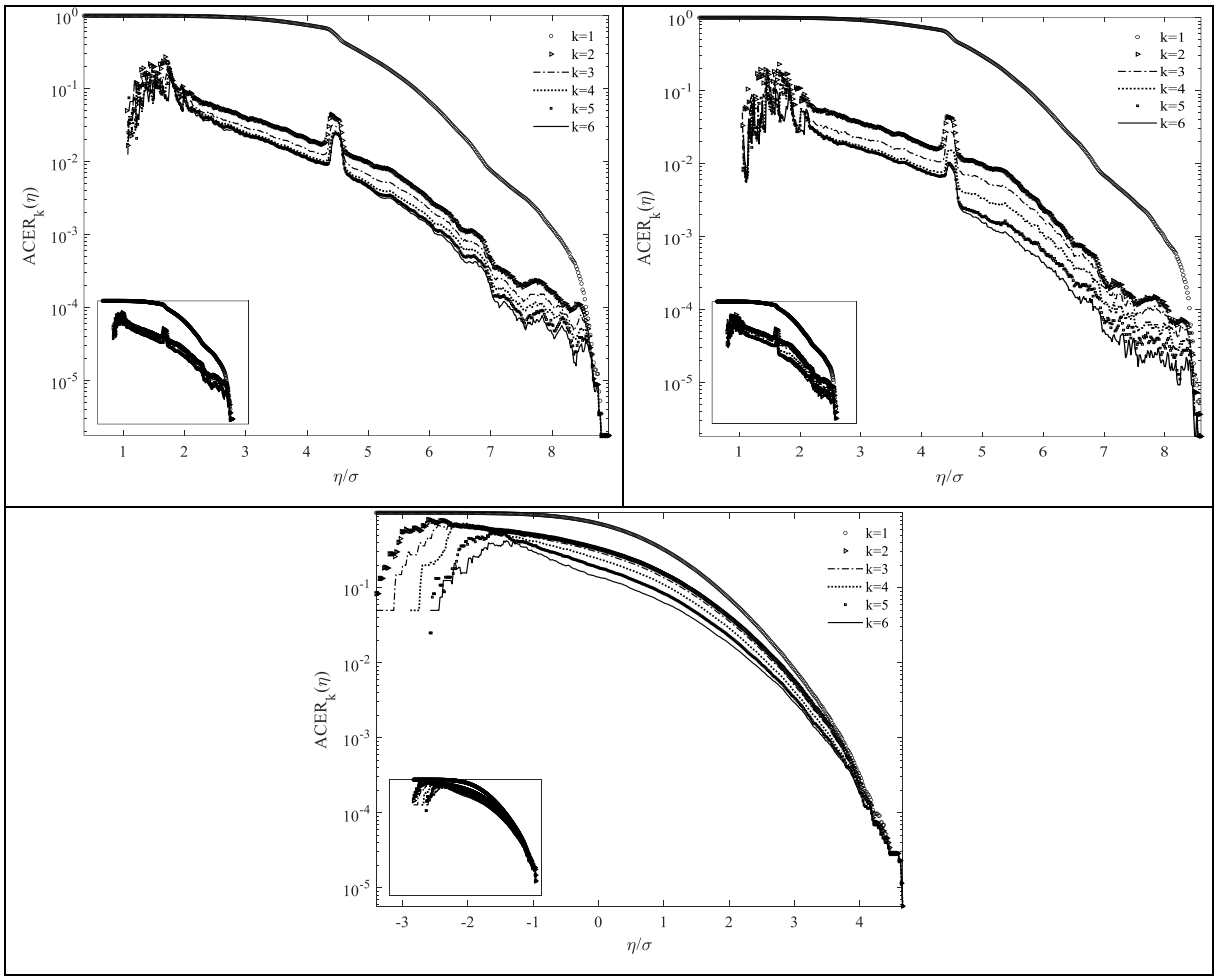

Figure 17: Acer function for k = 1 : 6, q=1e-6. Top left: LC1 st1_planet_to_st1 _sun; Top Right: st2_planet1_to_sun (kN); Bottom : LC2 INP B Fy

The different k values are analysed in Table 3 concerning a q value of 10^{-6}. It shows extreme values calculated using the ACER method are robust, accurate and don't vary significantly for different values of k. Figure 17 shows that the k value tends to meet or merge for a value greater than two, and hence we select k=6 in this thesis. However, k=1 tends to provide an incorrect result, which is also the same case in the attached Paper 1.

Chapter 5 – Conclusion & Discussion

This thesis focused on the extreme response of a 10-MW wind turbine drivetrain using ACER and Gumbel methods. The drivetrains main shaft bearings forces, gear meshing forces on the planetary gear system stage 1 and stage 2 gears and gear meshing forces on the 3rd stage parallel gears are studied for the three operating environmental conditions of underrated wind speed, rated wind speed and above rated wind speed.

The extreme values calculated using Gumbel for the different load cases and return periods are almost similar due to the sharp incline at the upper tail end. Gumbel method is not a good tool for estimating the extreme response in the 10-MW wind turbine drive train compared to ACER. This can also be due to the insufficient size of the extreme value to fit the Gumbel distribution. In contrast, the ACER technique is much more precise and follows the exact shape of the data that is being analysed.

ACER technique is used in Paper 1 to determine the root flap-wise bending moments, main shaft tip up-down bending moment and tower bottom fore-aft bending moment of 10-MW FOWT. The paper also showed the accuracy and performance of ACER in estimating the extreme response in the upper tail region and emphasised the importance of the extrapolation method in determining the ULS loads. The paper also suggests that using different k values will not influence ACER results except when k tends to be 1, which is similar to the case in this thesis.

In Paper 2, the power performance and extreme load response of a 10-MW offshore wind turbine with different floater configurations are analysed using ACER and Gumbel method. It can be seen that the Gumbel method overpredicted responses when compared to the ACER method. On estimating the loads on the three different turbine configurations, the spar wind turbine experienced high tower bending moments due to the platform pitch motion during LC1, LC2 and LC3 load cases compared to semi-submersible and monopile. The return period calculated for five years is approximately 1.3 times higher. Therefore, it is essential to estimate the accurate extreme values and use the appropriate factor of safety values during the design stage.

The ACER method estimated the extreme aerodynamic loads transmitted to the 10-MW wind turbine gearbox model more accurately than the Gumbel method. It is vital to evaluate accurate extreme load response based on the environment load condition and the operating region. Accurate prediction of load response is essential in Ultimate Limit State, which provides a base for the selection of different factors of safety and design parameters. ACER will act as a novel method for estimating extreme loads in the 10-MW FOWT drivetrain and will help guide future research on large wind offshore turbines and reduce the knowledge gap.

We plotted 20 seeds simulation, and if we analyse the maximum value, there will be a variation because when we generate wind and waves that are random or stochastic data. Even though they have the same amplitude and frequency, they don't have the same phase for the wave and wind elevation, which cause different responses. We get only one maximum value if we do a single seed simulation. But if we do two seed simulations, we make an average value. The variation in the average maximum value will reduce if we make more seed simulations. It will be interesting to see how many seeds are required to achieve the accuracy of the response. If we do more simulation, it will take more simulation time, but if we do limited simulation, it will have some stochastic variation in the response. Identifying the most suitable number of simulations for analysis would be good to achieve an accurate response. If we make five seed simulations and find the average value difference minimal compared to the twenty seed simulations, we can recommend a way to use the five seed simulation to obtain the average load and save a lot of simulation time

O.Karpa et al.[36] used Monte Carlo simulation to determine the performance of ACER and Gumbel distribution by generating 100-yr data points showing that ACER results are better than Gumbel. The ACER method is applicable not only for the stationary time series but also for non-stationary time series with regard to some limitations. It has been studied and shown by Naess et al. [37] that ACER can't foresee long-term trends outside the data. For example, the ACER method cannot estimate the long-term response past the data available from the model. But more than the cons ACER has more advantages in estimating the extreme load responses in 10-MW wind turbine drivetrain gear box.

References

[1] "GWEC | GLOBAL WIND REPORT 2022." Accessed: May 11, 2022. [Online]. Available: https://gwec.net/wp-content/uploads/2022/03/GWEC-GLOBAL-WIND-REPORT-2022.pdf

[2] M. Shields, P. Beiter, J. Nunemaker, A. Cooperman, and P. Duffy, "Impacts of turbine and plant upsizing on the levelized cost of energy for offshore wind," *Applied Energy*, vol. 298, Sep. 2021, doi: 10.1016/J.APENERGY.2021.117189.

[3] M. Bilgili, A. Yasar, and E. Simsek, "Offshore wind power development in Europe and its comparison with onshore counterpart," *Renewable and Sustainable Energy Reviews*, vol. 15, no. 2, pp. 905–915, Feb. 2011, doi: 10.1016/J.RSER.2010.11.006.

[4] W. Musial *et al.*, "Offshore Wind Market Report: 2021 Edition," 2021.

[5] J. Keller, S. Sheng, Y. Guo, B. Gould, and A. Greco, "Wind Turbine Drivetrain Reliability and Wind Plant Operations and Maintenance Research and Development Opportunities," 2021. [Online]. Available: www.nrel.gov/publications.

[6] S. Sheng and W. Yang, "Wind Turbine Drivetrain Condition Monitoring - An Overview (Presentation), NREL (National Renewable Energy Laboratory)," 2013.

[7] K. Xu, M. Zhang, Y. Shao, Z. Gao, and T. Moan, "Effect of wave nonlinearity on fatigue damage and extreme responses of a semi-submersible floating wind turbine," *Applied Ocean Research*, vol. 91, Oct. 2019, doi: 10.1016/j.apor.2019.101879.

[8] Y. Xing and T. Moan, "Multi-body modelling and analysis of a planet carrier in a wind turbine gearbox," *Wind Energy*, vol. 16, no. 7, pp. 1067–1089, Oct. 2013, doi: 10.1002/WE.1540.

[9] Y. Xing, M. Karimirad, and T. Moan, "Modelling and analysis of floating spar-type wind turbine drivetrain," *Wind Energy*, vol. 17, no. 4, pp. 565–587, 2014, doi: 10.1002/we.1590.

[10] S. Wang, A. R. Nejad, and T. Moan, "Design and Dynamic Analysis of a Compact 10 MW Medium Speed Gearbox for Offshore Wind Turbines," *Journal of Offshore Mechanics and Arctic Engineering*, vol. 143, no. 3, Oct. 2020, doi: 10.1115/1.4048608.

[11] S. Wang, A. Nejad, E. E. Bachynski, and T. Moan, "A comparative study on the dynamic behaviour of 10 MW conventional and compact gearboxes for offshore wind turbines," *Wind Energy*, vol. 24, no. 7, pp. 770–789, Jul. 2021, doi: https://doi.org/10.1002/we.2602.

[12] "IEC TS 61400-3-2:2019 - Wind energy generation systems - Part 3-2: Design requirements for floating." https://standards.iteh.ai/catalog/standards/iec/b79529ca-da46-42d2-9b72-f8ea4a02882c/iec-ts-61400-3-2-2019 (accessed May 21, 2022).

[13] A. Naess, O. Gaidai, and O. Karpa, "Estimation of extreme values by the average conditional exceedance rate method," *Journal of Probability and Statistics*, 2013, doi: 10.1155/2013/797014.

[14] X. Xu, O. Gaidai, A. Naess, and P. Sahoo, “Extreme loads analysis of a site-specific semi-submersible type wind turbine,” *Ships and Offshore Structures*, vol. 15, no. S1, pp. S46–S54, 2021, doi: 10.1080/17445302.2020.1733315.

[15] Z. Cheng, H. A. Madsen, W. Chai, Z. Gao, and T. Moan, “A comparison of extreme structural responses and fatigue damage of semi-submersible type floating horizontal and vertical axis wind turbines,” *Renewable Energy*, vol. 108, pp. 207–219, 2017, doi: 10.1016/J.RENENE.2017.02.067.

[16] “FAST | Wind Research | NREL.” https://www.nrel.gov/wind/nwtc/fast.html (accessed May 22, 2022).

[17] “Marine operations and mooring analysis software | Sima.” https://www.dnv.com/services/marine-operations-and-mooring-analysis-software-sima-2324 (accessed May 23, 2022).

[18] “Simpack MBS Software | Dassault Systèmes.” https://www.3ds.com/products-services/simulia/products/simpack/ (accessed May 23, 2022).

[19] Translated and revised by Bernt J. Leira, *STOCHASTIC THEORY OF SEALOADS, PROBABILISTIC MODELLING AND ESTIMATION*, vol. KompendiumUK-2010-72. MARINE TECHNOLOGY CENTRE DEPARTMENT OF MARINE TECHNOLOGY TRONDHEIM, NORWAY & NORGES TEKNISK-NATURVITENSKAPELIGE UNIVERSITE, 2019.

[20] A. Naess, O. Gaidai, and P. S. Teigen, “Extreme response prediction for nonlinear floating offshore structures by Monte Carlo simulation,” *Applied Ocean Research*, vol. 29, no. 4, pp. 221–230, Nov. 2007, doi: 10.1016/J.APOR.2007.12.001.

[21] W. Chai, A. Naess, B. J. Leira, and G. Bulian, “Efficient Monte Carlo simulation and Grim effective wave model for predicting the extreme response of a vessel rolling in random head seas,” *Ocean Engineering*, vol. 123, pp. 191–203, Sep. 2016, doi: 10.1016/J.OCEANENG.2016.07.025.

[22] L. Li, Z. Gao, and T. Moan, “Joint Environmental Data at Five European Offshore Sites for Design of Combined Wind and Wave Energy Devices,” *Proceedings of the International Conference on Offshore Mechanics and Arctic Engineering - OMAE*, vol. 8, Nov. 2013, doi: 10.1115/OMAE2013-10156.

[23] D. Norske Veritas, “RECOMMENDED PRACTICE DET NORSKE VERITAS AS Environmental Conditions and Environmental Loads,” 2014, Accessed: May 27, 2022. [Online]. Available: www.dnvgl.com.

[24] J. F. Manwell, J. G. Mcgowan, and A. L. Rogers, *WIND ENERGY EXPLAINED Wind Energy Explained: Theory, Design and Application, Second Edition*. 2009. [Online]. Available: www.wiley.com.

[25] W. S. ; Yu, K. ; Müller, and F. ; Lemmer, “State-of-the-art model for the LIFES50+ OO-Star Wind Floater Semi 10MW floating wind turbine,” *Journal of Physics: Conference Series*, vol. 1104, no. 1, p. 12024, 2018, doi: 10.1088/1742-6596/1104/1/012024.

[26] J. Jonkman, S. Butterfield, W. Musial, and G. Scott, “Definition of a 5-MW Reference Wind Turbine for Offshore System Development,” 2009, Accessed: May 24, 2022. [Online]. Available: http://www.osti.gov/bridge

[27] C. ; Bak *et al.*, “General rights The DTU 10-MW Reference Wind Turbine). The DTU 10-MW Reference Wind Turbine. Sound/Visual production (digital),” 2013.

[28] “Dr.techn.Olav Olsen AS Archives - Lifes50+.” https://lifes50plus.eu/tag/dr-techn-olav-olsen-as/ (accessed May 25, 2022).

[29] W. Yu *et al.*, “LIFES50+ D4. 2: Public definition of the two LIFES50+ 10 MW floater 510 concepts. The University of Stuttgart,” 2017.

[30] F. Oyague, “Gearbox Reliability Collaborative (GRC) Description and Loading,” 2011, Accessed: May 26, 2022. [Online]. Available: http://www.osti.gov/bridge

[31] Y. Guo, J. Keller, W. Lacava, Y. Guo, J. Keller, and W. Lacava, “Combined Effects of Gravity, Bending Moment, Bearing Clearance, and Input Torque on Wind Turbine Planetary Gear Load Sharing Preprint Combined Effects of Gravity, Bending Moment, Bearing Clearance, and Input Torque on Wind Turbine Planetary Gear Load Sharing,” 2012, Accessed: May 26, 2022. [Online]. Available: http://www.osti.gov/bridge

[32] S. Wang, A. R. Nejad, and T. Moan, “On design, modelling, and analysis of a 10-MW medium-speed drivetrain for offshore wind turbines,” *Wind Energy*, vol. 23, no. 4, pp. 1099–1117, Apr. 2020, doi: 10.1002/WE.2476.

[33] Iec, “IEC 61400-4 INTERNATIONAL STANDARD Wind turbines-Part 4: Design requirements for wind turbine gearboxes,” 2012.

[34] J. Torsvik, A. R. Nejad, and E. Pedersen, “Main bearings in large offshore wind turbines: development trends, design and analysis requirements,” *Journal of Physics: Conference Series*, vol. 1037, p. 042020, Jun. 2018, doi: 10.1088/1742-6596/1037/4/042020.

[35] G. 1899-1982 Niemann and H. Winter, *Maschinenelemente : Entwerfen, Berechnen und Gestalten im Maschinenbau ; ein Lehr- und Arbeitsbuch.* Berlin: Springer, 2003.

[36] O. Karpa and A. Naess, “Extreme value statistics of wind speed data by the ACER method,” *Journal of Wind Engineering and Industrial Aerodynamics*, vol. 112, pp. 1–10, Jan. 2013, doi: 10.1016/J.JWEIA.2012.10.001.

[37] A. Naess and O. Gaidai, “Estimation of extreme values from sampled time series,” *Structural Safety*, vol. 31, no. 4, pp. 325–334, Jul. 2009, doi: 10.1016/J.STRUSAFE.2008.06.021.

Appendix A: Calculation

Extreme Value response using Acer and Gumbel

Load Case	ACER Vs Gumbel	ACER	GUMBEL	ACER	GUMBEL	ACER	GUMBEL
	Return Period	**1 yr**		**2 Yr**		**5 Yr**	
	Exceedance probability q	**7.19178E-05**		**5.70776E-05**		**2.28311E-05**	
LC 1, V_{hub} = 8 m/s	INPA_Fx (kN)	816.5 (784 , 842)	841.8 (657 , 1077)	826.2 (791 , 854)	841.8 (658 , 1077)	863.5 (819 , 897)	841.8 (658 , 1077)
	INPA_Fy (kN)	4849.9 (4849 ,5094)	4898.9 (3638,6599)	4937.3 (4533,5190)	4898.9 (3638,6600)	5274.6 (4792,5562)	4898.9 (3638,6600)
	INP A _Fz (kN)	2144.1 (1861, 2350)	2024.3 (1536,2671)	2222.5 (1896,2434)	2024.3 (1537,2671)	2520.8 (2141,2754)	2024.3 (1537,2671)
	INP B_Fx (kN)	650.2 (620 , 673)	673.7 (531 , 853)	659.5 (627 , 682)	673.7 (531 , 854)	694.9 (652 , 721)	673.7 (531 , 854)
	INP B_Fy (kN)	5539.7 (5324 ,5705)	5510.1 (4074,7458)	5622.9 (5405,5792)	5510.1 (4075,7458)	5939.4 (5716,6122)	5510.1 (4075,7458)
	INP B_Fz (kN)	6177.0 (5732, 6570)	6119.5 (5069,7395)	6279.4 (5815,6692)	6119.5 (5070,7396)	6673.8 (6131,7170)	6119.5 (5070,7396)
	st1_planet_to_st1 _sun (kN)	1103.2 (1066, 1140)	1189.4 (977 , 1450)	1120.4 (1080,1160)	1189.4 (977 , 1450)	1184.8 (1137,1239)	1189.4 (977 , 1450)
	st2_planet1_to_st2_ring (kN)	617.0 (588 , 647)	611.4 (473 , 791)	625.1 (595 , 658)	611.4 (473 , 791)	655.5 (621 , 696)	611.4 (473 , 791)
	st2_planet1_to_sun (kN)	579.2 (553 , 604)	584.1 (475 , 718)	587.7 (560 , 614)	584.1 (475 , 718)	619.9 (587 , 652)	584.1 (475 , 718)
	st3_wgear_to_st3_pgear (kN)	797.5 (757 , 833)	823.3 (666 , 1017)	809.8 (767 , 847)	823.3 (666 , 1017)	855.8 (805 , 903)	823.3 (666 , 1017)

Load Case	ACER Vs Gumbel	ACER	GUMBEL	ACER	GUMBEL	ACER	GUMBEL
	Return Period	**1 yr**		**2 Yr**		**5 Yr**	
	Exceedance probability q	**7.19178E-05**		**5.70776E-05**		**2.28311E-05**	
LC 2, V_{hub} = 12 m/s	INPA_Fx (kN)	1133.4 (1125 , 1140)	1154.2 (953 , 1398)	1137.7 (1128,1145)	1154.2 (953 , 1398)	1153.4 (1142 , 1162)	1154.2 (953 , 1398)
	INPA_Fy (kN)	6861.1 (6467,7117)	6921.5 (4484,10727)	7005.0 (6586,7267)	6921.5 (4484,0727)	7565.3 (7043,7856)	6921.5 (4484,10727)
	INP A _Fz (kN)	5442.4 (5005,5787)	5546.5 (4288,7183)	5592.4 (5136,5953)	5546.5 (4288,7183)	6172.0 (5618,6599)	5546.5 (4288 , 7183)
	INP B_Fx (kN)	943.3 (935 , 950)	962.6 (757 , 1224)	947.3 (938 , 954)	962.6 (757 , 1224)	961.9 (951 , 970)	962.6 (757 , 1224)
	INP B_Fy (kN)	7866.2 (7504,8146)	7777.1 (5722,10590)	7990.2 (7614,8281)	7777.1 (5722,10590)	8462.6 (8030,8796)	7777.1 (5722,10590)
	INP B_Fz (kN)	8440.5 (78689,8807)	8281.9 (6999 , 9802)	8637.6 (8638,9017)	8281.9 (6999 , 9802)	9411.5 (8647,9840)	8281.9 (6999 , 9802)
	st1_planet_to_st1 _sun (kN)	1419.4 (1402 , 1438)	1369.5 (1001 , 1874)	1429.9 (1411,1451)	1369.5 (1001 , 1874)	1471.6 (1445,1501)	1369.5 (1001 , 1874)
	st2_planet1_to_st2_ring (kN)	715.7 (714, 718)	706.8 (528 , 948)	719.3 (718 , 723)	706.8 (528 , 948)	733.9 (733 , 738)	706.8 (528 , 948)
	st2_planet1_to_sun (kN)	997.5 (861 , 1331)	679.6 (552 , 838)	1087.2 (907 , 1566)	679.6 (552 , 838)	1642.9 (1155,3408)	679.6 (552 , 838)
	st3_wgear_to_st3_pgear (kN)	1206.1 (1127, 1329)	952.0 (794 , 1140)	1264.6 (1167,1422)	952.0 (794 , 1140)	1566.6 (1360,1933)	952.0 (794 , 1140)

Load Case	ACER Vs Gumbel	ACER	GUMBEL	ACER	GUMBEL	ACER	GUMBEL
	Return Period	**1 yr**		**2 Yr**		**5 Yr**	
	Exceedance probability q	**7.19178E-05**		**5.70776E-05**		**2.28311E-05**	
LC 3 , V_{hub} = 16 m/s	INPA_Fx (kN)	862.4 (830 , 882)	957.2 (756 , 1213)	875.3 (840 , 897)	957.2 (756 , 1213)	925.9 (880 , 952)	957.2 (756 , 1213)
	INPA_Fy (kN)	7728.3 (7346, 8053)	8034.9 (7253 , 8909)	7870.9 (7474,8212)	8034.9 (7253, 8909)	8419.0 (8419,8827)	8034.9 (7253, 8909)
	INP A _Fz (kN)	6623.1 (6343, 6822)	6527.0 (5304 , 8047)	6754.1 (6465,6955)	6527.0 (5304, 8047)	5921.2 (5697,6110)	6527.0 (5304,8047)
	INP B_Fx (kN)	693.3 (664 , 710)	780.0 (617 , 988)	705.2 (673 , 723)	780.0 (617 , 988)	751.7 (709 , 773)	780.0 (617 , 988)
	INP B_Fy (kN)	8174.0 (7806, 8485)	8152.7 (5856,11354)	8319.3 (7934,8645)	8152.7 (5856,11354)	8875.3 (8422,9261)	8152.7 (5856,11354)
	INP B_Fz (kN)	8142.4 (7839 ,8455)	7246.3 (5355 , 9818)	8319.3 (7934,8645)	7246.4 (5355 , 9818)	8875.3 (8422,9261)	7246.4 (5355 , 9818)
	st1_planet_to_st1 _sun (kN)	1296.0 (1294, 1298)	1307.4 (718 , 2385)	1297.2 (1294,1299)	1307.4 (718 , 2385)	1301.7 (1299,1304)	1307.4 (718 , 2385)
	st2_planet1_to_st2_ring (kN)	675.3 (674 , 677)	683.6 (559 , 837)	676.7 (676 , 678)	683.6 (559 , 837)	682.2 (680 , 684)	683.6 (559 , 837)
	st2_planet1_to_sun (kN)	637.4 (636 , 638)	642.6 (498 , 830)	638.0 (637 , 634)	642.6 (498 , 830)	640.4 (639 , 641)	642.6 (498 , 830)
	st3_wgear_to_st3_pgear (kN)	894.0 (893 , 895)	900.1 (495 , 1637)	894.7 (894 , 896)	900.1 (495 , 1637)	897.4 (896 , 899)	900.1 (495 , 1637)

Appendix B: Appended Papers

Paper 1

Characterisation of extreme load responses of a 10-MW floating semi-submersible type wind turbine

Heliyon

Characterisation of extreme load responses of a 10-MW floating semi-submersible type wind turbine

--Manuscript Draft--

Manuscript Number:	HELIYON-D-22-08553
Article Type:	Original Research Article
Section/Category:	Engineering
Keywords:	Floating wind turbine; FAST; Extreme value analysis; ACER method; Gumbel method
Manuscript Classifications:	30.140.170.180: Wind Energy
Corresponding Author:	Shuaishuai Wang, PhD NTNU TRONDHEIM, NORWAY
First Author:	Yihan Xing
Order of Authors:	Yihan Xing
	Shuaishuai Wang, PhD
	Anuraj Karuvathil
	Rajiv Balakrishna
	Oleg Gaidai
Abstract:	Offshore wind turbines have been steadily increasing in size, with the global average size increasing from 1.5 MW to 6 MW from 2000 to 2020. With this backdrop, the research community has recently looked at very large offshore wind turbines (OWTs) in the 10 to 15 MW class. The larger rotor, nacelle structure and tower have larger structural flexibility. The larger structural flexibility, controller dynamics, aerodynamics, hydrodynamics, and various environmental conditions result in complex structural responses. The structural load effects of a very large OWT could be more severe than that of the lower MW classes. Accurate quantification of the extreme dynamic responses of OWT systems is essential in the Ultimate Limit State (ULS) based design due to the fully-coupled interaction between the OWT system and environmental conditions. Motivated by this, this paper uses the average conditional exceedance rate (ACER) and Gumbel methods to predict the extreme responses of the 10 MW semi-submersible type floating OWT under the operating conditions of 8, 12, and 16 m/s mean wind speed, representing the below-rated, rated and above-rated regions, respectively. The aim is to guide future research on very large OWTs by indicating the ULS loads expected.
Suggested Reviewers:	Zhiyu Jiang zhiyu.jiang@uia.no
	Puyang Zhang zpy_td@163.com
	Chana Sinsabvarodom chana.sinsabvarodom@ntnu.no
Opposed Reviewers:	

29 April 2022

Subject: Manuscript Submission to *Heliyon*

Dear Editor,

On behalf of my co-authors Yihan Xing, Anuraj Karuvathil, Rajiv Balakrishna and Oleg Gaidai I would like to submit the manuscript entitled “Characterisation of extreme load responses of a 10-MW floating semi-submersible type wind turbine” for consideration of publication in *Heliyon*.

Sincerely yours,

Shuaishuai Wang

Post-doctor researcher, Norwegian University of Science and Technology, Norway

Email: shuaishuai.wang@ntnu.no

Characterisation of extreme load responses of a 10-MW floating semi-submersible type wind turbine

Yihan Xing[1], Shuaishuai Wang[2,*], Anuraj Karuvathil[1], Rajiv Balakrishna[1], Oleg Gaidai[3]

[1]Department of Mechanical and Structural Engineering and Materials Science, University of Stavanger, Norway

[2]Norwegian University of Science and Technology, Trondheim, Norway

[3]Shanghai Engineering Research Centre of Marine Renewable Energy, College of Engineering Science and Technology, Shanghai Ocean University, Shanghai, China

[*]Corresponding author: shuaishuai.wang@ntnu.no

Abstract

Offshore wind turbines have been steadily increasing in size, with the global average size increasing from 1.5 MW to 6 MW from 2000 to 2020. With this backdrop, the research community has recently looked at very large offshore wind turbines (OWTs) in the 10 to 15 MW class. The larger rotor, nacelle structure and tower have larger structural flexibility. The larger structural flexibility, controller dynamics, aerodynamics, hydrodynamics, and various environmental conditions result in complex structural responses. The structural load effects of a very large OWT could be more severe than that of the lower MW classes. Accurate quantification of the extreme dynamic responses of OWT systems is essential in the Ultimate Limit State (ULS) based design due to the fully-coupled interaction between the OWT system and environmental conditions. Motivated by this, this paper uses the average conditional exceedance rate (ACER) and Gumbel methods to predict the extreme responses of the 10 MW semi-submersible type floating OWT under the operating conditions of 8, 12, and 16 m/s mean wind speed, representing the below-rated, rated and above-rated regions, respectively. The aim is to guide future research on very large OWTs by indicating the ULS loads expected.

Keywords: Floating wind turbine, FAST, Extreme value analysis, ACER method, Gumbel method

1. Introduction

Offshore wind has been developing quickly from the past decade. From the global wind report 2021 [1] issued by the global wind energy council, it is seen that the cumulative offshore installations have grown on average by 22 % annually in the past decade. The cumulative installed wind energy was 35 GW in 2020, 14 times higher than a decade ago. Further, it is estimated that there will be over 235 GW new installations over the next decade, which demonstrates a great prospect.

One observation over the years in the technological development of wind turbines is that wind turbine capacities have consistently increased. This is particularly true of offshore wind turbines (OWTs). Larger wind turbine sizes enable the same power output with fewer turbines, foundations, converters, and cables and lower maintenance costs, thus reducing the overall cost of energy. The global average offshore wind turbine size has increased from 1.5-MW in 2000 to 6.0-MW in 2020 [1]. The trend continues with the research community recently starting conceptual studies for 15-20 MW-class offshore turbines, such as the IEA 15-MW offshore reference wind turbine [2].

Accurate quantification of the extreme dynamic responses of OWT systems is essential in the Ultimate Limit State (ULS) based design. Due to the fully-coupled interaction between the OWT system and environmental conditions, the responses are strongly nonlinear and highly dynamic. A robust set of design requirements must ensure that the extreme load effects over the entire design lifetime are correctly assessed with corresponding structural capacities designed in the OWT. Estimating these extreme load effects can be challenging. Direct calculation of extreme structural responses could obtain accurate results, but this method needs many dynamic simulations and substantial computational costs. A statistical extrapolation method, as proposed in IEC 61400-3 [3], for ultimate strength analysis makes it possible to evaluate the extreme load effects of OWTs by using a much smaller amount of data, thereby saving a great deal of computational time.

Many studies have evaluated the effectiveness of various statistical extrapolation methods when used for the extreme load and load effect analysis for OWTs. Saha et al. [4] studied the extreme short-term responses of a jacket foundation of a 5 MW OWT. The authors studied the sensitivity of the extreme responses to sample sizes. Three extreme value analysis methods were investigated: the mean up crossing rate method, the Weibull tail method, and the global maxima method. It was found that the up crossing rate method performs better for both Gaussian and non-Gaussian responses than the other two methods. Dimitrov [5] compared three different methods for extracting independent responses peaks of wind turbine loads. Low-speed shaft torsion moment, tower base side-side bending moment, and flapwise blade root bending moment were compared. The results showed that the statistical load extrapolation method could reasonably estimate the statistical distribution of extreme loads under normal operating conditions. In contrast, uncertainties in the extrapolation approach exist in other conditions such as emergency stops, faults, grid drops, storms. Further, the behaviour is influenced by the turbine controller strategy. Using measurement data, Lott and Cheng [6] presented different methods to perform statistical extrapolations of extreme loads at wind turbine tower base and blade root. It was shown that the choices of the distribution function and the fitting method, and the database selection are important in determining the extrapolated extreme loads. Cao et al. [7] proposed a stochastic programming formulation based on statistical extrapolation techniques to mitigate long-term extreme loads in wind turbines. It is found that significant improvements in power extraction can be obtained while within the extreme mechanical loads. Cheng et al. [8] compared the extreme structural response and fatigue damage of a 5 MW horizontal axis floating wind turbine and a 5 MW vertical type. Li et al. [9] estimated the extreme values of the tower base fore-aft bending moments and mooring line tension forces of an integrated wind, wave and tidal energy system based on an extrapolated up-crossing rate method. Xu et al. [10] investigated the effect of wave nonlinearity on the fatigue damage and extreme responses of a 5MW semi-submersible floating wind turbine. Gumbel fitting and average conditional exceedance rate (ACER) methods were used to estimate the extreme responses of the tower base bending moments and mooring line tensions in extreme conditions.

Most studies on extreme structural response were performed on small-scale or medium-scale OWTs. Minimal effort has been devoted to very large (10-15 MW) floating OWTs. Very large floating OWT has longer blades, larger swept areas, and taller tower heights, leading to larger aerodynamic loads. In addition, it has a heavier rotor-nacelle-assembly (RNA) system and a larger support structure which leads to larger inertial loads. Further, studies performed by Wang et al. [11]-[12] indicated that larger wind turbines could be at risk of resonance. The larger rotor, nacelle structure and tower could be sufficiently flexible so their natural frequencies can be close to the low-frequency wind and wave excitations. The generally larger load effects mean that the structural load effects of a very large OWT could be more severe than that of the lower

MW classes. This highlights the importance of accurately quantifying the dynamic load effects of these very large OWTs, which is paramount in their ULS design.

Motivated by the above, the present work will characterise the extreme structural responses of a 10-MW floating semi-submersible OWT using the widely used Gumbel fitting and ACER methods. The paper will investigate the critical locations at the blades-hub, rotor-main shaft, and the tower base-floating platform interfaces. Representative operating conditions at below-rated, rated, and above-rated wind speeds are studied. The aim is to guide future research on very large OWTs by indicating the ULS loads expected.

2. System description

A 10-MW floating wind turbine (FWT) system [13] which is illustrated in Figure 1, is used in this work. The FWT system will be expounded in two parts in the following sections. Firstly, the reference wind turbine will be described, then the properties of the semi-submersible floater and the mooring system will be introduced.

Figure 1 The 10-MW OO-Star floating wind turbine [13].

2.1. DTU 10-MW Reference Wind Turbine

The DTU 10-MW reference wind turbine (RWT) [14] is used in this paper. The wind turbine was designed following International Electrotechnical Commission (IEC) Class 1A wind regime. It is a traditional three-bladed, clockwise rotation-upwind turbine and uses a variable speed and collective pitch control system. The DTU 10-MW RWT numerical model has been developed and studied by many researchers such as Muggiasca et al. [15], Yu et al. [16], Wang et al. [17], and Hu et al. [18]. The summary of the DTU 10-MW RWT is presented in Table 1.

Table 1 Key parameters of the DTU 10-MW reference wind turbine [14].

Parameter	**Value**
Rating	10-MW
Type	Upwind/3 blades
Control	Variable speed, collective pitch
Drivetrain	Medium-speed, multiple stage gearbox
Cut-in, rated and cut-out wind speed (m/s)	4, 11.4, 25
Minimum and maximum rotor speed (rpm)	6.0, 9.6
Maximum generator speed (rpm)	480
Rotor diameter (m)	178.3
Hub height (m)	119.0
Rotor mass (kg)	227962
Nacelle mass (kg)	446036
Tower mass (kg)	1.257×10^6

2.2. OO-Star Semi-submersible Wind Floater and mooring system

This paper considers the 10-MW RWT mounted on the semi-submersible developed by Dr.techn. Olav Olsen AS [13]-[14] in the LIFES 50+ project [13]. The floater is constructed using post-tensioned concrete. It has a central main column and three outer columns located radially outwards. The four columns are mounted on a star-shaped pontoon through a slab attached at the bottom. Three catenary mooring lines are used for station keeping. Clumped masses are attached at the middle of each mooring line for increased mooring tension. More details of the OO-Star Wind Floater and its mooring system are shown in Table 2 and Table 3, respectively.

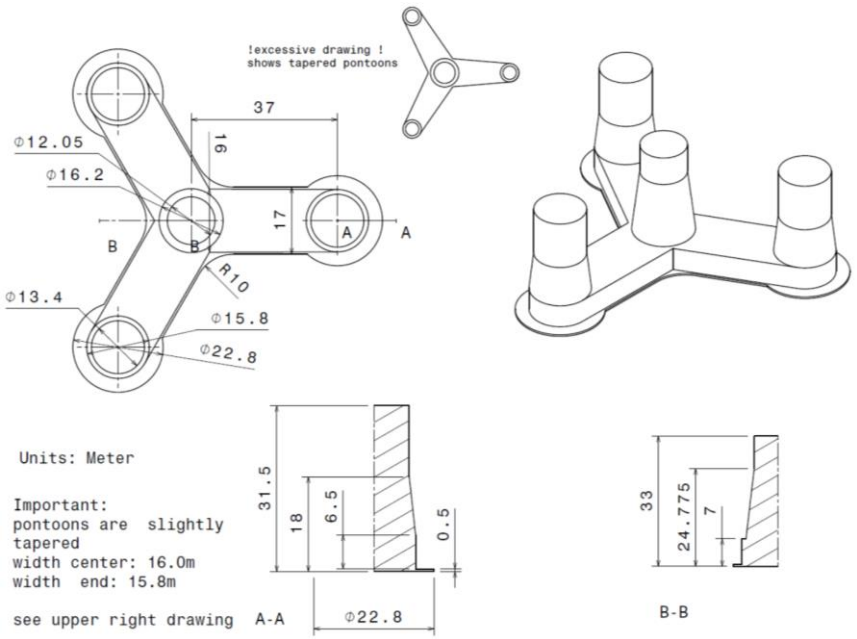

Figure 2 Main dimensions of the OO-Star floater of the 10-MW wind turbine [19].

Table 2 The main properties for the 10-MW OO-Star wind floater.

Parameter	Value
Water depth (m)	130
Draft (m)	22
Tower-base interface above mean sea level (m)	11
Displacement (kg)	24158
Overall gravity, including ballast (kg)	21709
Roll and pitch inertia about center of gravity (kg·m^2)	1.4462 x 10^{10}
Yaw inertia about center of gravity (kg·m^2)	1.63 x 10^{10}
Center of gravity height below mean sea level (m)	15.23
Center of buoyancy height below mean sea level (m)	14.236

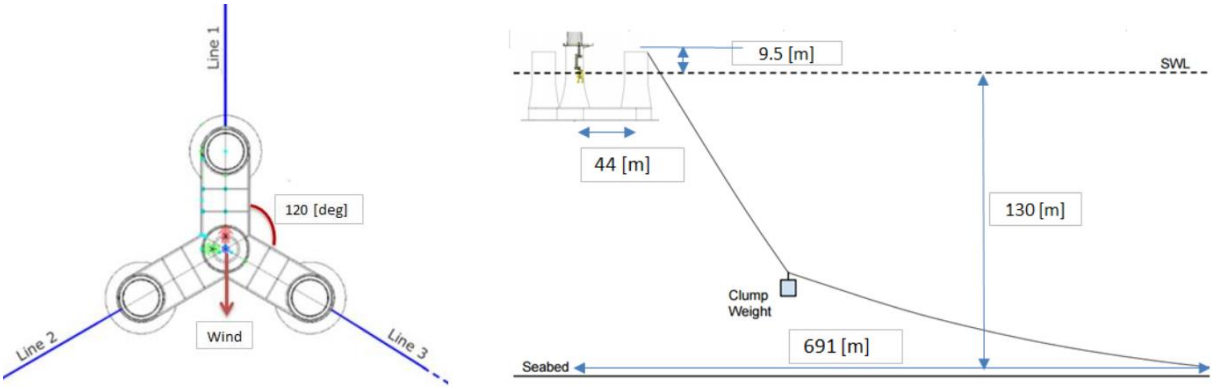

Figure 3 Sketch of the mooring system in the 10-MW FWT (left: top view; right: side view) [19].

Table 3 The main properties for the mooring system of the 10-MW FWT.

Parameter	Value
Radius to anchors from platform centerline (m)	691
Anchor position below MSL (m)	130
Initial vertical position of clump mass below MSL (m)	90.45
Initial radius to clump mass from centerline (m)	148.6
Length of clump mass upper segment (kg)	118
Length of clump mass lower segment (kg)	585
Equivalent weight per length in water (N/m)	3200.6
Extentional stiffness (N/m)	1.506 x 10^9

3. Methodology

3.1. Aero-hydro-elastic-servo dynamic analysis of the 10-MW FWT

The simulation tool used to simulate a wind turbine is an open-source code called FAST (v8.16.00a-bjj) developed by the National Renewable Energy Laboratory (NREL). FAST is an acronym for Fatigue, Aerodynamics, Structures and Turbulence. As its name suggests, it is a coupled aero-hydro-elastic-servo tool that has been used to execute the dynamic analysis of the 10-MW FWT. The five codes are implemented via MATLAB, and they work concurrently together to produce the aerodynamic and hydrodynamic loads, and control, structural and mooring system dynamics are commonly known as AeroDyn [20], HydroDyn [21], ServoDyn, and MoorDyn [22]. Furthermore, FAST can accept and analyse time-varying stochastic wind as an input for its time-domain simulations. FAST has been successfully used to execute various projects such as the OC3: Offshore Code Comparison Collaboration [23] and OC4: IEA (International Energy Agency) Task Wind 30 [24], with its modelling capability verified in the Netherlands [25].

Aerodynamics

In a wind turbine, the blades aerodynamic loads are measured using the quasi-steady Blade Element Momentum (BEM) theory, where the momentum and blade element theory are used together. The BEM method includes various corrections such as tip loss, hub loss, skewed inflow, and dynamic stall corrections in its calculation. While the Pitt and Peters' model minimises the error by correcting the skewed inflow, the Boddoes-Leishman model helps correct the dynamic stall. Similarly, the Prandtl corrections and Glauert correction account for the blade's hub, tip losses, and induction factors. The AeroDyn theory manual can be used as a reference to understand the calculation of the aerodynamic load executed by the FAST code [20].

Hydrodynamics

The drag term from Morison's equation and potential flow theory are used together to calculate the hydrodynamic loads present in the semi-submersible floater. The wave pressures and viscous loads are accounted for in this method. Next, the panel code, WAMIT [26], as per the potential flow theory, is used to estimate the hydrodynamic coefficient and first-order wave excitation load transfer function. The hydrodynamic coefficient is made up of the added mass and damping coefficients. After that, the convolution technique is initiated to transform the hydrodynamic coefficients to obtain the solutions in the time domain [27].

Structural dynamics

To ensure that the structural dynamics of the FWT is accounted for in the FAST code uses the combined multi-body and modal structural approach. The blades, tower, and driveshaft are designed as flexible bodies in this approach. In contrast, the nacelle, hub, and floater are designed as rigid bodies. A coupled dynamics equation from Kane's approach is used to calculate the structural dynamic responses for the time-domain [28]. At the same time, the Rayleigh damping coefficient is used in design for the blade's inherent structural damping in both the blades and tower.

Control system dynamics

The 10-MW FWT's control system functions differently according to its operational modes. These modes are primarily called the below-rated or full-rated regions. In the below-rated region, speeds that are lower than the FWT's rated speed, the generator torque-speed curve controls the rotational speed of the rotor according to the optimal tip speed ratio, allowing the turbine to reach its maximum power. While at the full-rated region, speeds higher than the

FWT's rated speed, the blade pitch is adjusted using a proportional-integral (PI) algorithm to control the rotational speed of the rotor to maintain the rated power generation. The PI parameters used in the FWTs differ from those used in land-based RWT since it is vital to avoid the negative damping effects that can significantly affect the FWTs.

3.2. Extreme value prediction

In any stochastic process *X(t)* taken across a time period (*T*), the extreme value is classified as the largest maxima extracted from a group of individual maxima.

$$X_e = \boldsymbol{max}\{X_{m1}, X_{m2}, X_{m3}, \dots., X_{mn}\}\ , \qquad i = 1, \dots, n \tag{1}$$

where X_e describes the largest maximum value and X_{mi} describes the individual maxima. Therefore, from this assumption, it is observed that the individual maxima are independently and identically distributed across the common distribution function $F_{Xm}(x)$. Therefore, from the equation below, the distribution of X_e is labelled as:

$$F(x) = \boldsymbol{Prob}\{X_e \leq x\} = \ [F_{Xm}(x)]^n\ , \qquad i = 1, \dots, n \tag{2}$$

Various statistical methods have been used to approximate an extreme value distribution. Examples of the extreme value methods used in the study of wind turbines includes an estimation of extreme structural responses in a floating vertical axis wind turbines by Cheng et al. [29] and extreme responses due to wave nonlinearity on a semi-submersible floating wind turbine by Xu et al. [30]. The two methods used in this paper are the ACER method (Section 3.3) and the Gumbel method (Section 3.4).

3.3. ACER (Average Conditional Exceedance Rate)

This paper uses the ACER method to estimate extreme structural responses. The method was proposed by Naess and Gaidai [31], and it is derived for a discretely sampled response process. The cascade of conditional approximation is the basis for calculating the exceedance probability for extreme value estimation. The primary purpose of the ACER method is to accurately determine the distribution function of the extreme value, which is denoted as $M_N = max\{X_j;\ j = 1,\ \cdots,\ N\}$. Let $P_\eta = Prob(M_N \leq \eta)$ denotes the probability of the occurrence of the extreme value η and it follows:

$$P_\eta = Prob(M_N \leq \eta) = Prob(X_1 \leq \eta,\ \cdots,\ X_N \leq \eta) \tag{3}$$

To solve this equation efficiently, a cascade of conditional approximation $P_k(\eta)$ is used, where $P_k(\eta)$ tends to close to P_η as k increases. For $N \gg 1$ and $k = 1,2,\cdots, P_k(\eta)$ is represented as:

$$P_k(\eta) \approx exp(-\sum_{j=k}^{N} \alpha_{kj}(\eta)) \quad (4)$$

where $\alpha_{kj}(\eta) = Prob\big(X_1 > \eta | X_{j-1} \ll \eta, \cdots, X_{j-k+1} \leq \eta\big)$, and it represents the exceedance probability conditional on $k-1$ previous non-exceedances.

Equation (4) will be calculated based on the ACER, which is defined as:

$$\varepsilon_k(\eta) = \frac{1}{N-k+1} \sum_{j=k}^{N} \alpha_{kj}(\eta), k = 1,2, \cdots \quad (5)$$

For $k \geq 2$, $\tilde{\varepsilon}_k(\eta)$ is used instead of $\varepsilon_k(\eta)$ because it is easier to use for nonstationary or long-term statistics, and it is defined as:

$$\tilde{\varepsilon}_k(\eta) = \lim_{N \to \infty} \frac{\sum_{j=k}^{N} a_{kj}(\eta)}{N-k+1} \quad (6)$$

where $a_{kj}(\eta)$ is the realised values for the observed time series, and $\lim_{N \to \infty} \frac{\tilde{\varepsilon}_k(\eta)}{\varepsilon_k(\eta)} = 1$.

For both stationary and nonstationary time series, the sample estimate of the ACER can be denoted as:

$$\hat{\varepsilon}_k(\eta) = \frac{1}{R} \sum_{r=1}^{R} \hat{\varepsilon}_k{}^{(r)}(\eta) \quad (7)$$

where *R* is the number of samples, and

$$\hat{\varepsilon}_k{}^{(r)}(\eta) = \frac{\sum_{j=k}^{N} a_{kj}{}^{(r)}(\eta)}{N-k+1} \quad (8)$$

where *r* denotes the realisation number.

When the realisations are sufficiently numerous and assumed to be independent, then the 95 % confidence interval (CI) for the ACER can be estimated as:

$$CI(\eta) = \hat{\varepsilon}_k(\eta) \pm 1.96 \, {\hat{s}_k(\eta)}\Big/{\sqrt{R}} \quad (9)$$

where $\hat{s}_k(\eta)$ refers to the standard deviation of samples and can be estimated by:

$$\hat{s}_k(\eta)^2 = \frac{1}{R-1}\sum_{r=1}^{R}(\hat{\varepsilon}_k^{(r)}(\eta) - \hat{\varepsilon}_k(\eta))^2 \quad \textbf{(10)}$$

The above equations for estimation of average exceedance rate are based on direct numerical simulations. In contrast, an extrapolation technique can reduce the computational time.

Assuming the mean exceedance rate in the tail behaves similarly to $exp\{-a(\eta-b)^c\}(\eta \geq \eta_0 \geq b)$, where *a*, *b* and *c* are suitable constants. The ACER will therefore be assumed by:

$$\varepsilon_k(\eta) \approx q_k(\eta)exp\{-a_k(\eta-b_k)^{c_k}\}, \eta \geq \eta_0 \quad \textbf{(11)}$$

where the function $q_k(\eta)$ varies slowly compared to the exponential function $exp\{-a_k(\eta - b_k)^{c_k}\}$ in the tail region, thus it can be replaced by a constant for a suitable choice of the tail marker η_0.

Finally, the Levenberg-Marquardt least-squares optimisation method can be used to determine the constants *a*, *b*, *c* and *q*. Based on this, the probability of the occurrence of the extreme value can be obtained by the ACER method. In the studies of Naess et al. [32] and Chai et al.[33] it is shown that the extrapolation technique can achieve a satisfactory estimation of the extreme values but saves significant simulation time. Detailed descriptions of the ACER method can be found in the reference [34].

3.4. Gumbel fitting method

Extreme value distribution Eq. (2) has been proven on numerous occasions to converge to the Gumbel, Fréchet or Weibull distribution if the sample size (*n*) is large enough. Therefore, these distributions are also recognised as the Type I, II and III extreme value distributions, respectively and are a family of cumulative distribution probability that combines the generalised extreme value (GEV) distribution.

$$F_{X_e}(x) = exp\left(-\left(1+\gamma\left(\frac{x-\mu}{\beta}\right)\right)^{-\frac{1}{\gamma}}\right) \quad \textbf{(12)}$$

where β describes the scale parameter, γ describes the shape parameter, and μ describes the location parameter. The limiting of $\gamma \to 0$ allows the approximation to fit the Gumbel distribution, commonly used as a recommendation when modelling marine structures [35].

$$F_{X_e}(x) = exp\left(-exp\left(-\frac{x-\mu}{\beta}\right)\right) \quad \textbf{(13)}$$

Eq. (13) can be rewritten by using logarithm on the equation, allowing it to become a linear function.

$$-ln\left(ln\left(F_{X_e}(x)\right)\right) = \frac{x}{\beta} - \frac{\mu}{\beta} \quad \textbf{(14)}$$

The parameters β and μ can be approximated from the original data using the least-square fitting method from the cumulative distribution probability, i.e., a straight line on a probability paper [36].

3.5. Load cases and environmental conditions

In this paper, the wind and wave data were generated using the hindcast data obtained from the North Sea from 2001 to 2010. The long-term joint wind and wave distribution consisted of 1-hour mean wind speed located 10 m above the sea level (U_{10}), wave spectral peak period (T_p) and significant wave height (H_s) [37]. The long-term joint wind and wave distribution are described below:

$$f_{U_{10},H_s,T_p}(u,h,t) = f_{U_{10}}(u) \cdot f_{H_s|U_{10}}(h|u) \cdot f_{T_p|U_{10},H_s}(t|u,h) \quad \textbf{(15)}$$

where the marginal distribution of U_{10} is described by $f_{U_{10}}(u)$, $f_{H_s|U_{10}}(h|u)$ and $f_{T_p|U_{10},H_s}(t|u,h)$, the conditional distribution of H_s for given U_{10} and the conditional distribution of T_p for given U_{10} and H_s. Figure 4 shows a scattered diagram for the in situ values of H_s and T_p that are used to assign probabilities for the individual sea states.

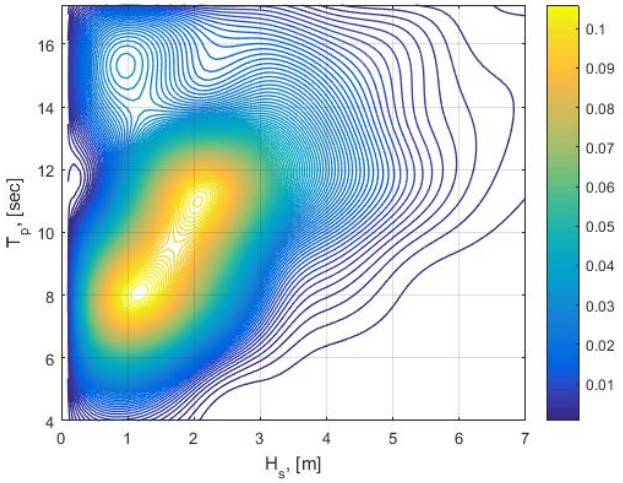

Figure 4 Scattered diagram: In situ values of H_s *and* T_p *used to assign* probabilities for the individual sea states.

Table 4 Load cases for numerical simulations.

Load cases	U_w (m/s)	T_I	H_s (m)	T_p (s)	Samples	Simulation length (s)
LC1	8	0.1740	1.9	9.7	20	4000
LC2	12	0.1460	2.5	10.1	20	4000
LC3	16	0.1320	3.2	10.7	20	4000

To replicate a highly probabilistic normal operational condition experienced by the turbine, three closely related load cases were selected, shown in Table 4. The wind speed used varied according to the turbine operating ranges, cut-in, rated and cut-out zones. The three-speed increased in blocks of 4 m/s. Each speed had its significant wave height and spectra peak period, and these values were measured using the joint distribution described in Eq. (15). In comparison, the turbulent wind and irregular waves used for all three cases were directionally aligned. Wind turbine Class C is used with normal turbulence and normal wind profiles. The wind speed profile is modelled using the wind power-law formulation described in Eq. (16).

$$U_w(z) = U_{hub}\,(\frac{\mathrm{Z}}{Z_{hub}})^{\alpha} \qquad \textbf{(16)}$$

where $U_w(z)$ is the mean wind speed taken from height z above the still water level, u_{hub} is the mean wind speed w.r.t hub height, z_{hub} is the hub height w.r.t the still water level (119 m for the selected 10-MW FWT). α (power-law exponent) is equal to 0.14. These recommendations are from IEC 61400-3-2, see [38], used for offshore locations.

The 3-D wind turbulent fields generated using Turbsim is derived from the Kaimal's turbulence model [39]. At the same time, the JONSWAP (Joint North Sea Wave Project) spectrum allowed the modelling of the time-varying irregular waves with the respective H_s and T_p values.

Every simulation was conducted for a period of 4000s. The initial 400s of these simulations were disregarded to account for the transient effect often present during a turbine's start-up. Consequently, only 3600s of data is used to analyse the extreme value. Accordingly, each environmental condition had sea states with 20 random wind and wave conditions samples.

4. Response variables

The loads at the three measurement points presented in Figure 5 are considered. These are the blade 1 root flapwise bending moment (RootMyb1), main shaft tip up-down bending moment (LSSTipMys) and tower bottom fore-aft bending moment (TwrBsMyt).

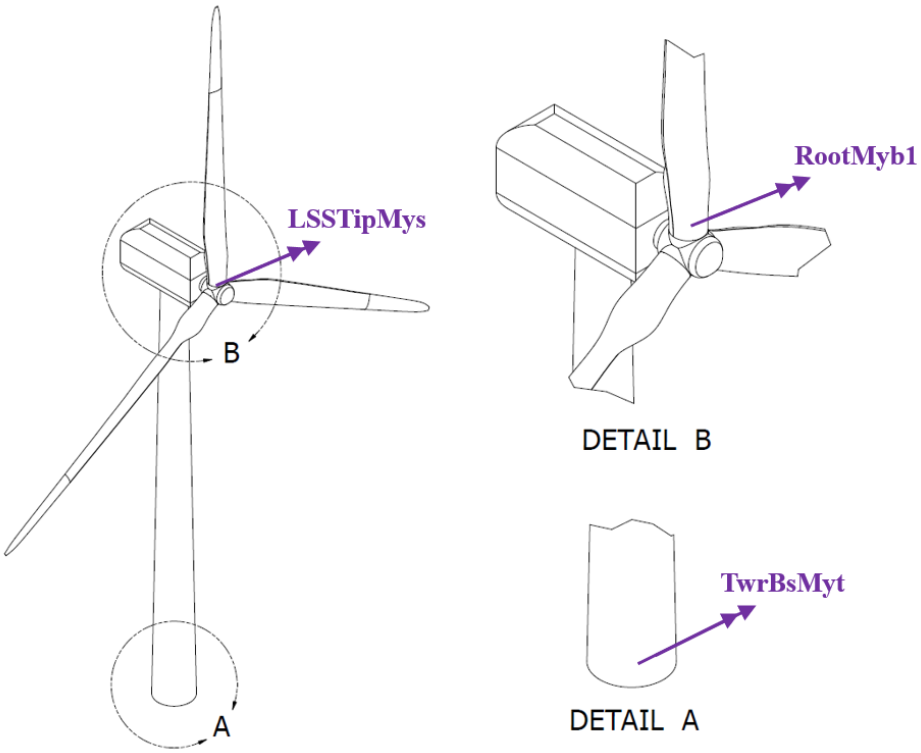

Figure 5 Location of points where bending moments are measured.

5. Results and discussions

This paper presents the methodology for estimating the 10 MW DTU WT-OO-Star's extreme loads during operating conditions. The empirical data is based on accurate numerical simulations using a FAST model as presented in Section 3.1. The Gumbel and ACER methods presented in Sections 3.3 and 3.4 are used.

5.1. Time-domain responses, PSD, and maximum values

The time-domain responses for one portion of a realisation, the power spectral distributions (PSDs) for a full realisation and the maximum values of each realisation are presented in Figure 6, Figure 7, and Figure 8, respectively. These results of each load case, i.e., LC1, LC2 and LC3 are taken from one of the 20 realisations calculated. The wind and wave elevation time series and PSDs are also plotted for reference.

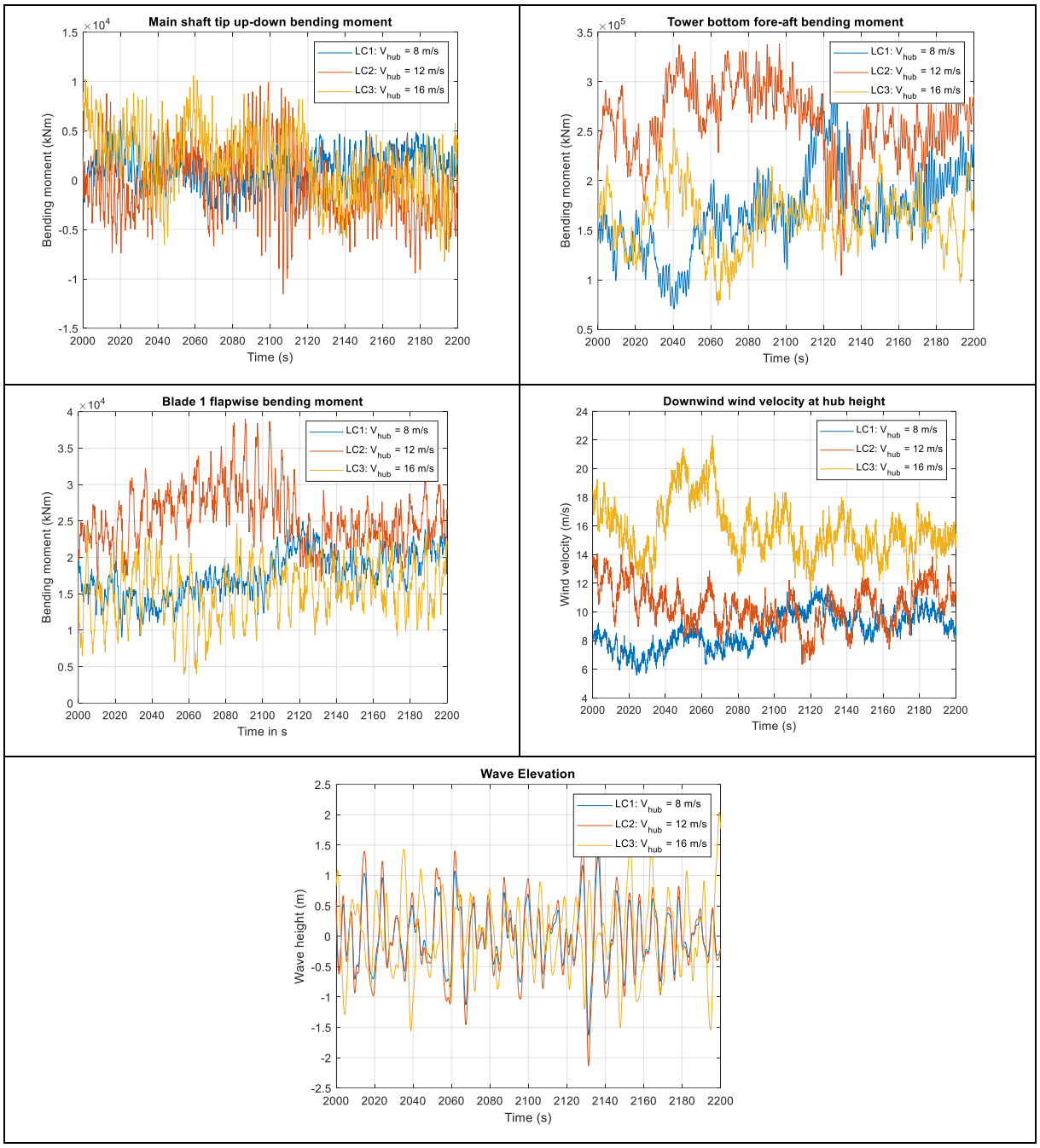

Figure 6 Example time domain results. Top-left: Main shaft tip up-down bending moment (LSSTipMys); Top-right: Tower bottom fore-aft bending moment (TwrBsMyt); Centre-left: Blade 1 root flapwise bending moment (RootMyb); Centre-right: Downwind wind velocity at hub height; Bottom: Wave elevation

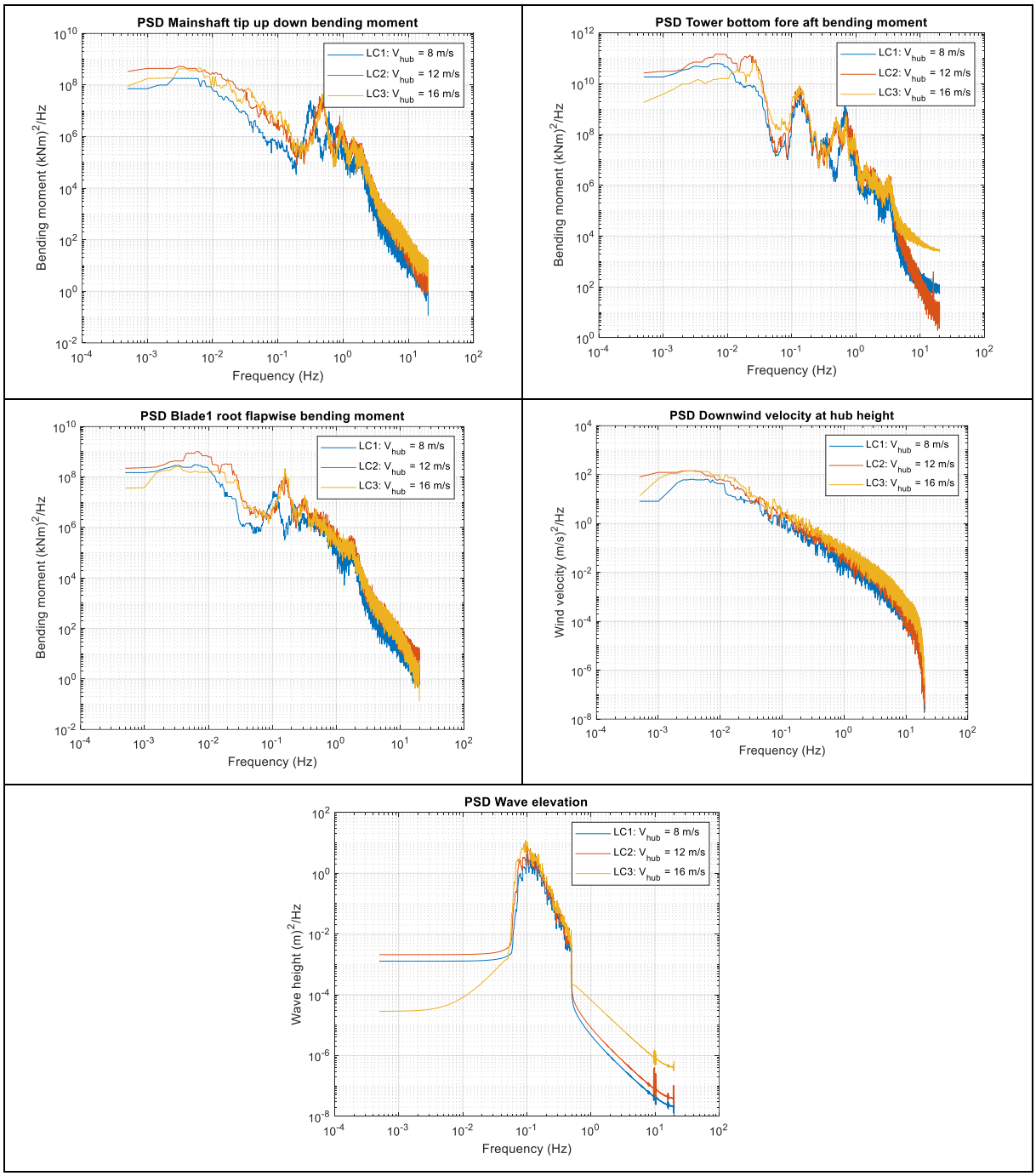

Figure 7 Power spectral distributions. Top-left: Main shaft tip up-down bending moment (LSSTipMys); Top-right: Tower bottom fore-aft bending moment (TwrBsMyt); Centre-left: Blade 1 root flapwise bending moment (RootMyb); Centre-right: Downwind wind velocity at hub height; Bottom: Wave elevation

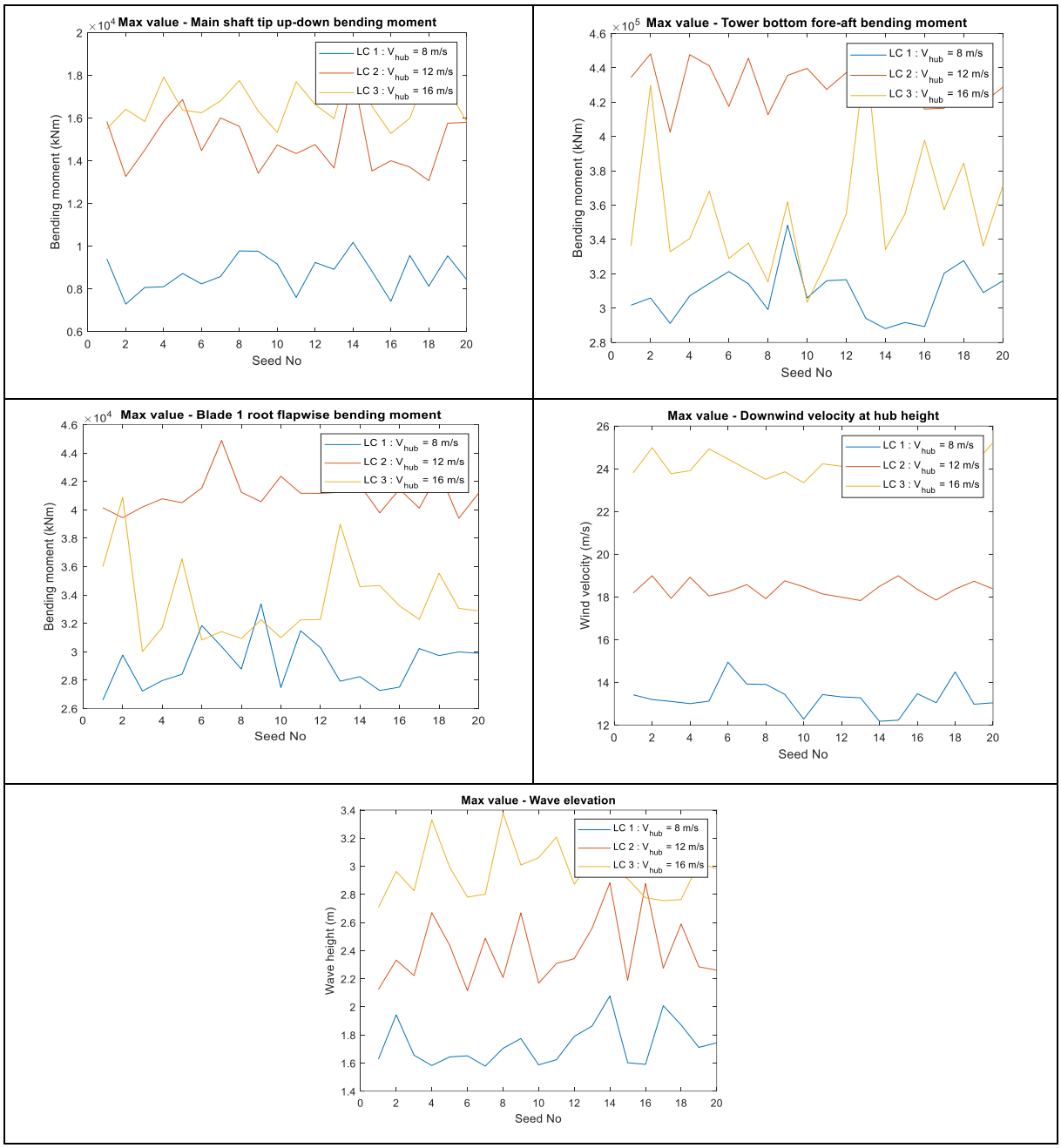

Figure 8 Maximum value in each realisation. Top-left: Main shaft tip up-down bending moment (LSSTipMys); Top-right: Tower bottom fore-aft bending moment (TwrBsMyt); Centre-left: Blade 1 root flapwise bending moment (RootMyb); Centre-right: Downwind wind velocity at hub height; Bottom: Wave elevation

5.2. Extreme load responses using ACER and Gumbel methods

This section presents the extreme load responses using the ACER and Gumbel methods for the three operating conditions (LC1 – LC3) presented in Table 4. k = 6 is used. For illustration, example plots of the ACER extrapolation and Gumbel fitting are presented in Figure 9 and Figure 10, respectively.

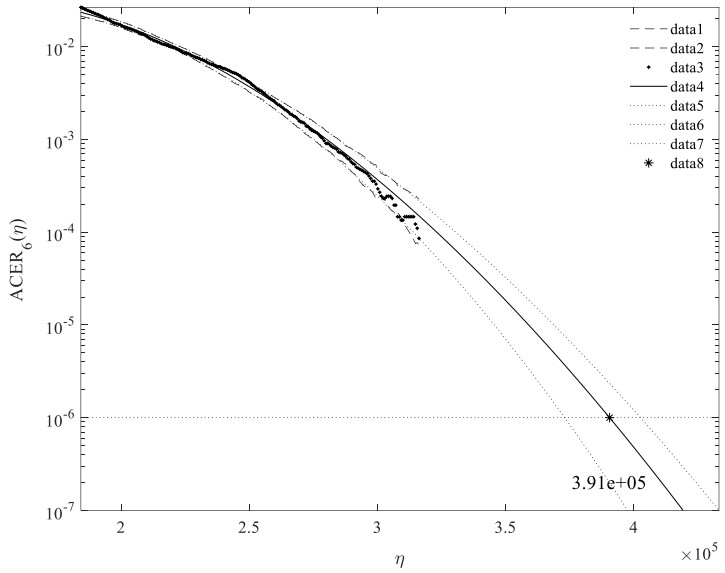

Figure 9 Example plot of ACER extrapolation,TwrBsMyt, LC1 – V_{hub} =8 m/s, Realisation #1

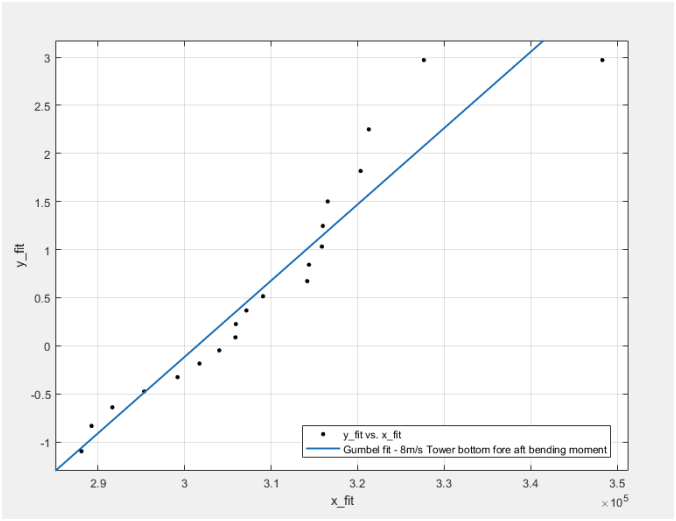

Figure 10 Example plot of Gumbel fitting, TwrBsMyt, LC1 – V_{hub} = 8 m/s, Realisation #1

As illustrated by the significantly smaller confidence intervals, the ACER method can lead to more accurate results as it does not assume a distribution. The ACER method does not assume any extreme value distribution. Instead, it follows the exact shape of the data points as presented in Figure 9. On the other hand, from Figure 10, it is observed that the Gumbel distribution does fit the upper-end tail well. The data points tend to curve up towards the left for increasing response values and are above the Gumbel line. This means the Gumbel distribution will tend to overpredict the extreme value responses. This example shows the advantages of the ACER method.

The extreme load responses together with the 95 % CIs from both ACER and Gumbel methods are then plotted in Figure 11, Figure 12 and Figure 13 for RootMyb, LSSTipMys and TwrBsMyt, respectively. The numerical values of the results are also presented in Table 6 and

Table 7 of the Appendix for extreme values calculated by the ACER and Gumbel methods, respectively.

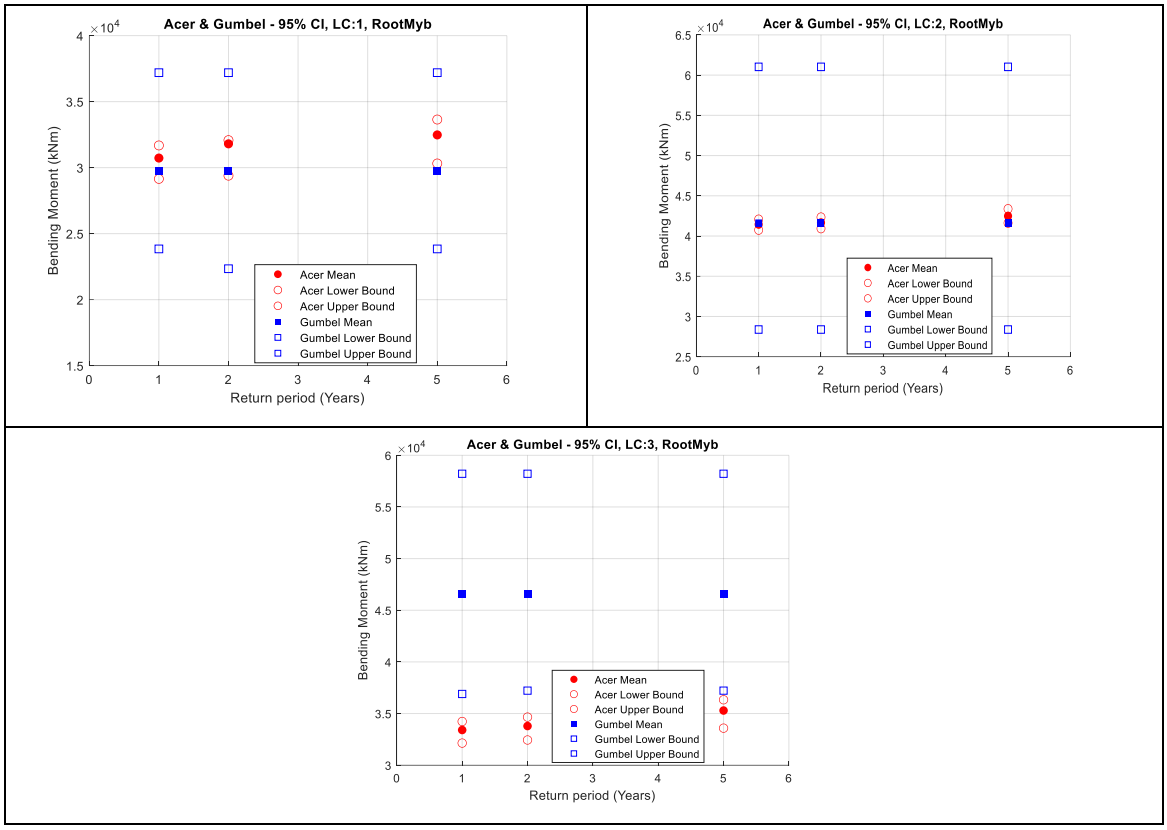

Figure 11 Blade 1 root flapwise bending moment. ACER and Gumbel with 95 % CI; Top-left: LC1, V_{hub} = 8 m/s; Top-right: LC2, V_{hub} = 12 m/s; Bottom: LC3, V_{hub} = 16 m/s.

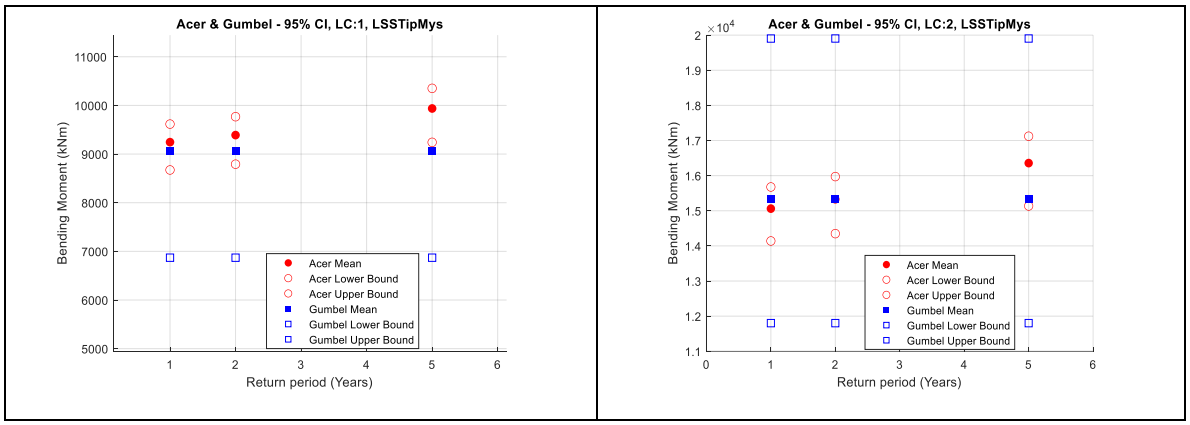

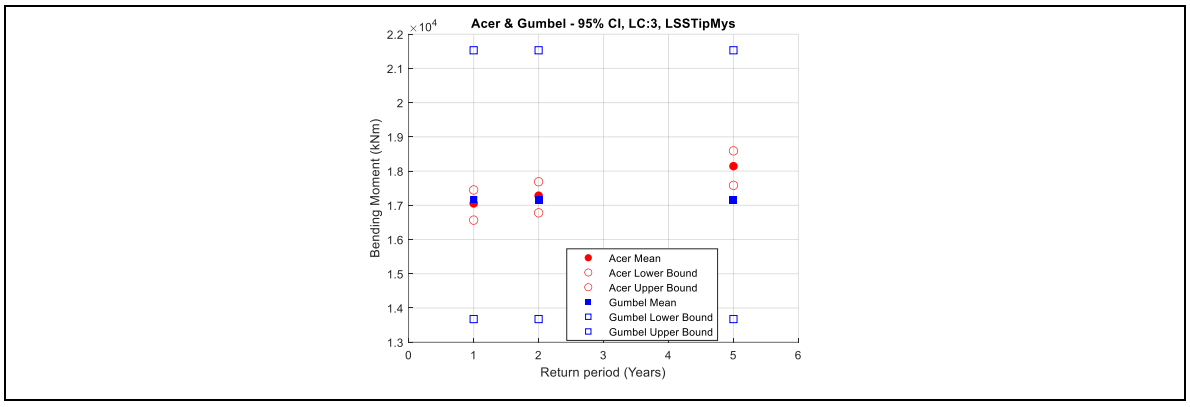

Figure 12 Main shaft tip up-down bending moment. ACER and Gumbel with 95 % CI; Top-left: LC1, V_{hub} = 8 m/s; Top-right: LC2, V_{hub} = 12 m/s; Bottom: LC3, V_{hub} = 16 m/s.

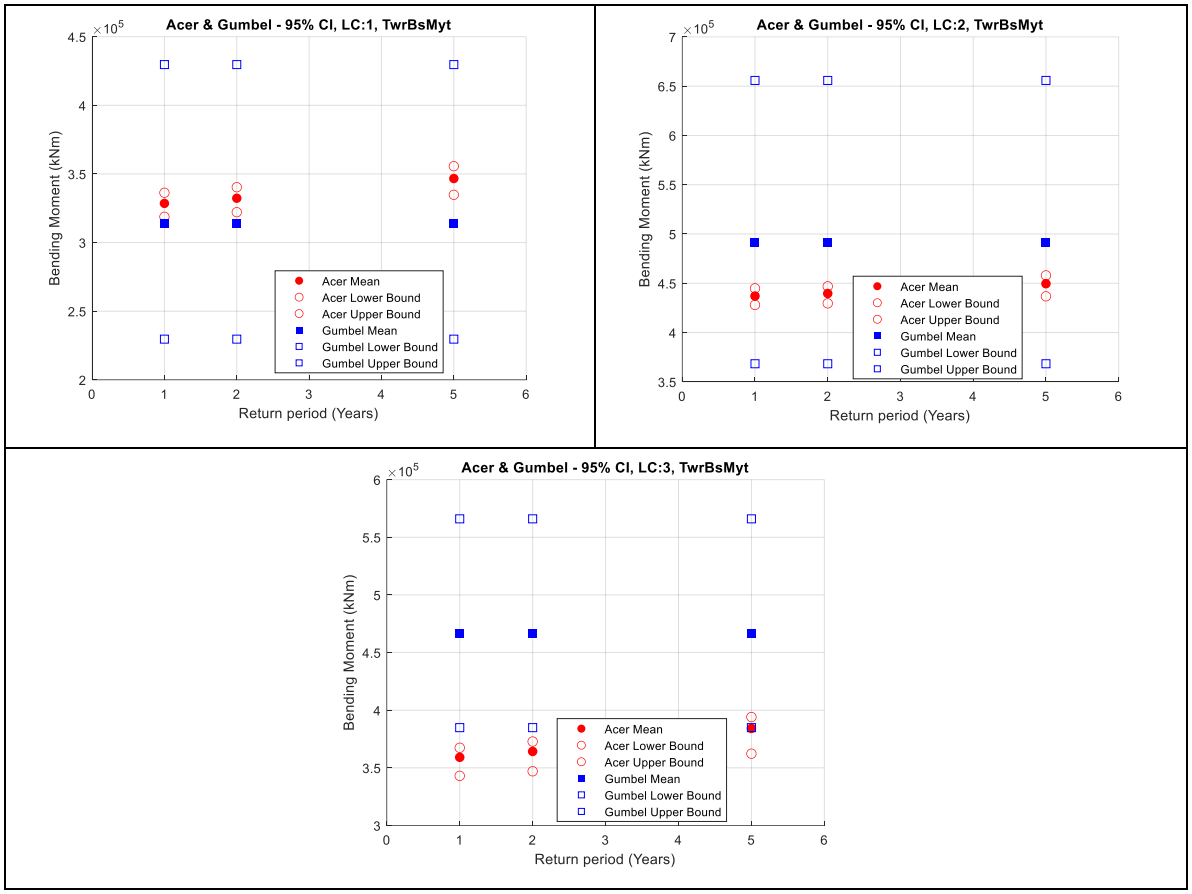

Figure 13 Tower bottom fore-aft bending moment. ACER and Gumbel with 95 % CI; Top-left: LC1, V_{hub} = 8 m/s; Top-right: LC2, V_{hub} = 12 m/s; Bottom: LC3, V_{hub} = 16 m/s.

The following observations are made:

- The 1, 2 and 5-year extreme values are generally 1.1-1.3 times larger than the maximums of single 1-hour realisations. The relatively large range of values (about 20 %) indicates the importance of using extrapolation methods that are accurate in predicting extreme values that can be used to define appropriate design values that can be utilised in deterministic engineering design.

- The 95 % CIs of the results calculated using the ACER method are significantly smaller than those of the Gumbel method. This highlights the benefits of the ACER in not assuming a distribution in the extrapolation of extreme values.
- The 95 % Cis of the results calculated using the Gumbel method are larger. This indicates that the Gumbel distribution does not fit the extreme value responses very well.
- Further, the 1, 2, and 5-year extreme values calculated using the Gumbel method are relatively similar. This is due to the inaccurate fit of the probability distribution at the upper tail end. The fitted Gumbel probability density distribution slope is too steep at the upper tail end. This leads to very small changes in the response values for a unit change in probability.

5.3. Choice of *k* value in ACER method

It is recommended to perform sensitivity analyses of the *k* values used when studying new responses [31]. Therefore, the choice of *k* value is investigated in this section for a *q* value of 10^{-6}. The results for *k* = 2, 4 and 6 are presented in Table 5. The ACER function plots for *k* = 1 to 6 are presented in Figure 14.

Table 5 Extreme values calculated from the ACER method considering different values of *k*.

Load Case	***q* value**	**10^{-6}**		
	***k* value**	**2**	**4**	**6**
LC1, V_{hub} = 8 m/s	RootMyb (kNm)	36103	36441	37018
	LSSTipMys (kNm)	11509	11580	11592
	TwrBsMyt (kNm)	380076	368822	390514
LC2, V_{hub} = 12 m/s	RootMyb (kNm)	44536	44626	44951
	LSSTipMys (kNm)	19511	19228	19607
	TwrBsMyt (kNm)	476606	479938	480159
LC3 , V_{hub} = 16 m/s	RootMyb (kNm)	38980	40385	40214
	LSSTipMys (kNm)	20747	20803	20670
	TwrBsMyt (kNm)	450802	447620	450217

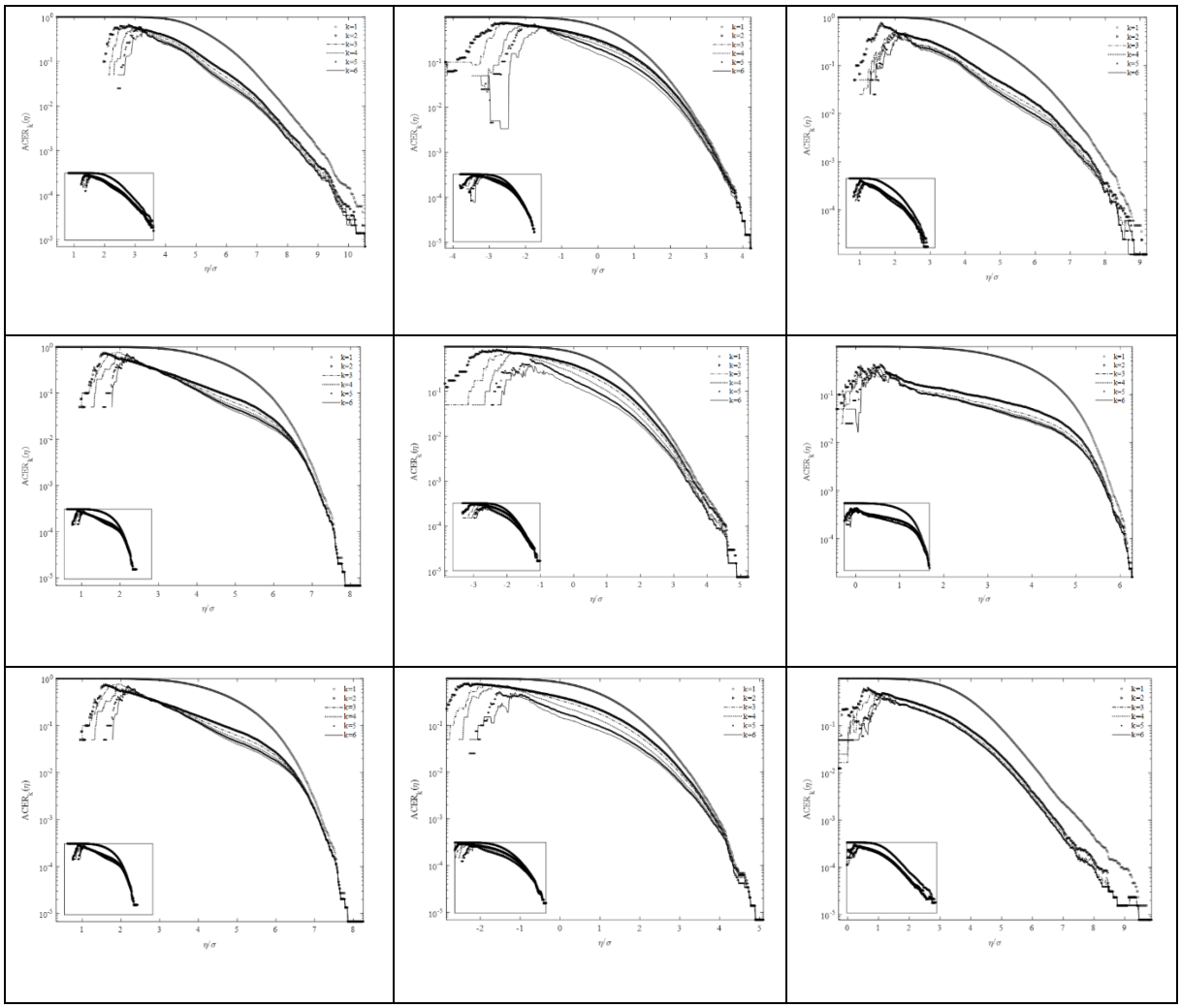

Figure 14 ACER functions for various k values. Top: LC1, V_{hub} = 8 m/s; Centre: LC2, V_{hub} = 12 m/s; Bottom: LC3, V_{hub} = 16 m/s; Left: Blade 1 root flapwise bending moment (RootMyb); Centre: Mainshaft tip up-down bending moment (LSSTipMys); Right: Tower bottom fore-aft bending moment (TwrBsMyt).

In general, the extreme values calculated do not vary significantly with the value of *k* used. A *k* value of 1 was found to lead to incorrect results. The extreme values estimated also increase for increasing values of *k* used. It was observed that the responses converged for $k > 2$. Therefore, it was decided to use $k = 6$ for the analyses in this paper.

6. Conclusions

This paper investigated the extreme responses for a 10 MW semi-submersible type FWT using ACER and Gumbel methods. The responses are based on fully coupled nonlinear numerical analysis, including structural flexibility, aerodynamics, hydrodynamics, control dynamics, interaction with combined turbulent wind and stochastic waves. The following conclusions are made:

- The 1, 2 and 5-year responses of the FWT were in general 1.1-1.3 times larger than the maximums of single 1-hour realisations. This reinforces the importance of using extrapolation methods to determine extreme loads to be used as ULS loads.

- The ACER results have a smaller 95 % CI than the Gumbel results. This means the ACER method is more accurate than the Gumbel method.
- The 1, 2 and 5-year responses predicted by the Gumbel method are quite similar. This is due to poor Gumbel fitting of the data at the upper tail. On the other hand, the ACER does not assume any distributions and therefore does not have the same poor fit issue at the tail end.
- The better performance of the ACER method is because, in contrast to Gumbel, it does not assume that the extreme responses follow a designated probability distribution.
- Lastly, it was found that $k = 1$ would lead to incorrect results and cannot be used, but otherwise, the choice of the k values does not affect the ACER results. When new responses are studied, it is also recommended to perform sensitivity studies on the k values.

References

[1] Murdock, H. E., Gibb, D., Andre, T., Sawin, J. L., Brown, A., Ranalder, L., ... & Brumer, L. (2021). Renewables 2021-Global status report.

[2] Bak, C., Zahle, F., Bitsche, R., Kim, T., Yde, A., Henriksen, L. C., ... & Natarajan, A. (2013). The DTU 10-MW reference wind turbine. In Danish wind power research 2013.

[3] Turbines—Part, W. (2009). 3: design requirements for offshore wind turbines. Proceedings of the IEC, 61400-3.

[4] Saha, N., Gao, Z., Moan, T., & Naess, A. (2014). Short-term extreme response analysis of a jacket supporting an offshore wind turbine. Wind Energy, 17(1), 87-104.

[5] Dimitrov, N. (2016). Comparative analysis of methods for modelling the short-term probability distribution of extreme wind turbine loads. Wind Energy, 19(4), 717-737.

[6] Lott, S., & Cheng, P. W. (2016, September). Load extrapolations based on measurements from an offshore wind turbine at alpha ventus. In Journal of Physics: Conference Series (Vol. 753, No. 7, p. 072004). IOP Publishing.

[7] Cao, Y., Zavala, V. M., & D'Amato, F. (2018). Using stochastic programming and statistical extrapolation to mitigate long-term extreme loads in wind turbines. Applied energy, 230, 1230-1241.

[8] Cheng, Z., Madsen, H. A., Chai, W., Gao, Z., & Moan, T. (2017). A comparison of extreme structural responses and fatigue damage of semi-submersible type floating horizontal and vertical axis wind turbines. Renewable Energy, 108, 207-219.

[9] Li, L., Cheng, Z., Yuan, Z., & Gao, Y. (2018). Short-term extreme response and fatigue damage of an integrated offshore renewable energy system. Renewable Energy, 126, 617-629.

[10] Xu, K., Zhang, M., Shao, Y., Gao, Z., & Moan, T. (2019). Effect of wave nonlinearity on fatigue damage and extreme responses of a semi-submersible floating wind turbine. Applied Ocean Research, 91, 101879.

[11] Wang, S., Nejad, A. R., Bachynski, E. E., & Moan, T. (2020). Effects of bedplate flexibility on drivetrain dynamics: Case study of a 10 MW spar type floating wind turbine. Renewable Energy, 161, 808-824.

[12] Wang, S., Moan, T., & Nejad, A. R. (2021). A comparative study of fully coupled and de-coupled methods on dynamic behaviour of floating wind turbine drivetrains. Renewable Energy, 179, 1618-1635.

[13] Yu, W., Müller, K., Lemmer, F., Bredmose, H., Borg, M., Sanchez, G., & Landbo, T. (2017). Public definition of the two LIFES50+ 10MW floater concepts. LIFES50+ Deliverable, 4.

[14] Bak, C., Zahle, F., Bitsche, R., Kim, T., Yde, A., Henriksen, L. C., ... & Natarajan, A. (2013). The DTU 10-MW reference wind turbine. In Danish wind power research 2013.

[15] Muggiasca, S., Taruffi, F., Fontanella, A., Di Carlo, S., Giberti, H., Facchinetti, A., & Belloli, M. (2021). Design of an aeroelastic physical model of the DTU 10MW wind turbine for a floating offshore multipurpose platform prototype. Ocean Engineering, 239, 109837.

[16] Yu, Z., Amdahl, J., Rypestøl, M., & Cheng, Z. (2022). Numerical modelling and dynamic response analysis of a 10 MW semi-submersible floating offshore wind turbine subjected to ship collision loads. Renewable Energy, 184, 677-699.

[17] Wang, S., Moan, T., & Jiang, Z. (2022). Influence of variability and uncertainty of wind and waves on fatigue damage of a floating wind turbine drivetrain. Renewable Energy, 181, 870-897.

[18] Hu, R., Le, C., Gao, Z., Ding, H., & Zhang, P. (2021). Implementation and evaluation of control strategies based on an open controller for a 10 MW floating wind turbine. Renewable Energy, 179, 1751-1766.

[19] Yu, W., Müller, K., Lemmer, F., Schlipf, D., Bredmose, H., Borg, M., ... & Andersen, H. (2018). LIFES50+ D4. 2: Public definition of the two LIFES50+ 10 MW floater concepts. University of Stuttgart.

[20] Moriarty, P. J., & Hansen, A. C. (2005). AeroDyn theory manual (No. NREL/TP-500-36881). National Renewable Energy Lab., Golden, CO (US).

[21] Damiani, R., Jonkman, J., & Hayman, G. (2015). SubDyn user's guide and theory manual (No. NREL/TP-5000-63062). National Renewable Energy Lab.(NREL), Golden, CO (United States

[22] Wendt, F. F., Andersen, M. T., Robertson, A. N., & Jonkman, J. M. (2016, June). Verification and validation of the new dynamic mooring modules available in FAST v8. In The 26th International Ocean and Polar Engineering Conference. OnePetro.

[23] Jonkman, J., & Musial, W. (2010). Offshore code comparison collaboration (OC3) for IEA Wind Task 23 offshore wind technology and deployment (No. NREL/TP-5000-48191). National Renewable Energy Lab.(NREL), Golden, CO (United States).

[24] Robertson, A., Jonkman, J., Musial, W., Popko, W., & Vorpahl, F. (2014). IEA Wind Task 30 Offshore Code Comparison Collaboration Continued.

[25] Coulling, A. J., Goupee, A. J., Robertson, A. N., Jonkman, J. M., & Dagher, H. J. (2013). Validation of a FAST semi-submersible floating wind turbine numerical model with DeepCwind test data. Journal of Renewable and Sustainable Energy, 5(2), 023116.

[26] Wamit I. Wamit user manual. WAMIT Inc.: Chestnut Hill, MA, USA, 2006.

[27] Faltinsen O. Sea loads on ships and offshore structures[M]. Cambridge university press, 1993.

[28] Kane, T. R., & Levinson, D. A. (1983). The use of Kane's dynamical equations in robotics. The International Journal of Robotics Research, 2(3), 3-21.

[29] Cheng, Z., Madsen, H. A., Chai, W., Gao, Z., & Moan, T. (2017). A comparison of extreme structural responses and fatigue damage of semi-submersible type floating horizontal and vertical axis wind turbines. Renewable Energy, 108, 207-219.

[30] Xu, K., Zhang, M., Shao, Y., Gao, Z., & Moan, T. (2019). Effect of wave nonlinearity on fatigue damage and extreme responses of a semi-submersible floating wind turbine. Applied Ocean Research, 91, 101879.
[31] Næss A, Gaidai O. Estimation of extreme values from sampled time series[J]. Structural safety, 2009, 31(4): 325-334.
[32] Naess A, Gaidai O, Teigen P S. Extreme response prediction for nonlinear floating offshore structures by Monte Carlo simulation. Applied Ocean Research, 2007, 29(4): 221-230.
[33] Chai W, Naess A, Leira B J, et al. Efficient Monte Carlo simulation and Grim effective wave model for predicting the extreme response of a vessel rolling in random head seas. Ocean Engineering, 2016, 123: 191-203.
[34] Naess, A., & Moan, T. (2013). Stochastic dynamics of marine structures. Cambridge University Press.
[35] Peeringa, J. M. (2009). Comparison of extreme load extrapolations using measured and calculated loads of a MW wind turbine. Petten: ECN.
[36] Lott, S., & Cheng, P. W. (2016, September). Load extrapolations based on measurements from an offshore wind turbine at alpha ventus. In Journal of Physics: Conference Series (Vol. 753, No. 7, p. 072004). IOP Publishing.
[37] Li, L., Gao, Z., & Moan, T. (2013, June). Joint environmental data at five european offshore sites for design of combined wind and wave energy devices. In International Conference on Offshore Mechanics and Arctic Engineering (Vol. 55423, p. V008T09A006). American Society of Mechanical Engineers.
[38] Turbines-Part, W. (2009). 3: design requirements for offshore wind turbines. Proceedings of the IEC, 61400-3.
[39] Jonkman, B. J. (2009). TurbSim user's guide: Version 1.50 (No. NREL/TP-500-46198). National Renewable Energy Lab.(NREL), Golden, CO (United States).

Appendix

Table 6 Extreme value responses using ACER method for various return periods; 95 % confidence interval in paratheses.

Load Case	Return period	1 yr	2 yr	5 yr
	Exceedance probability, q	**7.19×10^{-5}**	**5.71×10^{-5}**	**2.28×10^{-5}**
LC1 V_{hub} = 8 m/s	RootMyb (kNm)	30726 (29149, 31682)	31084 (29393, 32082)	32479 (30315, 33645)
	LSSTipMys (kNm)	9245 (8673, 9616)	9390 (8792, 9768)	9937 (9241, 10351)
	TwrBsMyt (kNm)	328555 (318797, 336312)	332314 (322130, 340328)	346662 (334792, 355663)
LC2 V_{hub} = 12 m/s	RootMyb (kNm)	41445 (40752, 42073)	41662 (40934, 42338)	42485 (41615, 43372)
	LSSTipMys (kNm)	15061 (14140, 15677)	15327 (14349, 15973)	16357 (15136, 17122)
	TwrBsMyt (kNm)	437049 (428032, 444853)	439643 (429627, 446865)	449561 (436751, 457982)
LC3 V_{hub} = 16 m/s	RootMyb (kNm)	33406 (32141, 34231)	33790 (32440, 34657)	35293 (33587, 36335)
	LSSTipMys (kNm)	17054 (16567, 17449)	17282 (16780, 17688)	18144 (17584, 18591)
	TwrBsMyt (kNm)	359140 (343069, 367411)	364244 (347041, 372826)	384245 (362296, 394070)

Table 7 Extreme value responses using Gumbel method for various return periods; 95 % confidence interval in paratheses.

Load Case	Return period	1 yr	2 yr	5 yr
	Exceedance probablity, q	**7.19×10^{-5}**	**5.71×10^{-5}**	**2.28×10^{-5}**
LC1, V_{hub} = 8 m/s	RootMyb (kNm)	29772 (23844, 37194)	29772 (22344, 37194)	29772 (23844, 37195)
	LSSTipMys (kNm)	9061 (6870, 11953)	9061 (6870, 11953)	9061 (6870, 11953)
	TwrBsMyt (kNm)	314083 (229636, 429680)	314083 (229636, 429680)	314084 (229636, 429681)
LC2, V_{hub} = 12 m/s	RootMyb (kNm)	41593 (28380, 61026)	41593 (28380, 61026)	41593 (28380, 61026)
	LSSTipMys (kNm)	15321 (11801, 19903)	15321 (11801, 19904)	15321 (11801, 19904)
	TwrBsMyt (kNm)	491364 (368347, 655777)	491364 (368347, 655778)	491365 (368348, 655779)
LC3, V_{hub} = 16 m/s	RootMyb (kNm)	46542 (36896, 58215)	46542 (37218, 58215)	46542 (37218, 58215)
	LSSTipMys (kNm)	17168 (13676, 21530)	17168 (13676, 21530)	17168 (13676, 21530)
	TwrBsMyt (kNm)	466508 (384880, 566002)	466510 (384880, 566003)	466510 (384882, 566004)

Paper 2

A comparison study of power performance and extreme load effects of large 10-MW offshore wind turbines

A comparison study of power performance and extreme load effects of large 10-MW offshore wind turbines

Journal:	*IET Renewable Power Generation*
Manuscript ID	RPG-2022-05-0205
Wiley - Manuscript type:	Original Research
Date Submitted by the Author:	27-May-2022
Complete List of Authors:	Wang, Shuaishuai; Norwegian University of Science and Technology Xing, Yihan; University of Stavanger Karuvathil, Anuraj; University of Stavanger Gaidai, Oleg; Shanghai Ocean University
Keywords:	wind power, wind power plants, statistical analysis, dynamic response, failure (mechanical), finite element analysis
Abstract:	The utilisation of offshore wind turbines has rapidly increased in the last decade, which has resulted in a steady increase in wind turbine sizes. The global average offshore wind turbine size has increased from 1.5 MW to 6 MW in the last two decades. The research community has started to investigate huge 10 to 15 MW offshore wind turbines in recent years, resulting in the study of very innovative floating wind turbines using various substructure technologies. With this backdrop, this paper will investigate and thoroughly compare the power performance of extreme load effects of a large offshore 10 MW turbine installed on the monopile, spar, and semisubmersible substructures. This is performed by using the average conditional exceedance rate (ACER) and Gumbel methods to predict the extreme responses under the operating conditions of 8, 12, and 16 m/s mean wind speed, representing the below-rated, rated, and above-rated regions, respectively. The aim is to consolidate and close the knowledge gap in understanding wind turbine responses across the most common offshore substructure technologies. The results show that the extreme loads experienced depends significantly on the operating regions. Further, the spar wind turbine generally experiences larger extreme loads due to larger platform pitch motion.

A comparison study of power performance and extreme load effects of large 10-MW offshore wind turbines

Shuaishuai Wang[1], Yihan Xing[2,*], Anuraj Karuvathil[2], Oleg Gaidai[3]

[1]Norwegian University of Science and Technology, Trondheim, Norway

[2]Department of Mechanical and Structural Engineering and Materials Science, University of Stavanger, Norway

[3]Shanghai Engineering Research Centre of Marine Renewable Energy, College of Engineering Science and Technology, Shanghai Ocean University, Shanghai, China

[*]Corresponding author: yihan.xing@uis.no

Abstract

The utilisation of offshore wind turbines has rapidly increased in the last decade, which has resulted in a steady increase in wind turbine sizes. The global average offshore wind turbine size has increased from 1.5 MW to 6 MW in the last two decades. The research community has started to investigate huge 10 to 15 MW offshore wind turbines in recent years, resulting in the study of very innovative floating wind turbines using various substructure technologies. With this backdrop, this paper will investigate and thoroughly compare the power performance of extreme load effects of a large offshore 10 MW turbine installed on the monopile, spar, and semisubmersible substructures. This is performed by using the average conditional exceedance rate (ACER) and Gumbel methods to predict the extreme responses under the operating conditions of 8, 12, and 16 m/s mean wind speed, representing the below-rated, rated, and above-rated regions, respectively. The aim is to consolidate and close the knowledge gap in understanding wind turbine responses across the most common offshore substructure technologies. The results show that the extreme loads experienced depends significantly on the operating regions. Further, it was observed that the spar wind turbine generally experiences larger extreme loads due to larger platform pitch motion.

Keywords: Floating wind turbine, FAST, Extreme value analysis, ACER method, Gumbel method

1. Introduction

Low-carbon technologies have been becoming essential because they can effectively facilitate the transformation from fossil fuels to renewable energy and thus promote the realisation of the global sustainable energy goal. Wind power is one of the significant renewable energy sources in accelerating the global energy transition. Even though the onshore wind market dominates, offshore wind power demonstrates excellent potential for rapid development due to the vast untapped resources.

According to the substructure type, offshore wind turbines (OWTs) can be categorised by fixed types, such as Triple, Tripod, Gravity base, Jacket, Monopile; and floating types, such as spar, semisubmersible, barge, and tension-leg platform (TLP). In the offshore wind report by Wind Europe [1], by the end of 2020, Monopile OWT in Europe reached a cumulative 4681 units and remained the most used type with a market share of approximately 81.2%. In contrast, all floating wind turbines (FWTs) account for only about 0.2% of total units. This is because FWTs are usually installed at distant shore locations where the wind resources are more stable and abundant than the near coast; the installations of the bottom-fixed offshore turbine in regions with water depth exceeding 50-60 m are not economically attractive [2]. However, floating offshore wind has been attracted significant attention in recent years and shows a massive prospect for rapid development.

To promote the successful evolvement of offshore wind from shallow water to deep water regions, a significant reduction of the levelized cost of energy (LCOE) is necessary. FWTs are generally based on classical substructure design, such as the spar, semisubmersible, and TLP, developed by learning from the oil and gas industry [3]. However, different design criteria are needed to design OWT substructures compared to the offshore oil and gas platforms. This is because offshore oil and gas platforms mainly withstand wave loads, while OWTs also have to withstand substantial wind loads. OWTs are usually designed following the international standard IEC 61400-3 [4], covering additional wave, current, and tidal conditions in the general sea states. However, the IEC 61400-3 standard cannot be used as the basis for FWT design yet.

Compared to the bottom-fixed OWTs, FWTs are still in the early stage of technology, mainly due to the superficial understanding of complex dynamics. FWTs present strong nonlinearity in the dynamic behaviour because of the interactions of the aerodynamic and hydrodynamic loads, the structural flexibility, the advanced controller system, and the stochastic turbulent wind and irregular wave conditions. In addition, various conditions, including start-up, normal operating, faulted and emergent shutdown, and parked conditions, increase the complexity of the dynamic behaviour of FWTs.

The power and dynamic load effect performance of OWTs differ in different substructure supports, which have been presented in several studies, i.e., [5][6][7][8]. Although these studies addressed specific comparisons between different OWTs, much more efforts need to be devoted to getting more profound insight into the dynamic behaviour of FWTs, which will be the basis for technology improvement and LCOE reduction. Extreme response analysis is an essential aspect of OWTs because the extreme responses are the basis for the

ultimate limit state (ULS) check, a fundamental criterion for OWT structural design. Aggarwal et al. [9] studied 3-h short term extreme motions for a 5-MW spar-type FWT. Chen et al. [10] presented a modified environmental contour method (MECM) for long-term extreme response analysis of OWTs. Tower base and monopile extreme loads of a 5-MW bottom-fixed OWT estimated by full long-term analysis, ECM, and MECM methods were compared, and the results showed that the proposed MECM could achieve a more accurate prediction of the extreme structural loads than the traditional ECM. Xu et al. [11] proposed an averaged conditional exceedance rate (ACER) method to investigate the extreme structural responses of a 5-MW semisubmersible FWT. The focus of the work was to compare the ACER method with the conventional Gumbel method, and the results showed that the proposed ACER method could perform the extreme value analysis for FWTs more accurately and efficiently.

However, there is a lack of comparison of extreme responses between different support type OWTs, which can be an essential basis in contributing to the improvement of the design guidelines for FWTs. To close this knowledge gap, this study proposes a comparative study of the power generation and extreme response analysis for three 10-MW OWTs supported on the bottom-fixed, spar, and semisubmersible substructures, respectively.

2. Floating wind turbine concepts

Three 10-MW offshore wind turbine concepts: a monopile bottom-fixed, a spar and a semisubmersible type, are used in this study. The Technical University of Denmark (DTU)10-MW reference wind turbine (RWT) [12] is employed in the three offshore concepts, which were developed by upscaling from the National Renewable Energy Laboratory (NREL) 5-MW wind turbine but emphasised the optimised design of the rotor blades. The 10-MW RWT is a three-bladed upwind clockwise rotating wind turbine with varying speed pitch control arrangement... The wind turbine is designed with a cut in speed of 4m/s, a rated speed of 11.4m/s and a cut-out speed of 25 m/s. In addition, the minimum and maximum rotor speeds are 6.0 rpm and 9.6 rpm, respectively. More detailed information about the DTU0-MW RWT can be found in the technical report [12].

The sketches of the monopile-, spar- and semi-submersible-type offshore wind turbines are illustrated in Fig. 1. Each offshore wind turbine concept is described in greater detail in Sections 2.1-2.3, respectively.

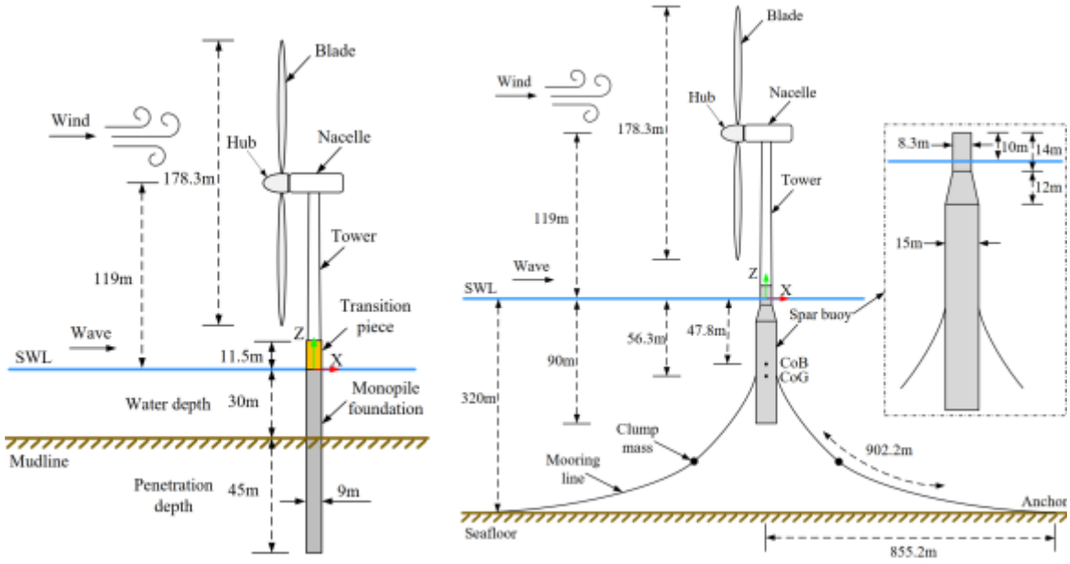

(a) bottom-fixed monopile [2] (b) floating spar type [3]

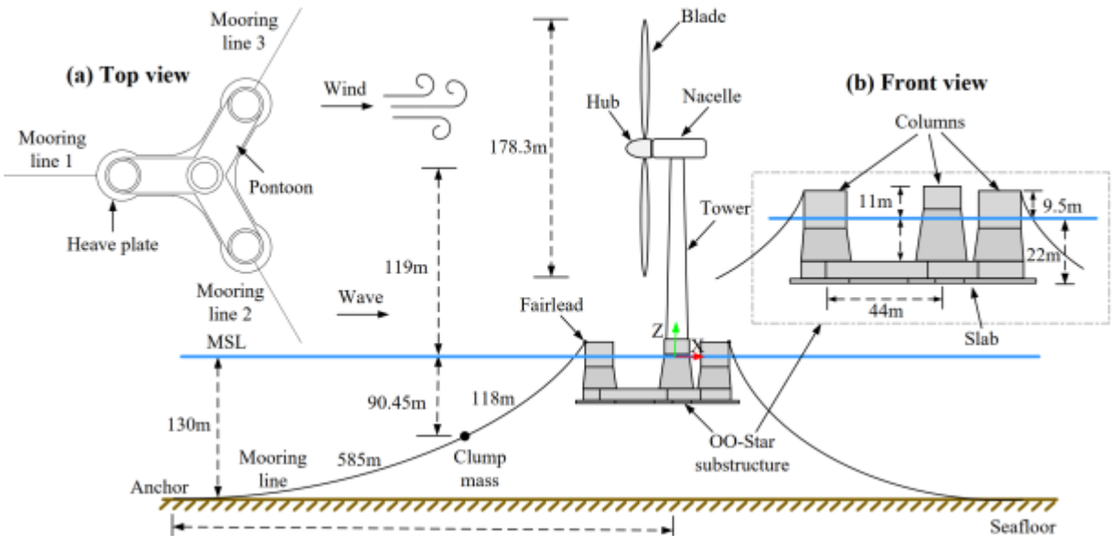

(c) floating semisubmersible type [4]

Fig. 1. Sketches of the 10-MW bottom-fixed monopile, floating spar-, and semisubmersible types offshore wind turbine concepts.

2.1. Bottom-fixed monopile concept

The 10-MW bottom-fixed monopile wind turbine concept used in the present work was designed by Velarde and Bachynski [13]. The monopile foundation was designed for a water depth of 30 m. Parameters of the pile diameter, thickness, penetration depth of the monopile foundation, and the tower material, diameter, and thickness are determined to obtain the desired natural frequency. The desired natural frequency of the monopile turbine structure is in a soft-stiff region and falls outside the blade 1P and 3P excitation regions to avoid structural resonance. A natural frequency of 0.251 Hz was realised based on the design considerations. Detailed specifications of the monopile-support wind turbine are illustrated in Fig. 1 (a) and are presented in the paper [13].

2.2. Spar-type floating concept

Hegseth and Bachynski [14] designed the spar platform for supporting the 10-MW RWT. The spar support structure was developed from the OC3-Hywind spar concept [15], but the draft of the hull for the 10-MW RWT model was reduced to 90m to make it applicable in intermediate water depths. To improve the hydrodynamic stability and buoyancy, the diameter of the hull and the ballast mass was increased. A heavy ballast was also placed at the bottom of the hull to improve stability.

The spar platform consists of two cylinders with different diameters and is connected by a taper section, as illustrated in Figure 1(b). The tower length and bottom diameter are modified from the DTU 10-MW RWT to join the spar platform. As a result, the dimensions of the tower sections are adjusted accordingly to maintain the same hub height as the land-based RWT; meanwhile, to make the natural frequencies in tower bending moment modes above the rotor 3P excitation range.

The spar-type floating wind turbine with the catenary mooring system improves the yaw stiffness by using a rotational spring. The fairleads are placed at the centre of gavity (COG) to reduce the coupling of surge and pitch motions. The 10-MW spar-type floating wind turbine was introduced in greater detail in Figure 1(b) and the reference [14].

2.3. Semisubmersible type floating concept

The semisubmersible platform for supporting the 10-MW Reference Wind Turbine was designed and developed by Dr.techn. Olav Olsen as described in the LIFES 50+ project [16]. In the LIFES 50+ project, two semisubmersible concrete concepts were designed, and the OO-Star concrete concept is used in the present work. The OO-Star platform consists of three outer columns and a central column where the turbine is installed on the central column. The four columns are mounted on three pontoons, and each pontoon connects an outer column and the main column. A heave plate is attached at the bottom of the pontoons to increase the natural heave period.

Because the central column of the platform has an 11m height above the mean sea level, the tower length is shortened accordingly to maintain the same hub height of the land-based RWT. Moreover, the outer diameter of the tower bottom is modified to match the interface of the platform's central column. Then, the wall thickness and outer diameter of each tower segment were adjusted to avoid the resonance of the coupled tower-platform structure.

Three catenary mooring lines are used for station keeping, and the horizontal angle between two adjacent lines is 120 degrees. A clumped mass is attached to each mooring line to increase the mooring tension. More details of the OO-Star semisubmersible FWT system are demonstrated in Fig. 1 (c) and inthe LIFES50+ project reports [16][17].

3. Methodology

3.1. Aero-hydro-servo-elastic dynamic analysis of the 10-MW OWT models

The aero-hydro-servo-elastic fully coupled numerical analysis of the 10-MW monopile, spar, and semisubmersible OWT models are carried out by using the simulation tool SIMA [18]. SIMA is sophisticated software for marine operations and mooring analysis, and it has been successfully used for bottom-fixed and floating OWT dynamic analysis. The simulation tool integrates two computer codes: SIMO and RIFLEX. SIMO calculates the hydrodynamic loads and dynamic motions of floating structures. RIFLEX is a nonlinear finite element solver for calculating the structural responses of flexible elements, and it also provides an external controller for blade pitch and shaft torque controls. The simulation software can reasonably account for the aerodynamics, hydrodynamics, structural dynamics, and control system dynamics for OWT analysis.

The identical rotor, hub, and nacelle are used in the monopile, spar and semisubmersible OWT models. The hub, nacelle, spar and semisubmersible floating platforms are considered rigid bodies. The blades, tower, shaft and monopile are modelled by nonlinear beams. Nonlinear p-y curves model the laterally of the monopile below the mud line. Mooring lines in the spar and semisubmersible FWTs are modelled by nonlinear bar elements, where only the axial stiffness is considered.

Blade element momentum theory is used to calculate the forces on the wind turbine. The momentum theory refines the induced velocities calculation is used to analyse the aerodynamics loads on the rotor of the monopile, spar and semisubmersible. Advanced corrections include Prandtl and Glauert for hub and tip loss, dynamic wake correction, tower shadow, dynamic stall, and skewed inflow corrections.

Hydrodynamic loads on the monopile and mooring lines are calculated based on Morison's equation, where both the drag and inertial terms are included. The hydrodynamic loads on the spar and semisubmersible hulls are computed using the potential flow theory and Morison's equation. First-order wave loads on the structural hulls

are first obtained in the panel model's frequency domain; then, they are applied in the time domain using the convolution techniques. The drag term of Morison's equation is used to account for the viscous forces omitted in the potential flow theory in the two FWTs.

The control system for the three OWT models consists of the blade pitch control and the generator torque control, and they are written in JAVA and applied through the interface in RIFLEX. The proportional and integral coefficients, KP and KI, of the controller in the monopile OWT are those of the original values used in the onshore RWT. However, the controller coefficients used in the spar and semisubmersible FWTs are modified to avoid the negative damping effect and thus prevent unstable pitch motions.

3.2. Extreme value prediction

In any stochastic process *X(t)* taken across a period (*T*), the extreme value is the largest maxima extracted from a group of individual maxima.

$$X_e = \boldsymbol{max}\{X_{m1},X_{m2},X_{m3},....,X_{mn}\}\ ,\ i = 1,...,n \qquad (1)$$

where X_e describes the largest maximum value and X_{mi} describes the individual maxima. Therefore, from this assumption, it is observed that the individual maxima are independently and identically distributed across the common distribution function $F_{Xm}(x)$. Thus, from the equation below, the distribution of X_e is labelled as:

$$F(x) = \boldsymbol{Prob}\{X_e \leq x\} = \ [F_{Xm}(x)]^n\ ,\ i = 1,...,n \qquad (2)$$

Various statistical methods have been used to approximate an extreme value distribution. Examples of the extreme value methods used in the study of wind turbines include an estimation of extreme structural responses in floating vertical axis wind turbines by Cheng et al. [19] and extreme responses due to wave irregularity on an offshore floating wind turbine by Xu et al. [20]. The two popular techniques used in this paper the ACER method (Section 3.3) and the Gumbel method (Section 3.4).

3.3. ACER (Average Conditional Exceedance Rate)

This paper uses the ACER method to estimate extreme structural responses. The method was proposed by Naess and Gaidai [21], and it is derived for a discretely sampled response process. The cascade of conditional approximation is the basis for calculating the exceedance probability for extreme value estimation. The primary purpose of the ACER method is to accurately determine the distribution function of the extreme value, which is denoted as $M_N = max\{X_j; j = 1, \cdots, N\}$. Let $P_\eta = Prob(M_N \leqslant \eta)$ denotes the probability of the occurrence of the extreme value η and it follows:

$$P_\eta = Prob(M_N \leqslant \eta) = Prob(X_1 \leqslant \eta, \cdots, X_N \leqslant \eta) \qquad (3)$$

To solve this equation efficiently, a cascade of conditional approximation $P_k(\eta)$ is used, where $P_k(\eta)$ tends to be close to P_η as k increases. For N "1 and $\mathrm{k} = 1,2, \cdots, P_k(\eta)$ is represented as:

$$P_k(\eta) \approx exp(-\sum_{j=k}^{N}\alpha_{kj}(\eta)) \qquad (4)$$

where $\alpha_{kj}(\eta) = Prob(X_1 > \eta | X_{j-1}"\eta, \cdots, X_{j-k+1} \leqslant \eta)$ And it represents the exceedance probability conditional on $\mathrm{k}-1$ previous non-exceedances.

Equation (4) will be calculated based on the ACER, which is defined as:

$$\varepsilon_k(\eta) = \frac{1}{N-k+1}\sum_{j=k}^{N}\alpha_{kj}(\eta), k = 1,2,\cdots \qquad (5)$$

For $k \geq 2$, $\tilde{\varepsilon}_k(\eta)$ is used instead of $\varepsilon_k(\eta)$ because it is easier to use for nonstationary or long-term statistics, and it is defined as:

$$\tilde{\varepsilon}_k(\eta) = \lim_{N\to\infty} \frac{\sum_{j=k}^{N} a_{kj}(\eta)}{N-k+1} \quad (6)$$

where $a_{kj}(\eta)$ is the realised values for the observed time series, and $\lim_{N\to\infty} \frac{\tilde{\varepsilon}_k(\eta)}{\varepsilon_k(\eta)} = 1.$

For both stationary and nonstationary time series, the sample estimate of the ACER can be denoted as:

$$\hat{\varepsilon}_k(\eta) = \frac{1}{R}\sum_{r=1}^{R} \hat{\varepsilon}_k{}^{(r)}(\eta) \quad (7)$$

where *R* is the number of samples, and

$$\hat{\varepsilon}_k{}^{(r)}(\eta) = \frac{\sum_{j=k}^{N} a_{kj}{}^{(r)}(\eta)}{N-k+1} \quad (8)$$

where *r* denotes the realisation number.

When the realisations are sufficiently numerous and assumed to be independent, then the 95 % confidence interval (CI) for the ACER can be estimated as:

$$CI(\eta) = \hat{\varepsilon}_k(\eta) \pm 1.96 \hat{s}_k(\eta) / \sqrt{R} \quad (9)$$

where $\hat{s}_k(\eta)$ refers to the standard deviation of samples and can be estimated by:

$$\hat{s}_k(\eta)^2 = \frac{1}{R-1}\sum_{r=1}^{R} (\hat{\varepsilon}_k{}^{(r)}(\eta) - \hat{\varepsilon}_k(\eta))^2 \quad (10)$$

The above equations for estimation of average exceedance rate are based on direct numerical simulations. In contrast, an extrapolation technique can reduce the computational time.

Assuming the mean exceedance rate in the tail behaves similarly to $exp\{-a(\eta-b)^c\}(\eta \geq \eta_0 \geq b)$, where *a*, *b* and *c* are suitable constants. The ACER will therefore be assumed by:

$$\varepsilon_k(\eta) \approx q_k(\eta) exp\{-a_k(\eta-b_k)^{c_k}\}, \eta \geq \eta_0 \quad (11)$$

where the function $q_k(\eta)$ varies slowly compared to the exponential function $exp\{-a_k(\eta-b_k)^{c_k}\}$ in the tail region, thus it can be replaced by a constant for a suitable choice of the tail marker η_0.

Finally, the Levenberg-Marquardt least-squares optimisation method can be used to determine the constants *a*, *b*, *c* and *q*. Based on this, the probability of the occurrence of the extreme value can be obtained by the ACER method. In the studies of Naess et al. [22] and Chai et al.[23] it is shown that the extrapolation technique can achieve a satisfactory estimation of the extreme values but saves significant simulation time. Detailed descriptions of the ACER method can be found in the reference [24].

3.4. Gumbel fitting method

Extreme value distribution Eq. (2) has been proven to converge to the Gumbel, Fréchet or Weibull distribution if the sample size (*n*) is large enough. Therefore, these distributions are also recognised as the Type I, II and III

extreme value distributions, respectively and are a family of cumulative distribution probability that combines the generalied extreme value (GEV) distribution.

$$F_{X_e}(x) = exp\left(-\left(1 + \gamma\left(\frac{x-\mu}{\beta}\right)\right)^{-\frac{1}{\gamma}}\right) \quad (12)$$

where β describes the scale parameter, γ describes the shape parameter, and μ represents the location parameter. The limiting of γ→0 allows the approximation to fit the Gumbel distribution, commonly used as a recommendation when modelling marine structures [25].

$$F_{X_e}(x) = exp\left(-exp\left(-\frac{x-\mu}{\beta}\right)\right) \quad (13)$$

Eq. (13) can be rewritten by using a logarithm on the equation, allowing it to become a linear function.

$$-ln\left(ln\left(F_{X_e}(x)\right)\right) = \frac{x}{\beta} - \frac{\mu}{\beta} \quad (14)$$

The parameters β and μ can be approximated from the original data using the least-square fitting method from the cumulative distribution probability, i.e., a straight line on a probability paper [26].

3.5. Environmental conditions and load cases

The environmental conditions at site 14 in the Northern part of the North Sea are used in the presented work, where the 10-MW FWT is assumed to be installed. The environmental data are selected from a long-term joint distribution of mean wind speed at 10 m height above the sea level (U_{10}), significant wave height (H_s), and spectral peak period (T_p). The wind and wave distribution was developed by a hindcast model using the measured raw data from 2001-to 2010 of the location as a database, as proposed in the study of Li et al. [27].

The long-term joint wind and wave distribution can be written as:

$$f_{U_{10},H_s,T_p}(u,h,t) = f_{U_{10}}(u) \cdot f_{H_s|U_{10}}(h|u) \cdot f_{T_p|U_{10},\,H_s}(t|u,h) \quad (15)$$

where $f_{U_{10}}(u)$ represents the marginal distribution of the 1-h mean wind speed U_{10}, $f_{H_s|U_{10}}(h|u)$ denotes the conditional distribution of H_s for given U_{10}, and $f_{T_p|U_{10},\,H_s}(t|u,h)$ represents the conditional distribution of T_p for given U_{10} and H_s.

A two-parameter Weibull distribution represents the marginal distribution of the U10, and the probability density function (PDF) is given by:

$$f_{U_{10}}(u) = \frac{\alpha_U}{\beta_U}\left(\frac{u}{\beta_U}\right)^{\alpha_U - 1} exp\left[-\left(\frac{u}{\beta_U}\right)^{\alpha_U}\right] \quad (16)$$

where α_U and β_U represent the shape and scale parameters, and they are 2.029 and 9.409, respectively, for the specific sea location.

A two-parameter Weibull distribution describes the conditional PDF of Hs for given U10:

$$f_{H_s|U_{10}}(h|u) = \frac{\alpha_{HC}}{\beta_{HC}}\left(\frac{u}{\beta_{HC}}\right)^{\alpha_{HC} - 1} exp\left[-\left(\frac{u}{\beta_{HC}}\right)^{\alpha_{HC}}\right] \quad (17)$$

where α_{HC} and β_{HC} are the shape and scale parameters, respectively, and they are expressed by power functions of mean wind speed:

$$\alpha_{HC} = a_1 + a_2 u^{a_3}$$
$$\beta_{HC} = b_1 + b_2 u^{b_3} \quad (18)$$

where $a_1 = 2.136, a_2 = 0.013, a_3 = 1.709, b_1 = 1.816, b_2 = 0.024, b_3 = 1.787$ are the parameters for estimating the α_{HC} and β_{HC}.

The conditional PDF of T_p for given U_{10} and H_s is fitted by a lognormal distribution:

$$f_{T_p|U_{10},\,H_s}(t|u,h) = \frac{1}{\sqrt{2\pi}\sigma_{ln(Tp)}t} exp\left[-\frac{1}{2}\left(\frac{ln(t)-\mu_{ln(Tp)}}{\sigma_{ln(Tp)}}\right)^2\right] \quad (19)$$

where $\mu_{ln(Tp)}$ and $\sigma_{ln(Tp)}$ are the parameters in the conditional lognormal distribution and they are estimated by a detailed analysis in the study of Li et al. [27].

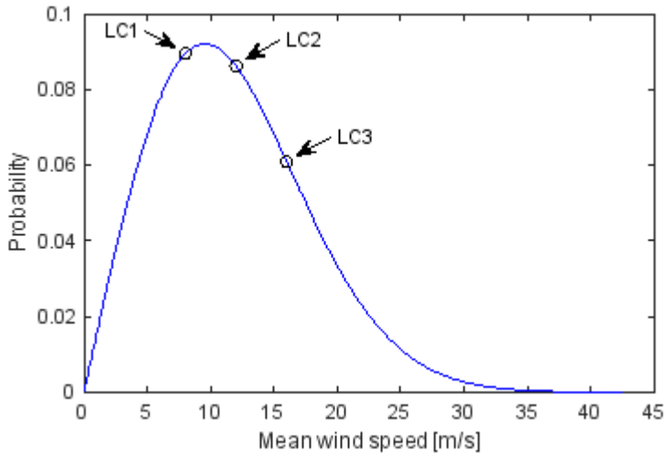

Figure 2 PDFof the average wind speed at wind turbine hub height.

Three representative environmental conditions using $U_{10,}$ H_s and T_p are considered in this paper. Correspondingly, different load cases with irregular wind and waves are analysed to study the power performance and extreme responses of the three OWTs. Mean wind speeds at the hub height are estimated based on the power-law formulation, as follows:

$$U_{10} = U_{hub}\left(\frac{10}{Z_{hub}}\right)^{\alpha} \quad (20)$$

where U_{hub} and U_{10} are the mean wind speeds at the hub height and 10 m height above the sea level, respectively. $Z_{hub} = 119m$ is the hub height of the 10-MW OWTs. According to international standard IEC 61400-3, the exponent in the power law is set at 0.14

The load cases for numerical simulations are listed in Table 4. The average wind speeds of 8m/s, 12m/s, and 16m/s at the hub height are chosen to account for the dynamics of the wind turbines under the cut-in, rated, and above rated operating zones illustrated in Fig. 2. For each given mean wind speed, the maximum probable H_s and T_p are selected according to the joint distributions of $U_{10,}$ H_s and T_p.

Table 1 Load cases for numerical simulations.

Load cases	U_{hub} **(m/s)**	T_I	H_s **(m)**	T_p **(s)**	**Samples**	**Simulation length (s)**
LC1	8	0.1740	1.9	9.7	20	4000
LC2	12	0.1460	2.5	10.1	20	4000
LC3	16	0.1320	3.2	10.7	20	4000

The turbulent wind fields are generated using the Turbsim program according to Kaimal's turbulence model defined in IEC 61400-3 [4]. Meanwhile,the JONSWAP (Joint North Sea Wave Project) spectrum modulates the

time-varying irregular waves with the respective H_s and T_p values. Wind and waves are considered to be directionally aligned in this work.

Each simulation lasted for a period of 4000 s. To remove the transient effects in the wind turbine during startup, the starting 400 s readings were eliminated. Consequently, one-hour data for each simulation is used for studying the results. 20 random wind and wave samples are considered for each environmental condition to account for the stochastic uncertainties. The power performance and extreme values are assessed based on the mean of the 20 one-hour simulations.

4. Response variables

The loads at the eight measurement points are considered. These are the tower My and Mz bending moment, blade 1 My and Mz bending moment, blade 2 My and Mz bending moment and blade 3 My and Mz bending moment

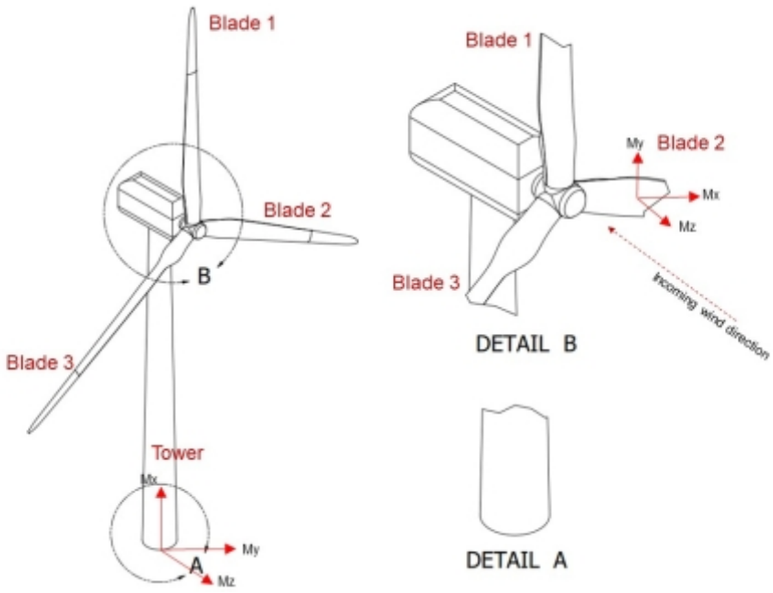

Figure 1 Bending moment measured locations.

5. Results and discussions

The empirical data is based on accurate numerical simulations using a SIMA model as presented in Section 3.1. The Gumbel and ACER methods presented in Sections 3.3 and 3.4 are used.

5.1. Time-domain responses, PSD, and maximum values

The time-domain responses for one portion of a realisation, the power spectral distributions (PSDs) for a full realisation and the maximum values of each realisation are presented in Figure 2, Figure 3, and Figure 4, respectively. These results of each load case, i.e., LC1, LC2 and LC3, are taken from one of the 20 realisations calculated. The wind and wave elevation time series and PSDs are also plotted for reference.

It is observed from the time domain responses represented in Figure 2 that the responses of the monopile and semisubmersible wind turbines are more similar compared to the spar wind turbine. The spar platform has more platform pitch responses than the semisubmersible platform; the monopile wind turbine is a fixed type offshore wind turbine with negligible pitch motion responses. Further discussions of the more significant pitch motions observed in the spar wind turbine are presented in Section 5.2.

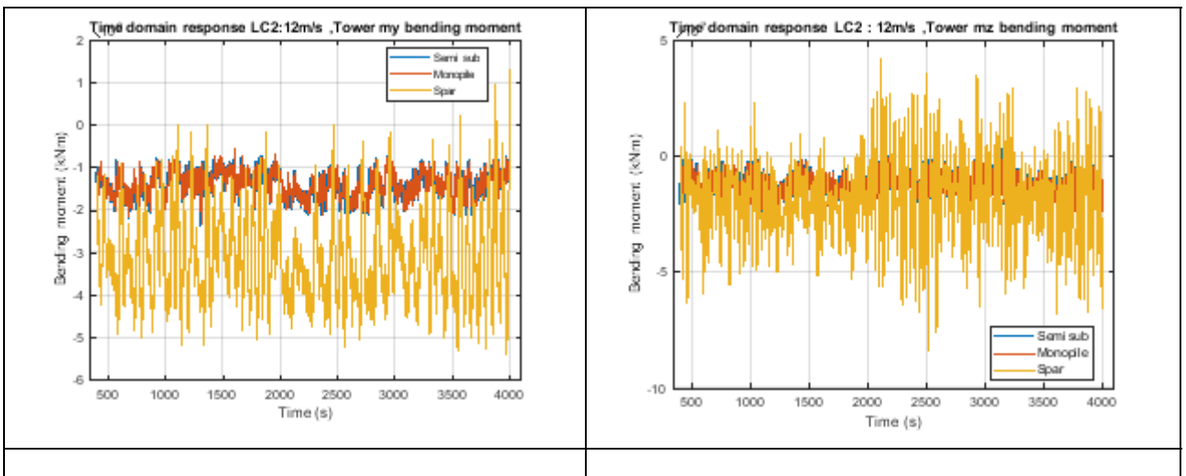

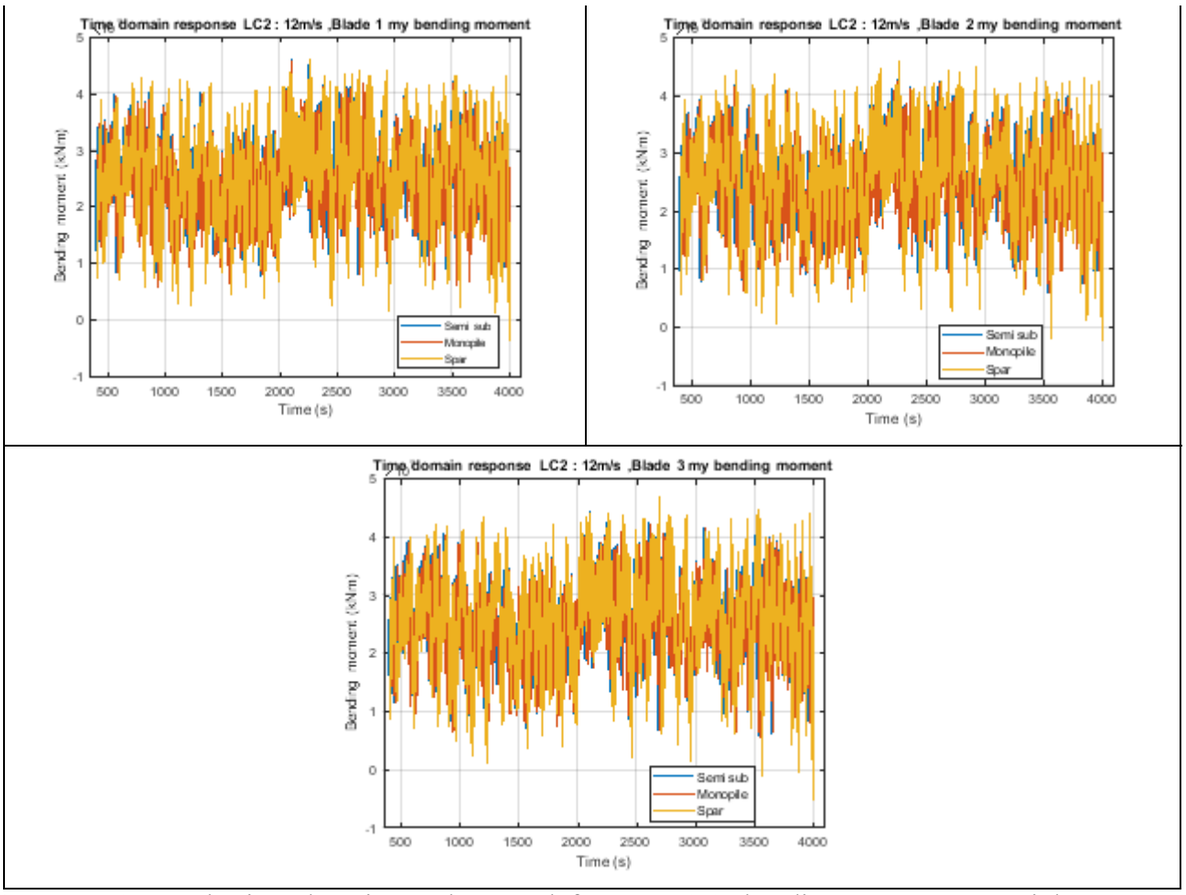

Figure 2 Example time-domain results. Top-left: Tower My bending moment; Top-right: Tower Mz bending moment; Centre-left: Blade 1 My bending moment; Centre-right: Blade 2 My bending moment; Bottom: Blade 3 My bending moment

Referring to Figure 3, the PDSs for the monopile and semisubmersible wind turbines are more similar to the spar wind turbine. These differences are due to the combined effect of the spar wind turbine's platform pitch motions and blade pitch controller, which is more prominent, leading to increased tower bottom bending and blade loads.

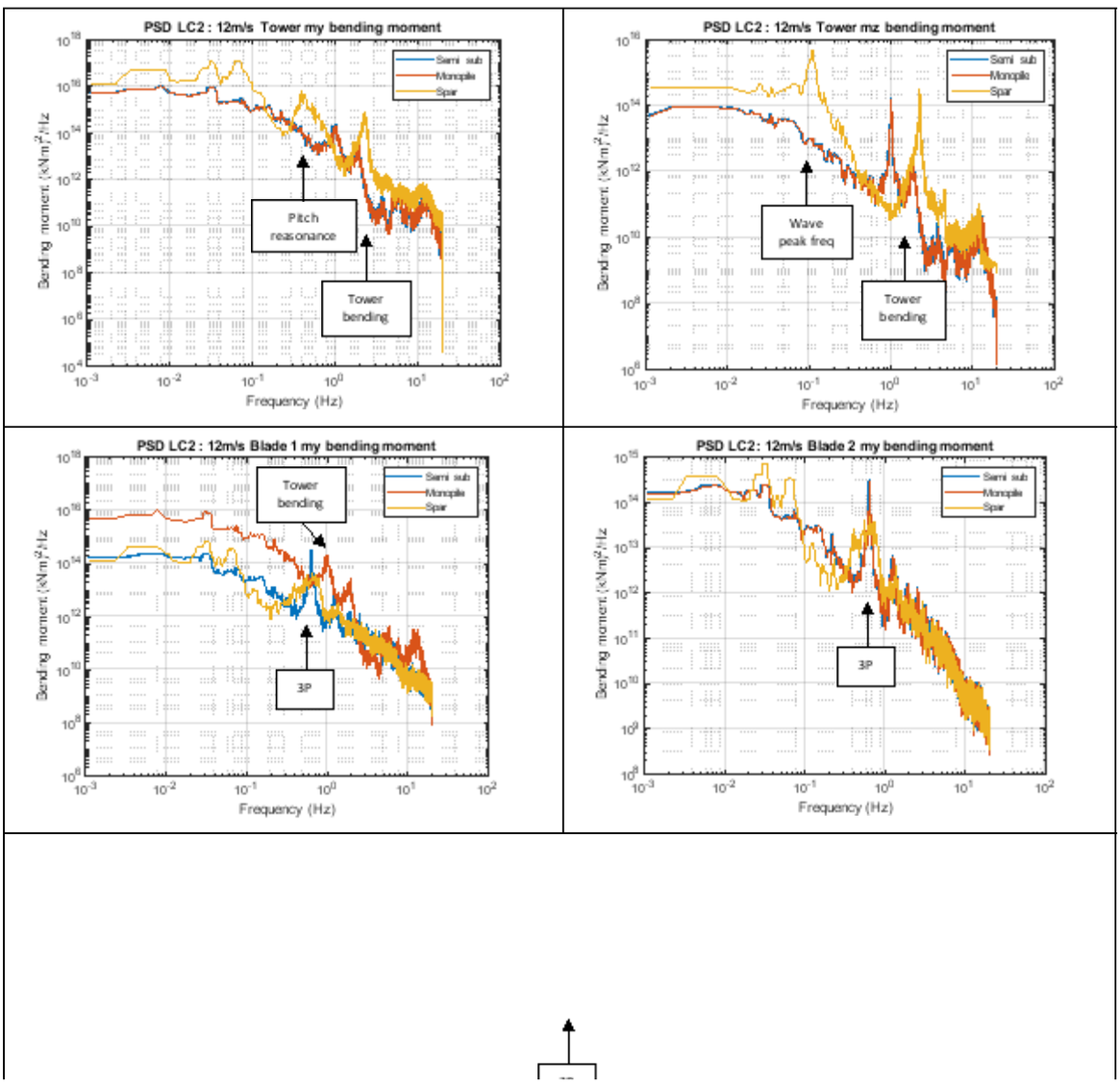

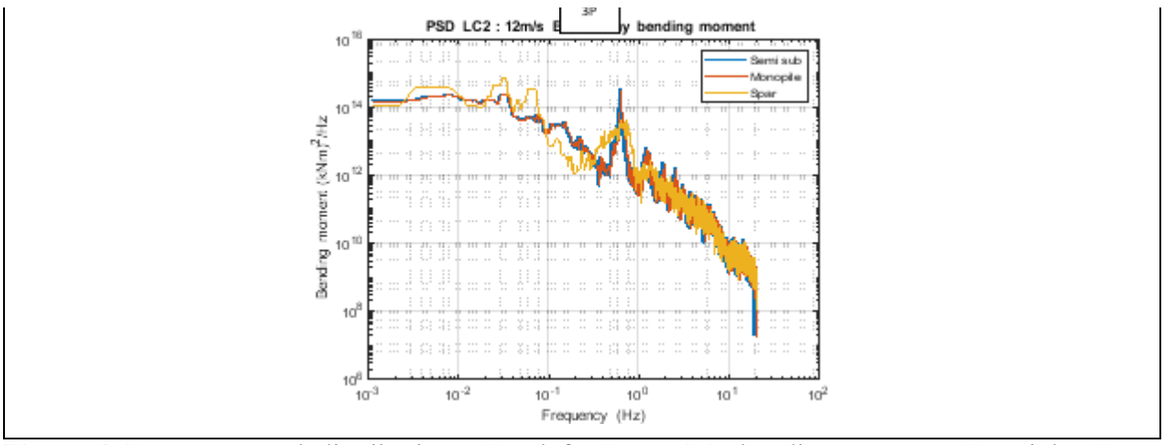

Figure 3 Power spectral distributions. Top-left: Tower My bending moment; Top-right: Tower Mz bending moment; Centre-left: Blade 1 My bending moment; Centre-right: Blade 2 My bending moment; Bottom: Blade 3 My bending moment

Several detailed observations can be made on the maximum values presented in Figure 4. The floating wind turbines have significantly larger maximum values for all responses considered; the monopile wind turbine has the smallest maximum values. For example, the blade My bending moments for the floating wind turbines are about 20 % larger than the fixed wind turbine. Further, the variation of the maximum values of the floating wind turbines is also significantly larger than the monopile wind turbine. For example, for the blade My bending moments, the variation for the floating wind turbines is about 10 %, while for the fixed wind turbine, they are about 5 %.

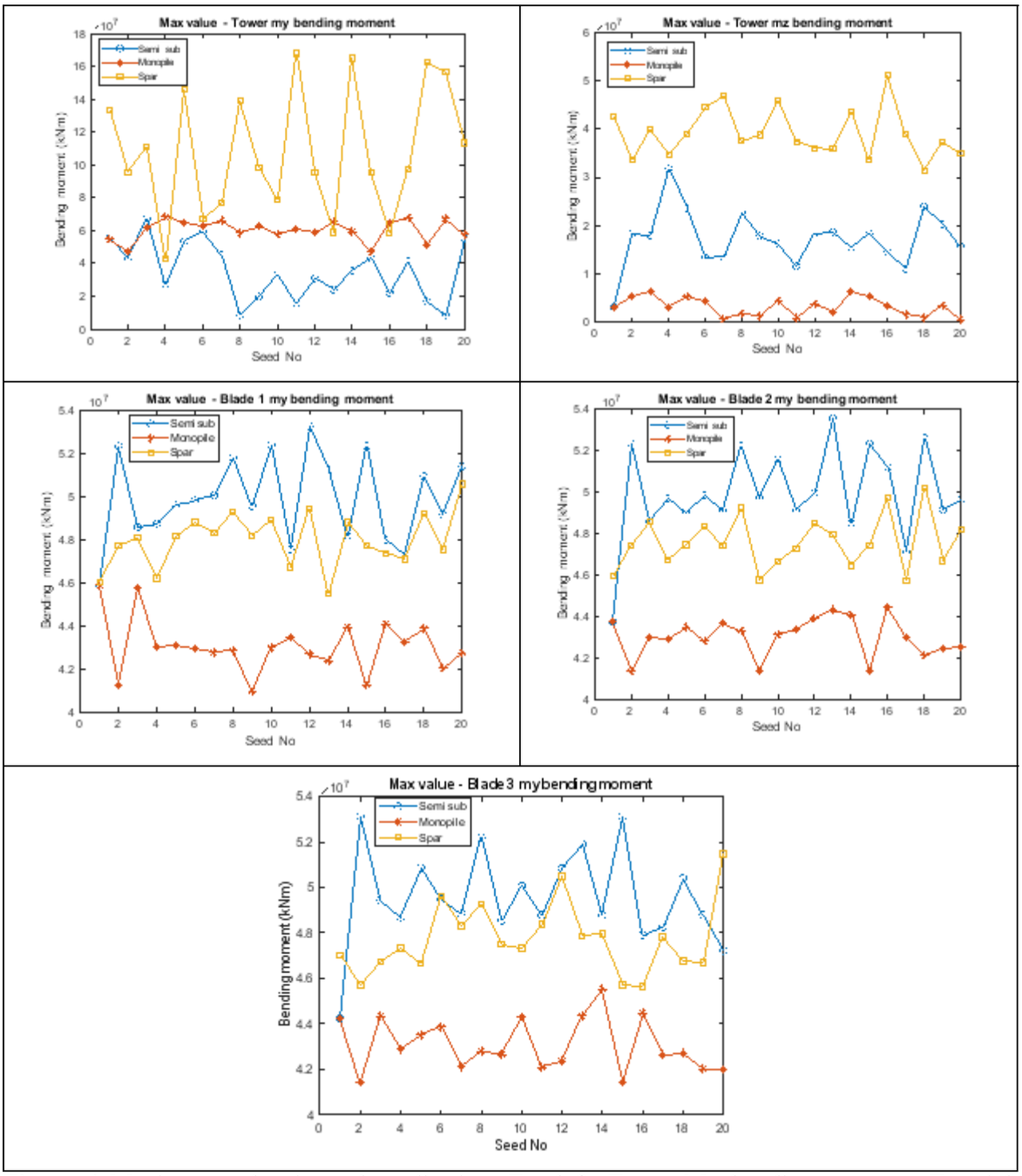

Figure 4 Maximum value in each realisation. Top-left: Tower My bending moment; Top-right: Tower Mz bending moment; Centre-left: Blade 1 My bending moment; Centre-right: Blade 2 My bending moment;

Bottom: Blade 3 My bending moment

5.2. Comparison of power performance

The power production values are presented in Figure 5 for the three environmental conditions. The mean values are presented on the left, while the standard deviations are presented on the right. The probability of the occurrence of the environmental conditions 8 m/s, 12 m/s, and 16 m/s are 0.0895, 0.0864, and 0.0611, respectively.

It is observed that the mean power production values are a little smaller for the spar concept compared to the fixed and semisubmersible turbines. This can be explained as follows. The spar turbine has a relatively small hydrostatic restoring pitch moment. The spar platform will have a mean pitch angle of some five degrees during operation. This mean pitch angle causes the rotor plane normal to be slightly out of the plane with the incoming wind, leading to less optimal power production. In contrast, the semisubmersible platform has a large hydrostatic restoring pitch moment due to the moment arms provided by the distance between the platform centre and the pontoon. This large hydrostatic restoring pitch moment leads to a small mean platform pitch angle. Therefore, the incoming wind will be aligned to the normal rotor plane, giving more optimal power production.

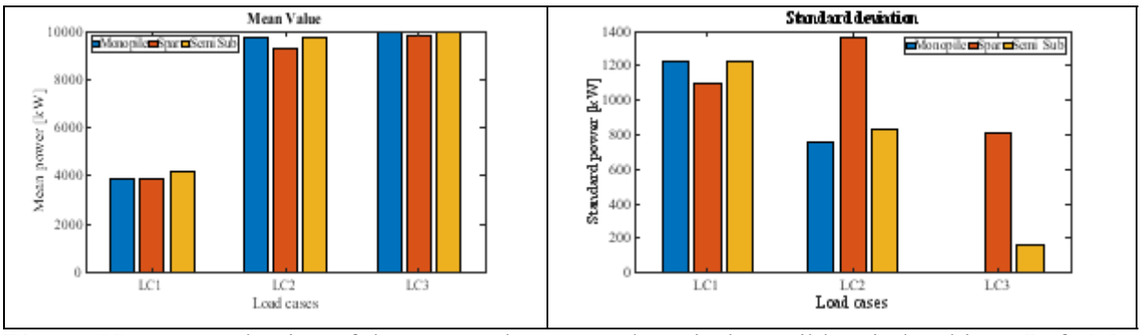

Figure 5 Power production of the monopole, spar and semisubmersible wind turbines. Left: Mean values; Right: Standard deviations.

It is observed that the standard deviations are generally large while the wind turbines are operating in the under-rated wind speed region. This is because the blade pitch controller is not active in this region, and the rotor will speed up or down accordingly to the incoming wind speed. This means the wind turbine has no control effort to limit the power fluctuations resulting from natural wind speed fluctuations. The standard deviations in the above-rated region are significantly smaller as the blade pitch controller is active and the wind turbines are limited at rated power. Tis means that the rotor speeds are constant in this region. For the fixed wind turbine, the rotor speed will be constant at the rated speed, and the wind turbine will produce at rated power without any noticeable power fluctuations. This explains the nearly zero standard deviation for the fixed wind turbine in LC3. The standard deviations in LC2 (rated wind speed) are smaller than LC3 except for the spar wind turbine. This is because, in this region, the wind turbine is operating half the time in the under-rated wind speed region and the other half in the above-rated wind speed region. Therefore, the blade pitch controller is active half the time and helps to reduce the power fluctuations in the fixed and semisubmersible wind turbines. The spar wind turbine's smaller hydrostatic pitch restoring ability leads to significantly more significant standard deviations in the power production values. This is due to more significant platform pitch motions.

5.3. Extreme load effects using ACER and Gumbel methods

5.3.1. Example extrapolation plots

This section presents the extreme load responses using the ACER and Gumbel methods for the three operating conditions (LC1 – LC3) presented in Table 1. k = 6 is used. For illustration, the example plots of the ACER extrapolation and Gumbel fitting are presented in Figure 6.

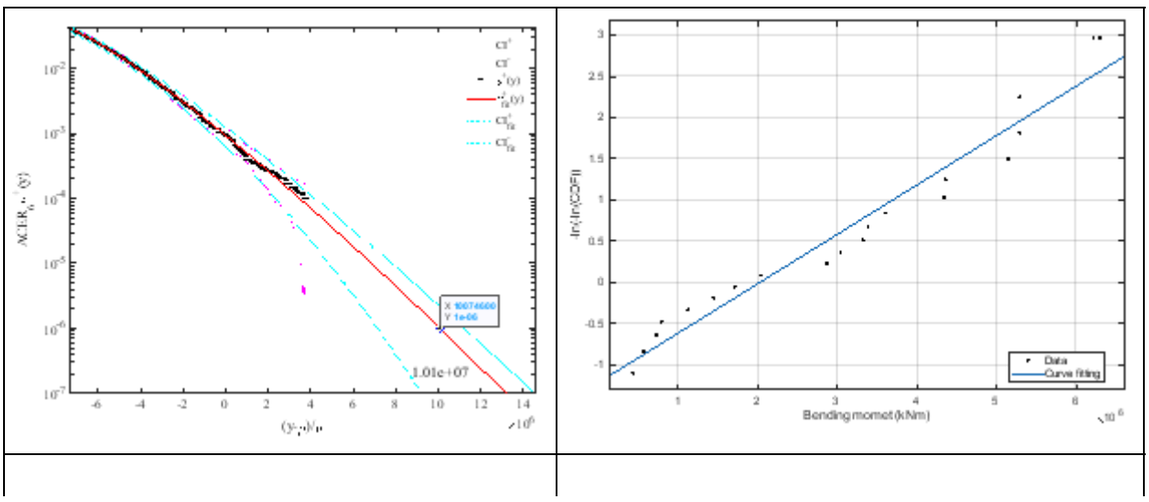

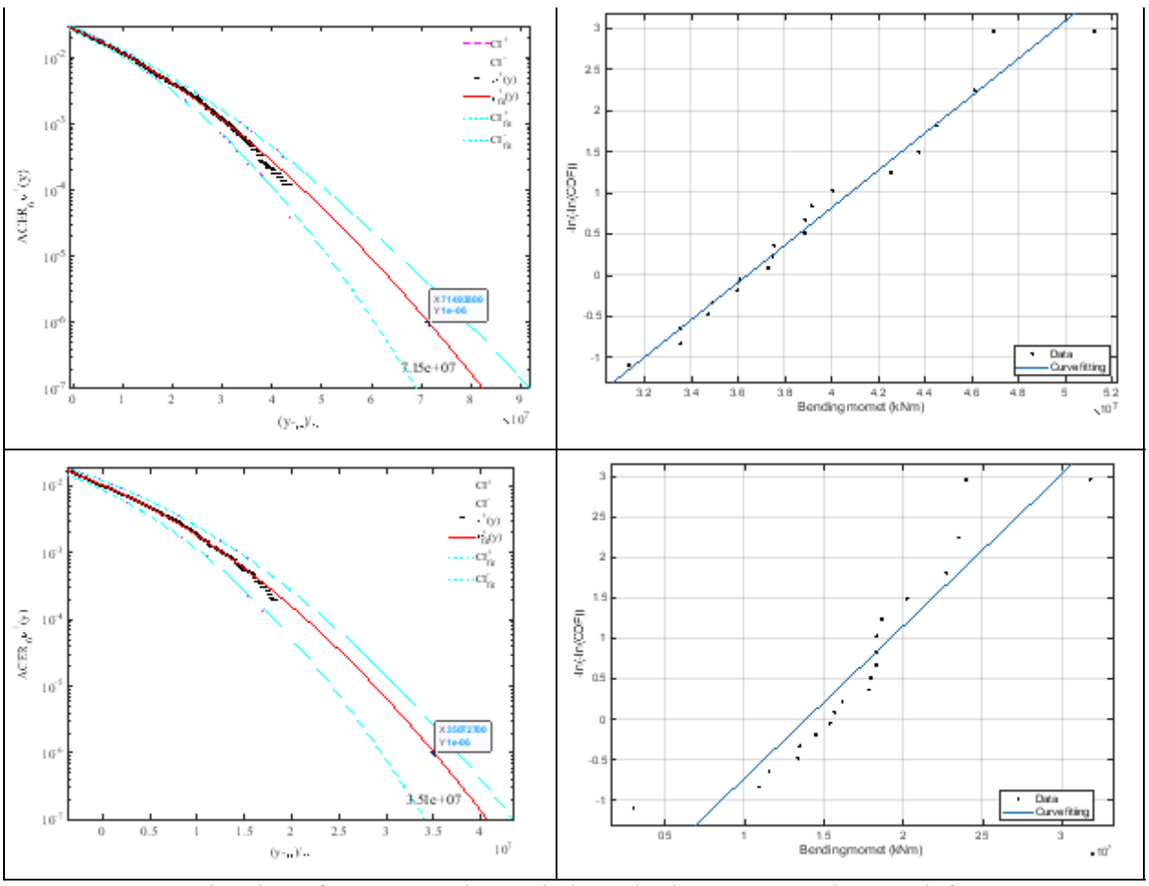

Figure 6 Example plot of ACER and Gumbel method LC 2: 12m/s. Top-left: ACER Monopile Tower Mz bending moment; Top-right: Gumbel Monopile Tower Mz bending moment; Centre-left: ACER Spar tower Mz bending moment; Centre-right: Gumbel Spar tower Mz bending moment; Bottom left: ACER Semi-submersible tower Mz bending moment; Bottom-right: Gumbel Semi-submersible tower Mz bending moment.

As illustrated by the significantly smaller confidence intervals, the ACER method can lead to more accurate results as it does not assume a distribution. The ACER method does not assume any extreme value distribution. Instead, it follows the exact shape of the data points as presented in Figure 6. On the other hand, it is observed that the Gumbel distribution does fit the upper-end tail well. The data points tend to curve up towards the left for increasing response values and are above the Gumbel line. This means the Gumbel distribution will tend to overpredict the extreme value responses. This example shows the advantages of the ACER method.

The extreme load responses and the 95 % CIs from both ACER and Gumbel methods are also plotted in Figure 6 for the example presented. The numerical values of all results are presented in Table 2 and Table 3 of the Appendix for extreme values calculated by the ACER and Gumbel methods, respectively.

5.3.2. Results and discussions

The extreme values of the bending moments are presented in Figure 7 to Figure 9 for the blade My bending moments and Figure 10 to Figure 11 for the tower bending moments. In general, the loads at below-rated wind are the smallest, these increase to the maximum at the rated wind speed and taper off in the rated wind region. Like the power values presented in Section 5.2, the extreme values for the spar wind turbine are larger than the monopile and submersible wind turbines. Further, the extreme loads of all blades are similar.

Below-rated wind

The blade extreme values for the monopile wind turbine are larger than the floating wind turbines. In this region, the pitch controller of the wind turbine is not active, and the rotor is allowed to adjust its speed freely to maintain an optimal tip speed ratio. Since the monopile wind turbine is fixed to the ground, it will not experience any platform pitch motion, and therefore it will extract the full potential from the aerodynamic power exerted by the wind on it. On the other hand, platform pitch motions in the floating wind turbines lead to a slightly less optimal aerodynamic extraction power. Consequently, the aerodynamic loads will be larger for the monopile wind turbine, leading to larger blade extreme loads.

The tower bending moments My (fore-aft) are significantly higher in the floating wind turbines than the monopile wind turbine. This is due to platform pitch responses in the floating wind turbines. The larger platform pitch results in increased bending moment acting on the tower bottom due to nacelle tilt. The tower bending moment Mz (side-side) for all three platforms are similar. This is because all three wind turbines experience similar aerodynamic shear forces.

Rated wind

In this region, the wind turbine is operating half the time in the below-rated (blade pitch controller not active) and the other half in the rated wind region (blade pitch controller active).

The blade pitch controller regulates the rotor speed when the above-rated wind speed. This reduces the wind turbine aerodynamic loads and, in general, will also reduce loads at other parts of the wind turbine. In the case of the monopile wind turbine, the effectiveness of the blade pitch controller is not affected by any platform pitch motion (since the turbine is fixed to the ground), and therefore, almost all of the controller effort is used in power regulation. This leads to lower blades and tower loads in the monopile wind turbine.

For the floating wind turbines, namely the spar and semisubmersible wind turbines, the effectiveness of the blade pitch controller is hampered by the platform pitch motion. The spar wind turbine has more significant platform pitch motions and is more affected. This leads to larger extreme loads for the spar wind turbine than the semisubmersible wind turbine for both blades and tower loads.

Above-rated wind

In this region, the blade pitch controller is constantly active. Therefore the combined effect of the blade pitch controller and the platform pitch motions on wind turbine loads will be even more prominent compared to in the rated-wind region.

The extreme loads on the monopile wind turbine are slightly lower than the loads in the rated-wind region. This is obvious as the blade pitch controller is acting to reduce aerodynamic loads all the time in this region. Note that even though there are larger waves (due to higher wind speeds) in this region, the wave loads on the monopile wind turbine are smaller than the wind loads.

The combined effect of the blade pitch controller and the platform pitch motions on the extreme loads is significant, particularly for the spar wind turbine. It is observed that the loads in the spar wind turbine are significantly larger for both the blade and tower.

ACER vs Gumbel

The extreme values presented using the ACER method are higher than the Gumbel method. However, 95 % CIs of the values predicted from the ACER method are significantly narrower than the 95 % CIs of the values predicted from the Gumbel method. This means that the ACER method is more accurate and highlights the benefits of the ACER in not assuming a distribution in the extrapolation of extreme values. Further, this indicates that the Gumbel distribution does not fit the extreme value responses very well. In addition, the 1, 2, and 5-year extreme values calculated using the Gumbel method are similar. This is due to the inaccurate fit of the probability distribution at the upper tail end. The fitted Gumbel probability density distribution slope is too steep at the upper tail end. This leads to minimal changes in the response values for a unit change in probability. The 1, 2 and 5-year extreme values are generally 1.1-1.3 times larger than the maximums of single 1-hour realisations. The relatively large range of values (about 20 %) indicates the importance of using accurate extrapolation methods to predict extreme values that can be used to define appropriate design values utilised in deterministic engineering design.

Blade 1 My bending moment, V_{hub} = 8m/s

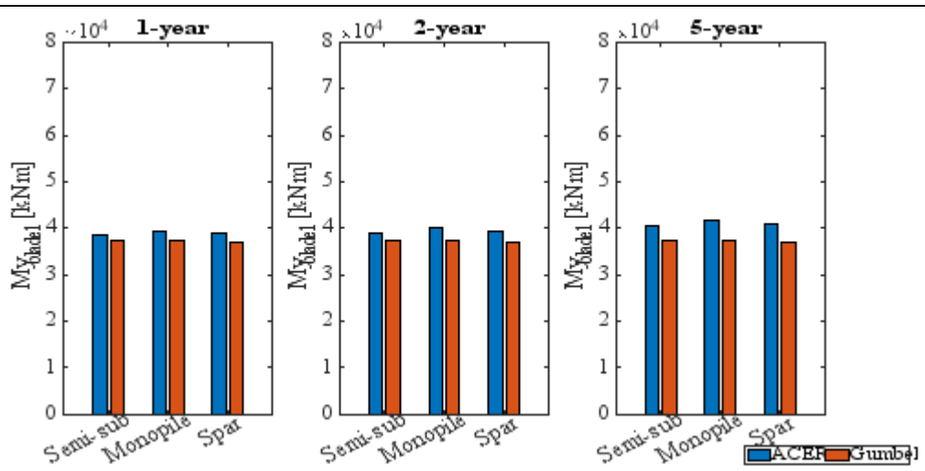

Blade 1 My bending moment, V_{hub} = 12m/s

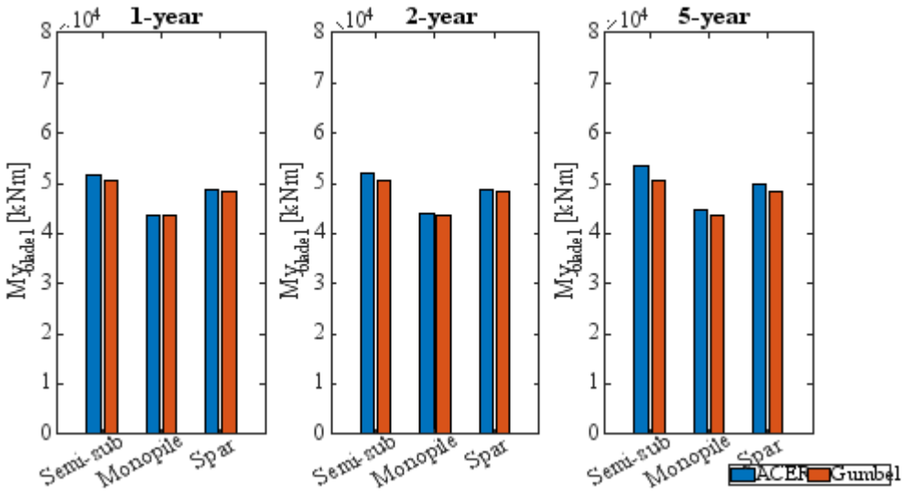

Blade 1 My bending moment, V_{hub} = 16m/s

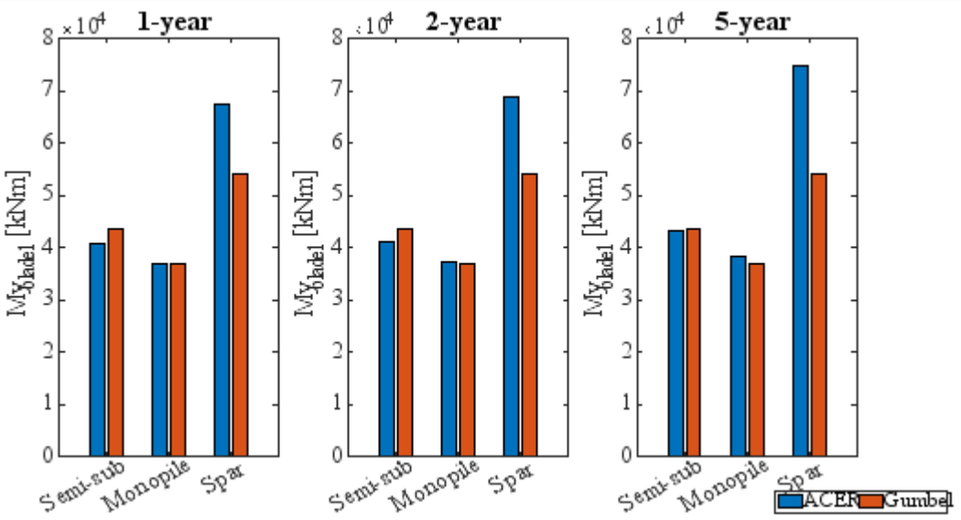

Figure 7 Extreme value responses of Blade 1 My bending moment

Blade 2 My bending moment, V_{hub} = 8m/s

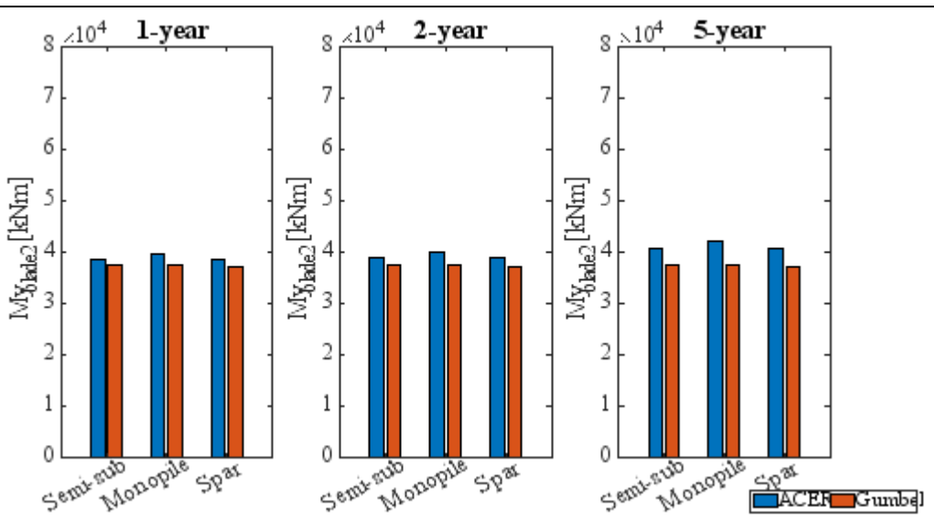

Blade 2 My bending moment, V_{hub} = 12m/s

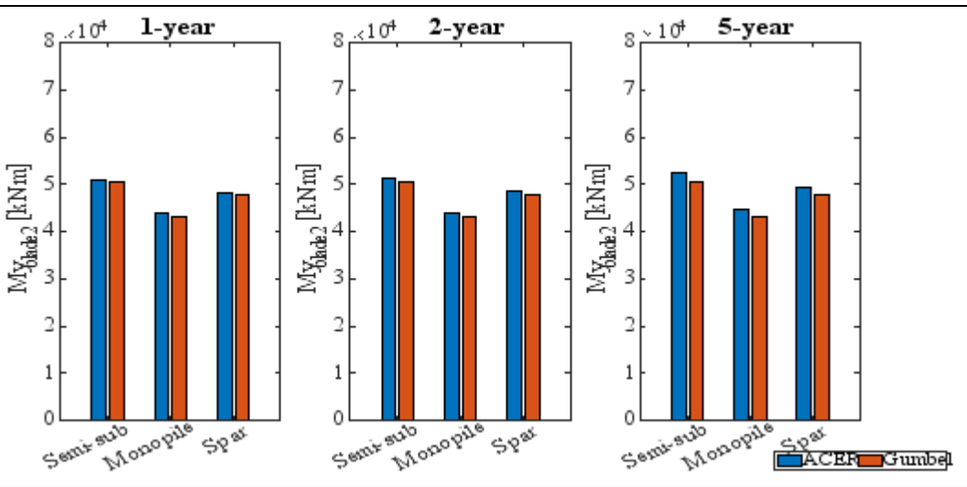

Blade 2 My bending moment, V_{hub} = 16m/s

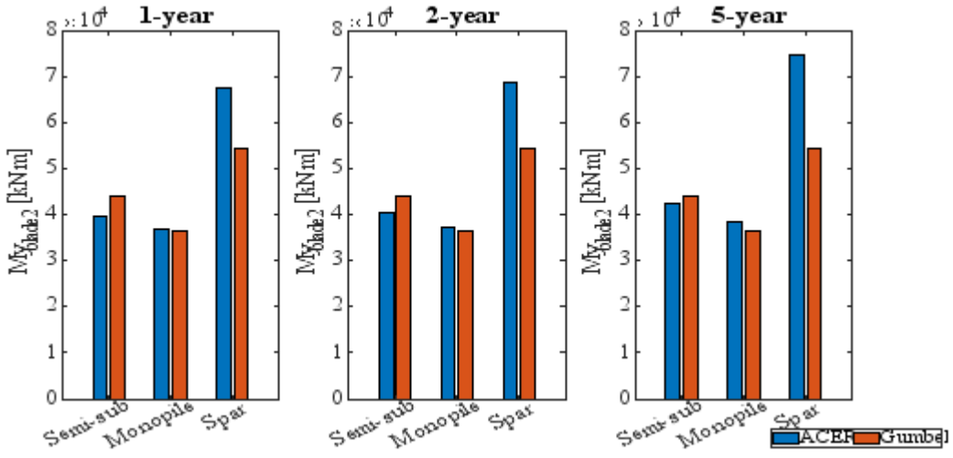

Figure 8 Extreme value responses of Blade 2 My bending moment

Blade 3 My bending moment, V_{hub} = 8m/s

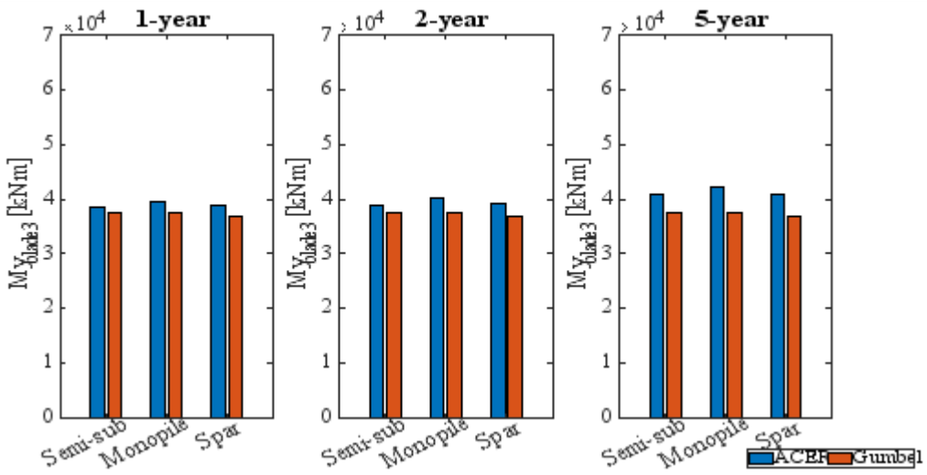

Blade 3 My bending moment, V_{hub} = 12m/s

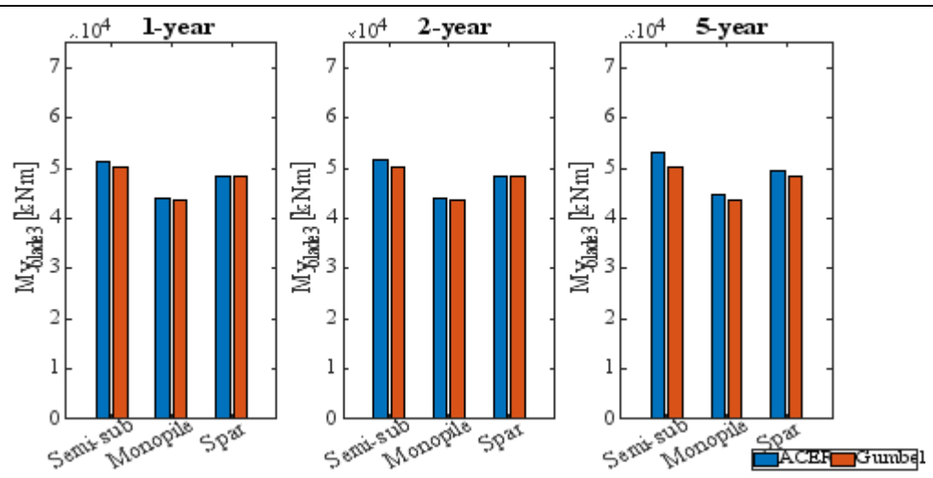

Blade 3 My bending moment, V_{hub} = 16m/s

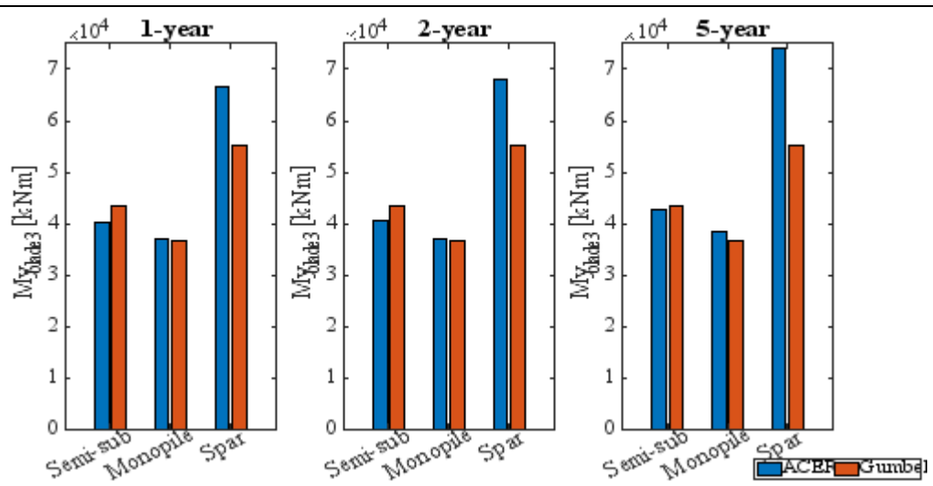

Figure 9 Extreme value responses of Blade 3 My bending moment

Tower My bending moment, V_{hub} = 8m/s

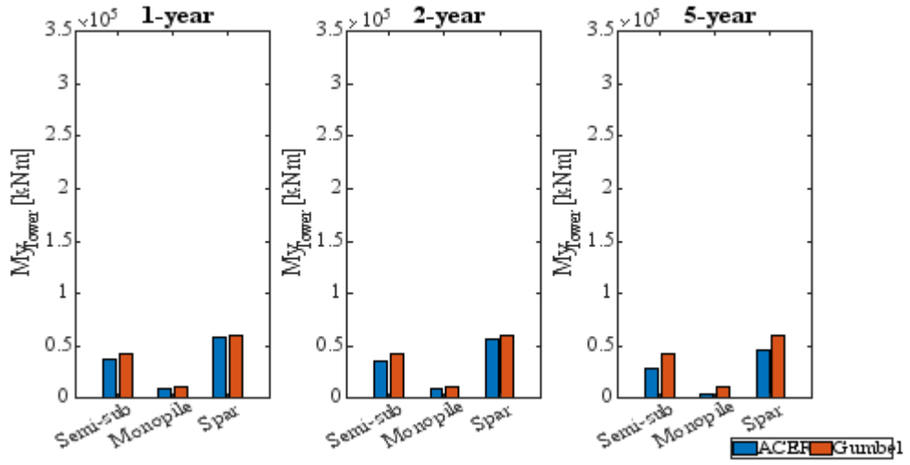

Tower My bending moment, V_{hub} = 12m/s

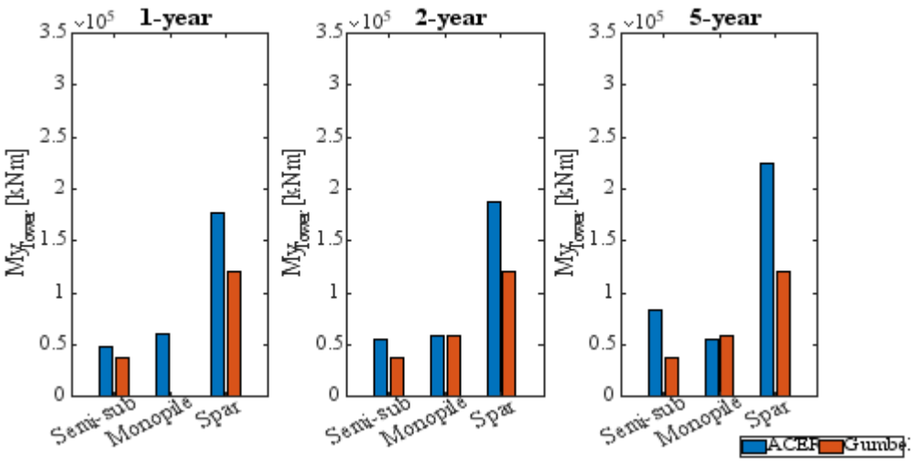

Tower My bending moment, V_{hub} = 16m/s

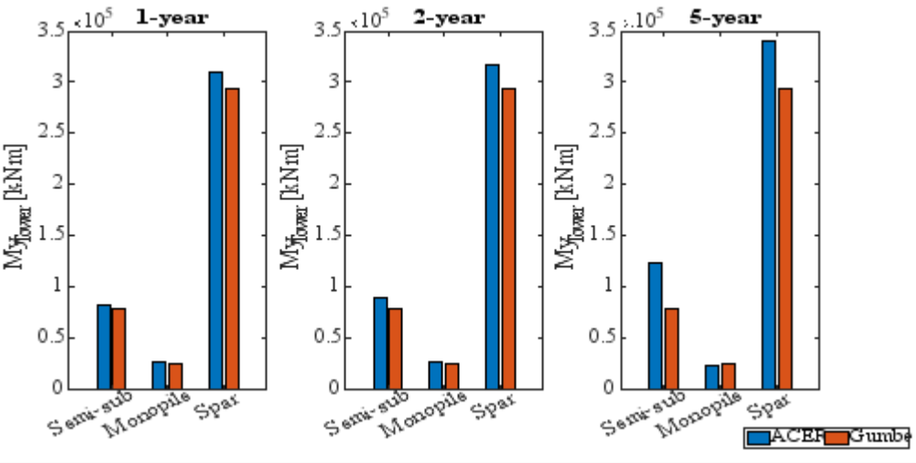

Figure 10 Extreme value responses of Tower My bending moment

Tower Mz bending moment, V_{hub} = 8m/s

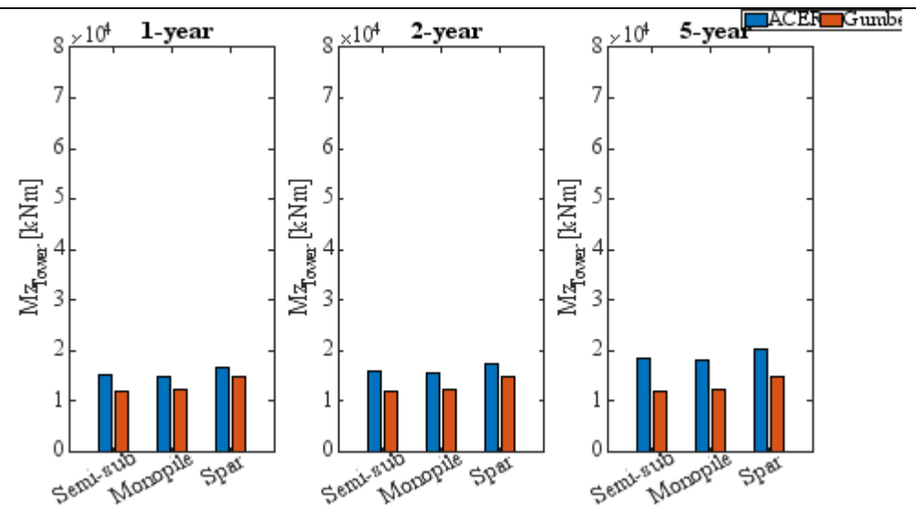

Tower Mz bending moment, V_{hub} = 12m/s

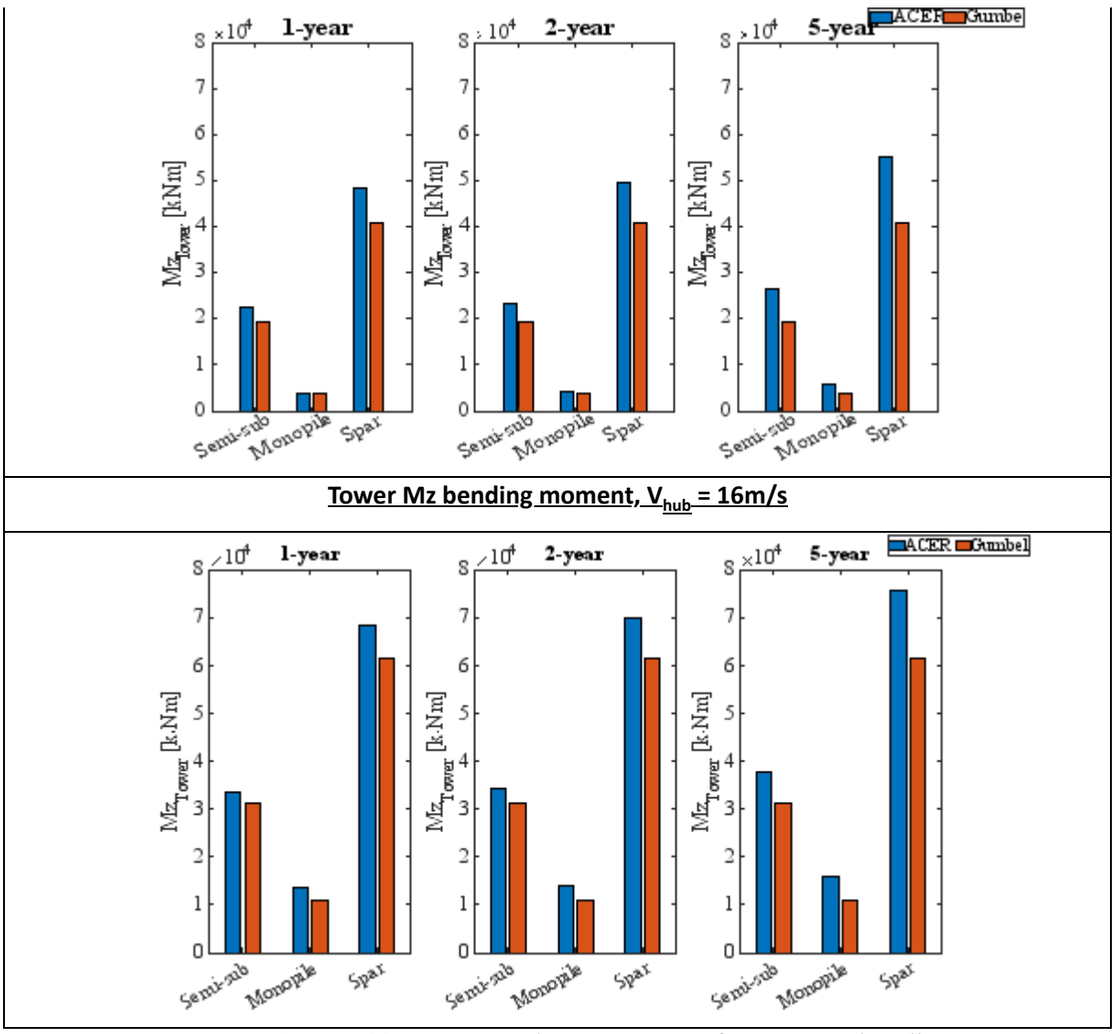

Figure 11 Extreme value responses of Tower Mz bending moment

6. Conclusions

This paper investigated the extreme responses for a 10 MW semisubmersible type FWT using ACER and Gumbel methods. The responses are based on fully coupled nonlinear numerical analysis, including structural flexibility, aero, hydrodynamics, control dynamics, interaction with combined turbulent wind and stochastic waves.

In general, the extreme loads of the spar wind turbine are larger than the monopile and submersible wind turbine, particularly for the rated and above-rated wind conditions. The extreme blade loads are similar in the below-rated and rated wind regions. In the above-rated region, the extreme blades loads for the spar wind turbine are significantly larger than the monopile and semisubmersible. The extreme blade loads of the submersible wind turbine are slightly larger than the monopile wind turbine. The extreme tower bending loads of the spar is the largest in all operating regions, followed by the semisubmersible wind turbine and the monopile wind turbine.

The 1, 2 and 5-year responses of the FWT were, in general, 1.1-1.3 times larger than the maximums of single 1-hour realisations. This reinforces the importance of using extrapolation methods to determine extreme loads to be used as ULS loads. The ACER results have a smaller 95 % CI than the Gumbel results. This means the ACER method is more accurate than the Gumbel method. The Gumbel method's 1, 2 and 5-year responses are quite similar. This is due to poor Gumbel fitting of the data at the upper tail. On the other hand, the ACER does not assume any distributions and therefore does not have the same poor fit issue at the tail end. The better performance of the ACER method is because, in contrast to Gumbel, it does not assume that the extreme responses follow a designated probability distribution.

References

[1] Wind Europe. Offshore Wind in Europe: Key Trends and Statistics 2020. Published February, 2021.

[2] IEA. Offshore Wind Outlook 2019. https://www.iea.org/reports/offshore-wind-outlook-2019.

[3] Musial, W., Beiter, P., Tegen, S., & Smith, A. (2016). Potential offshore wind energy areas in California: An assessment of locations, technology, and costs (No. NREL/TP-5000-67414). National Renewable Energy Lab.(NREL), Golden, CO (United States).

[4] IEC, I. (2009). 61400-3. Wind Turbines-Part 3: Design Requirements for Offshore Wind Turbines.

[5] Goupee, A. J., Koo, B. J., Kimball, R. W., Lambrakos, K. F., & Dagher, H. J. (2014). Experimental comparison of three floating wind turbine concepts. Journal of Offshore Mechanics and Arctic Engineering, 136(2).

[6] Souza, C. E. S., & Bachynski, E. E. (2019). Changes in surge and pitch decay periods of floating wind turbines for varying wind speed. Ocean Engineering, 180, 223-237.

[7] Wise, A. S., & Bachynski, E. E. (2020). Wake meandering effects on floating wind turbines. Wind Energy, 23(5), 1266-1285.

[8] Johlas, H. M., Martínez-Tossas, L. A., Churchfield, M. J., Lackner, M. A., & Schmidt, D. P. (2021). Floating platform effects on power generation in spar and semisubmersible wind turbines. Wind Energy, 24(8), 901-916.

[9] Aggarwal, N., Manikandan, R., & Saha, N. (2017). Nonlinear short term extreme response of spar type floating offshore wind turbines. Ocean Engineering, 130, 199-209.

[10] Chen, X., Jiang, Z., Li, Q., Li, Y., & Ren, N. (2020). Extended environmental contour methods for long-term extreme response analysis of offshore wind turbines. Journal of Offshore Mechanics and Arctic Engineering, 142(5), 052003.

[11] Xu, X., Gaidai, O., Naess, A., & Sahoo, P. (2020). Extreme loads analysis of a site-specific semisubmersible type wind turbine. Ships and Offshore Structures, 15(sup1), S46-S54.

[12] Bak, C., Zahle, F., Bitsche, R., Kim, T., Yde, A., Henriksen, L. C., ... & Natarajan, A. (2013). The DTU 10-MW reference wind turbine. In Danish wind power research 2013.

[13] Velarde, J., & Bachynski, E. E. (2017). Design and fatigue analysis of monopile foundations to support the DTU 10 MW offshore wind turbine. Energy Procedia, 137, 3-13.

[14] Hegseth, J. M., & Bachynski, E. E. (2019). A semi-analytical frequency domain model for efficient design evaluation of spar floating wind turbines. Marine Structures, 64, 186-210..

[15] Jonkman, J. (2010). Definition of the Floating System for Phase IV of OC3 (No. NREL/TP-500-47535). National Renewable Energy Lab.(NREL), Golden, CO (United States).

[16] Yu, W., Müller, K., Lemmer, F., Bredmose, H., Borg, M., Sanchez, G., & Landbo, T. (2017). Public definition of the two LIFES50+ 10MW floater concepts. LIFES50+ Deliverable, 4.

[17] Pegalajar-Jurado, A., Madsen, F. J., Borg, M., & Bredmose, H. (2018). State-of-the-art models for the two LIFES50+ 10 MW floater concepts (Vol. 4). tech. rep.

[18] SIMA. Marine operations and mooring analysis software. https://www.dnv.com/services/marine-operations-and-mooring-analysis-software-sima-2324. Accessed March 07, 2022.

[19] Cheng, Z., Madsen, H. A., Chai, W., Gao, Z., & Moan, T. (2017). A comparison of extreme structural responses and fatigue damage of semisubmersible type floating horizontal and vertical axis wind turbines. Renewable Energy, 108, 207-219.

[20] Xu, K., Zhang, M., Shao, Y., Gao, Z., & Moan, T. (2019). Effect of wave nonlinearity on fatigue damage and extreme responses of a semisubmersible floating wind turbine. Applied Ocean Research, 91, 101879.

[21] Næss, A., & Gaidai, O. (2009). Estimation of extreme values from sampled time series. Structural safety, 31(4), 325-334.

[22] Naess, A., Gaidai, O., & Teigen, P. S. (2007). Extreme response prediction for nonlinear floating offshore structures by Monte Carlo simulation. Applied Ocean Research, 29(4), 221-230.

[23] Chai, W., Naess, A., Leira, B. J., & Bulian, G. (2016). Efficient Monte Carlo simulation and Grim effective wave model for predicting the extreme response of a vessel rolling in random head seas. Ocean Engineering, 123, 191-203.

[24] Naess, A., & Moan, T. (2013). Stochastic dynamics of marine structures. Cambridge University Press.

[25] Peeringa, J. M. (2009). Comparison of extreme load extrapolations using measured and calculated loads of a MW wind turbine. Petten: ECN.

[26] Lott, S., & Cheng, P. W. (2016, September). Load extrapolations based on measurements from an offshore wind turbine at alpha ventus. In Journal of Physics: Conference Series (Vol. 753, No. 7, p. 072004). IOP Publishing.

[27] Li L, Gao Z, Moan T. Joint environmental data at five european offshore sites for design of combined wind and wave energy devices[C]//International Conference on Offshore Mechanics and Arctic Engineering. American Society of Mechanical Engineers, 2013, 55423: V008T09A006.

Appendix

Table 2 Extreme value responses using ACER method for various return periods; 95 % confidence interval in paratheses.

Load Case	**Return period**	**1 yr**	**2 yr**	**5 yr**
	Exceedance probability, q	**7.19×10^{-5}**	**5.71×10^{-5}**	**2.28×10^{-5}**
LC1 V_{hub} = 8 m/s	RootMyb (kNm)	30726 (29149, 31682)	31084 (29393, 32082)	32479 (30315, 33645)
	LSSTipMys (kNm)	9245 (8673, 9616)	9390 (8792, 9768)	9937 (9241, 10351)
	TwrBsMyt	328555	332314	346662

	(kNm)	(318797, 336312)	(322130, 340328)	(334792, 355663)
LC2 V_{hub} = 12 m/s	RootMyb (kNm)	41445 (40752, 42073)	41662 (40934, 42338)	42485 (41615, 43372)
	LSSTipMys (kNm)	15061 (14140, 15677)	15327 (14349, 15973)	16357 (15136, 17122)
	TwrBsMyt (kNm)	437049 (428032, 444853)	439643 (429627, 446865)	449561 (436751, 457982)
LC3 V_{hub} = 16 m/s	RootMyb (kNm)	33406 (32141, 34231)	33790 (32440, 34657)	35293 (33587, 36335)
	LSSTipMys (kNm)	17054 (16567, 17449)	17282 (16780, 17688)	18144 (17584, 18591)
	TwrBsMyt (kNm)	359140 (343069, 367411)	364244 (347041, 372826)	384245 (362296, 394070)

Table 3 Extreme value responses using Gumbel method for various return periods; 95 % confidence interval in paratheses.

Load Case	**Return period**	**1 yr**	**2 yr**	**5 yr**
	Exceedance probablity, q	**7.19×10^{-5}**	**5.71×10^{-5}**	**2.28×10^{-5}**
LC1, V_{hub} = 8 m/s	RootMyb (kNm)	29772 (23844, 37194)	29772 (22344, 37194)	29772 (23844, 37195)
	LSSTipMys (kNm)	9061 (6870, 11953)	9061 (6870, 11953)	9061 (6870, 11953)
	TwrBsMyt (kNm)	314083 (229636, 429680)	314083 (229636, 429680)	314084 (229636, 429681)
LC2, V_{hub} = 12 m/s	RootMyb (kNm)	41593 (28380, 61026)	41593 (28380, 61026)	41593 (28380, 61026)
	LSSTipMys (kNm)	15321 (11801, 19903)	15321 (11801, 19904)	15321 (11801, 19904)
	TwrBsMyt (kNm)	491364 (368347, 655777)	491364 (368347, 655778)	491365 (368348, 655779)
LC3, V_{hub} = 16 m/s	RootMyb (kNm)	46542 (36896, 58215)	46542 (37218, 58215)	46542 (37218, 58215)
	LSSTipMys (kNm)	17168 (13676, 21530)	17168 (13676, 21530)	17168 (13676, 21530)
	TwrBsMyt (kNm)	466508 (384880, 566002)	466510 (384880, 566003)	466510 (384882, 566004)